

https://dspace.org/

Source mechanism studies on Witwatersrand seismic events

Spottiswoode, Stephen Morrison

1980

http://hdl.handle.net/10539/22192

Spottiswoode, Stephen Morrison (1980) Source mechanism studies on Witwatersrand seismic events, University of the Witwatersrand, Johannesburg, <http://wiredspace.wits.ac.za/handle/10539/22192>

Downloaded from a DSpace repository. https://dspace.org/

SOURCE MECHANISM STUDIES ON WITWATERSRAND SEISMIC EVENTS.

Stephen Morrison Spottiswoode.

A Thesis submitted to the Faculty of Science, University of the Witwatersrand, Johannesburg, for the Degree of Doctor of Philosophy.

Johannesburg, 1980.

DECLARATION

Most of Chapter 4 has been published in a paper (Spottiswoode and McGarr, 1975). Dr. McGarr gave considerable assistance in the interpretation of this data. The data analysis and interpretation in the remainder of the thesis were done by the author.

All the information was obtained by the author while employed by the University of the Witwatersrand. This work has not been submitted for a higher degree at any other University.

Signed: S. M. Spottiswoode

July 1979

ACKNOWLEDGEMENTS.

Dr. A. McGarr supervised the work reported here and I am indebted to him for considerable advice and encouragement.

I benefited from discussions with many, especially Professor L.O. Nicolaysen, R.W.E. Green, N.C. Gay and W.D. Ortlepp. Dr. L.M. Fernandez has kindly allowed me unlimited access to the original seismological records of the Geological Survey of South Africa.

R.W.E. Green provided considerable support in the installation and maintenance of the seismic recording equipment used for this study.

Dr. L.R. Johnson kindly sent me a copy of his computer program for generating synthetic seismograms.

I would like to thank Mrs. V. Roberts for the final typing.

CONTENTS:

		Page.
Chapter 1	Introduction	1
Chapter 2	Location of E.R.P.M. Seismic events, 1976 - 1978.	
Chapter 3	Focal mechanism solutions.	
Chapter 4	Source parameters from body-wave spectra.	
Chapter 5	Seismic moments and source orientations from PRE L - P seismograms.	
Chapter 6	Fault gouge, driving stress and seismic efficiency.	
Appendix A1	Seidel's method of successive approximations.	
Appendix A2	Seismic Location program "SMSLOC"	
Appendix A3	PRE long-period response.	

ABSTRACT.

The physical processes at the source of mine tremors at the East Rand Proprietary Mines (E.R.P.M.) near Johannesburg were investigated. Source mechanisms and source parameters of seismic events with Richter magnitudes between 0 and 3,8 were studied by applying seismological techniques to data from geophones in and on the mine and at the seismograph station PRE at Pretoria, about 50 Km. north of E.R.P.M. A new method for determining the mean shear stress acting on a fault is presented.

Some 2 000 seismic events which occurred from 1976 to 1978 at E.R.P.M. were located using P- and S-wave arrival times by a computer location program "SMSLOC". This computer program incorporated a procedure for using arrival times which could be designated as uncertain. This procedure reduced the number of records which had to be reread due to poorly picked arrivals.

Focal mechanism solutions of five seismic events which occurred at E.R.P.M. during 1972 were studied using first motions of P-waves observed at underground geophone sites and P and S waves at a surface station at E.R.P.M. and at PRE. The data were consistent with shear faulting in a normal sense, in agreement with underground observations of burst zones.

Spectra of ground displacement of P and S waves were measured for 24 tremors using records from a seismograph station on the surface of E.R.P.M. The tremors occurred in close proximity to mining at depths of the order of 3,2 Km. below the station and had magnitudes ranging from about 0 to 3. Ground displacement due to P and S waves is, to a first approximation, a uni-directional pulse of the order of 0,05 to 0,2 sec. in width, although considerable complexity is often present in the wave forms. The corresponding spectra of displacement amplitude appear to be flat at low frequencies and generally diminish according to f^{-3} at high frequencies. Analysis of the spectra using the model of Brune for S waves and it's extension to P waves by Trifunac suggests source dimensions ranging from about 50 to 500 m and stress drops ranging from about 5 to 50 bars.

Moments estimated from the low-frequency limits of the spectra vary from 10^{18} to 10^{21} dyne-cm. Seismic energies calculated from the records of ground velocity are in good agreement with log E = 11,8 + 1,5 M; originally developed by Gutenberg and Richter for surface wave magnitudes. E is the energy in ergs.

Seismic events occurring near E.R.P.M. with magnitudes greater the 3,0 write simple looking records on the long-period seismograms at PRE, about 54 Km to the north. Observed seismograms from four seismic events occurring near E.R.P.M. during 1975 were analysed by calculating theoretical seismograms from generalised point sources with no net forces and no net torques. Synthetic seismograms calculated for sources that consist primarily of N - S striking normal faults give a reasonable fit to the observed seismograms. Agreement is improved if account is taken of Rayleigh-wave dispersion due to a surface layer 1 Km thick with a Rayleigh-wave velocity 10% less than that of the underlying material. Inferred seismic moments are in good agreement with the empirical relationship log M_0 = 17,7 + 1,2 M determined previously, where M_0 is the seismic moment in dyne-cm and M is the local magnitude.

The far-field measurements reported here indicate that mine tremors are highly similar, if not identical, to natural crustal earthquakes. This result is important because the source regions of mine tremors are far more accessible, as a consequence of the deep mining, than source regions of tectonic shocks. Furthermore, the rapid strain changes in the rock resulting from mining induce such a high level of seismicity that tremors of magnitude 2 and larger are recorded at least once per week in a region of the order of 1 Km in extent in the areas of ERPM that are currently being mined. Thus, the deep gold mines provide a convenient means of studying earthquake source processes at close hand.

Fault gouge formed in a mining-induced zone of shear failure at a depth of 2 Km. in E.R.P.M. was compared with gouge formed in laboratory samples tested to beyond failure in triaxial compression. The shear stress acting during the formation of the mining-induced zone of shear failure was found to be about 400 bars, determined using two different methods : using a relationship between seismicity and the volume of mining reported by McGarr and from values of the initial stress and stress drop reported by McGarr and others.

The specific crushing energy, or the work done on the gouge zone per unit surface area of gouge particles (determined here from particle-size distributions) was determined as about $3{,}6 \times 10^5$ ergs/cm^2 for gouge from three laboratory samples and about $4{,}5 \times 10^5$ ergs/cm^2 for mining-induced gouge. Alternatively, a crushing energy of $3{,}6 \times 10^5$ ergs/cm^2 can be applied to the mining-induced gouge to calculate an acting shear stress of 450 bars.

The value for driving stress was used together with empirical relationships between seismic energy, seismic moment and magnitude, to determine the seismic efficiency, η, of mine tremors as $\log\eta = 0.3\ M - 3.1$ for seismic events with magnitude, M, between 0 and 3. Resulting efficiencies range from 8×10^{-4} to 6×10^{-3}.

TABLE OF FIGURES.

Figure 1. Map of the East G and H stopes of E.R.P.M. with the face positions during March, 1972. Arrows indicate the direction of face advance for faces being mined at the time. Five seismic events are plotted together with their source mechanisms. Hatching indicates quadrants of compressional first motions.

Figure 2. Fault-plane solutions of events 1 and 2 on 3 February and 8 February, 1972.

Figure 3. Fault-plane solutions of events 3 and 4 on 10 February and 21 March, 1972, D marks the strike of the nearby dyke. Other symbols are the same as in Figure 2.

Figure 4. Fault-plane solution of event 5 on 23 March, 1972. A marks the strike of the 74 E H South abutment. Other symbols are the same as in Figure 2.

Figure 5. (a) Plan view of part of ERPM showing face on November, 1972, event location and seismograph station. 10 events are labelled. A for November 2, 1150A, B for November 2, 1150B,C for August 22, 1021,D for February 4, 2250,E for November 21, 0005,F for November 21, 0020A, G for November 21, 0020B, H for November 2, 2007,J for February 8, 1855, and K for February 4, 1537. (South African Standard Time is used throughout). (b) Section across strike, projected onto A - A'.

Figure 6. Velocity response of seismograph system. (Vertical scale is arbitrary.) Equation (1) is a fit to observed values.

Figure 7. Vertical and two horizontal seismograms of five of the events. The time scale of the two events on November 2, at 1150 is continuous, with the relative gain of A ten times that of B. Time windows used for calculating P (Z), S (NS) and S (EW) spectra and displacements are indicated.

Figure 8. Spectra and displacement for 10 events. The horizontal axis is log-frequency (Hz) and the vertical axis is log displacement spectral density (cm-sec). Our interpretation according to equation 3 is shown. ▲ is used for (3a) at ($f_0 \Omega(0)$), ■ for (3b) and ◆ for (3c). Hollow symbols are used when the theoretical fit is poor. The effect of $Q = 200$ is shown for the S (NS) spectral component of the event on February 4, at 2250.

Figure 9. Shear wave spectra of the 14 events not specifically discussed in the text. Symbols are explained in Figure 8.

Figure 10. Total seismic energy as a function of magnitude. Triangles are used for M from PRE, and magnitude deduced from seismograms recorded by the local station are indicated by circles.

Figure 11. $\Omega(0)$ as a function of f_0 or M_0 as a function of r_0 for P and S waves.

Figure 12. Magnitude as a function of fault dimension. Earthquake data and empirical relationships from Liebermann and Pomeroy (1970)

Figure 13. Moment as a function of magnitude. Symbols are explained in Figure 10.

Figure 14. f_o^P as a function of f_o^S. Hollow symbols are used when f_o^P or f_o^S is considered to be less reliably determined. Theoretical results of Berckhemer and Jacob (1968); Haskell (1964) and Brune (1970) as extended by Hanks and Wyss (1972) and Trifunac (1972a) are included for comparison.

Figure 15. L - P seismograms at PRE from four seismic events occurring near E.R.P.M. during 1975. Identified maxima and minima are indicated.

Figure 16. Synthetic seismograms at PRE from four canonical sources in a homogeneous half-space.

Figure 17. Synthetic seismograms from sources with net volume change (dashed lines) and with no net volume change (dotted lines) compared to observed seismograms.

Figure 18. Phase velocity dispersion inferred from PRE L - P seismograms.

Figure 19. The same as Figure 17, except that dispersion has been applied to the Rayleigh waves.

Figure 20. Seismic moment as a function of magnitude for the events discussed in Chapter 6. Log Mo = 17,7 + 1,2 M comes from Chapter 4.

Figure 21. Variation of axial strain with axial stress and lateral strain for three samples of E.R.P.M. quartzite. Broken lines are inferred values for unloading. (Figure courtesy of C. Heins).

Figure 22. Cumulative particle size distribution, by weight, for laboratory samples (20 + 22) and two mine-induced shear zone samples (A + B and C), plotted on log-probability scales.

Figure 23. A portion of the burst zone sampled for this study. Regions A, B and C in sketch are similar to regions sampled. Arrows indicate direction of movement. (Photograph courtesy of W.D. Ortlepp).

Figure A1. Locations of seismic events between the H and K sections of E.R.P.M. during December, 1976, to February, 1977. Circles indicate events which located in the hanging-wall and triangles events in the footwall. Crosses indicate geophone positions. The size of the symbols indicates the magnitude, ranging from about - 0,5 to 2,5.

Figure A2. Impulse response of PRE long-period systems.

CHAPTER 1.

INTRODUCTION.

Mine tremors have been associated with the gold mines in the Witwatersrand System since soon after mining activities started. With the increasing depth of mining, rockbursts caused by mine tremors are now a major cause of fatalities and loss of production on the gold mines, althougn the judicious use of safety pillars reduces the incidence of tremors (McGarr and Wiebols, 1977) and good support reduces their effect.

The main purpose of this thesis is to present some work done in studying the source mechanism of mine tremors.

The close relationship between mining and seismicity on the Witwatersrand was first demonstrated by Gane et al (1946, 1953) who found that seismic events occurred in the vicinity of actively mined areas. Cook (1963) described data from the first underground seismic network on the Witwatersrand at the East Rand Proprietary Mines (E.R.P.M.). He found that most seismic events originated within about 70m of advancing mine faces. Jouchin (1965) found a similar pattern at the Harmony Gold Mine.

McGarr et al (1975) presented locations of seismic events which occurred in the East Hercules region of E.R.P.M. We correlated the locations with induced stresses and with rock properties in the focal region. Chapter 2 discusses a computer program ("SMSLOC") which was used to locate seismic events occurring at E.R.P.M. between 1976 and 1978. Some 2 000 seismic events were located using P- and S-wave arrival times.

Increased depth of mining has resulted in an increase in seismicity and seismic investigations are now being carried out in many different mines, although most reported studies have been based on E.R.P.M. data.

Seismic activity in three gold mines in the Carletonville area are being studied at present (1979). An automatic seismic location system developed by Heunis (1976) is now being used to locate tremors at the Western Deep Levels Gold Mine at a rate of several thousand seismic events per month. Brink (1979) and D. O'Conner (personal communication 1979) have been studying the pattern of microseismic events within a region with dimensions of less than 200m and are looking for seismicity patterns which might be premonitory to larger events. Van Proctor (1978) studied the relationship of located seismic events to fracture development ahead of a stope which has been advanced by mechanical rock-cutting machines. He found that a small proportion of fractures occurred with sufficient violence to be detected as seismic events. I am at present studying tremors at the Blyvooruitzicht Gold Mine using a digital recording and replay system based on two mini-computers.

Van den Heever (1978) has shown that mine tremors near the gold mines in the Klerksdorp area are often related to the extensive normal faulting which displaces the gold-bearing reef in the area. He has found a good positive correlation between the throw of a fault and the magnitude of the largest event associated with it. A seismic network is being installed around the gold mines at Welkom (D. Lawrence, personal communication, 1979). These mining districts are each 10 to 20 Km. in extent.

MOTIVATION FOR THIS STUDY.

The purpose of the work reported here was to study the physical processes at work during mine tremors at E.R.P.M. The work was part of a contract between the Bernard Price Institute for Geophysical Research (B.P.I.) at the University of the Witwatersrand (Wits. University) and the Chamber of Mines of South Africa.

Analysis of first motions has been applied to tremors occurring at Harmony Gold Mine (Joughin, 1966) and at Western Deep Levels, Limited (Hallbauer, 1967). Both authors found that for a given event the most common distribution of first motions was one for which all or nearly all initial motions are toward the source. Hallbauer concluded that the predominant mechanism was "brittle failure of a volume of rock in compression". He stated that this type of source should excite P-waves only. This feature of his model does not agree with observations by Gane et al (1946) and Cook (1963) of very prominent S-waves. Cook, in fact, estimated that approximately 95% of the seismic energy was in the shear waves.

Joughin (1966), utilising results of Knopoff and Gilbert (1960) presented two focal mechanisms that yield initial motions toward the source (rarefactions) for radiation in all directions. Furthermore, both mechanisms produce shear waves. The two mechanisms are qualitatively described by Joughin as "the sudden failure of a volume of rock (double strain dislocation) or the collapse of fractured rock in the excavation". In addition to being consistent with first-motion patterns that are all, or nearly all, rarefactions, the two mechanisms proposed by Joughin are also compatible with data from convergence meters (Hodgson, 1967), which indicate that instantaneous convergence of the stope occurs at the time of a large seismic event.

Focal mechanism solutions of eleven seismic events at E.R.P.M. were studied by Spottiswoode et al (1971). We showed that first motions of E.R.P.M. seismic events are consistent with shear failure accompanying normal faulting. This result is in agreement with underground observations of burst zones; zones of violent shear failure which have often been associated with mine tremors (e.g. McGarr, 1971a). Chapter 3 presents another five focal mechanism solutions, using directions of first motion of S waves as well as P waves. These data are not consistent with the mechanism proposed by Joughin (1966).

P and S wave spectra of 24 seismic events at E.R.P.M. with magnitudes between 0 and 3 are analysed in Chapter 4 and interpreted in terms of source parameters such as seismic moment, extent of faulting and stress drop. The empirical relationship between seismic moment and magnitude determined in Chapter 4 (from Spottiswoode and McGarr, 1975) has been used in several studies. In particular McGarr (1976) and McGarr and Wiebols (1977) showed that a direct relationship exists for E.R.P.M. between closure volume and seismicity. Closure volume is generally expressed in terms of the Energy Release Rate (E.R.R.), half the gravitational energy available per unit area mined.

Stress drops inferred from seismic spectra, 5 to 50 bars (Chapter 4) are much lower than stress drops determined from laboratory samples which have failed under conditions of triaxial compression (about 1 Kbar). The presence of mine stopes nearby might be related to this apparent discrepency : McGarr et al (1979a) have suggested that the stopes, with a typical extent of 200m or more, control the rate of formation of the shear zone associated with the seismic event. Detailed analysis of data from underground geophones is required to solve the problem of the behaviour of stopes during seismic events.

Focal mechanism solutions of E.R.P.M. seismic events (Chapter 3) are consistent with underground observations of normal faulting (e.g. McGarr, 1971a). Focal mechanism solutions have been based principally on data from short-period instruments and therefore represent only the initiation of failure. Small-scale variations in the state of stress induced by mining can result in changes in the direction of faulting: Ortlepp (1978) found a change of about 25° in the dip angle of a mining-induced shear zone.

The long-period components at PRE write records for mine tremors at E.R.P.M. with magnitudes greater than about 3. The long-period records have a much less complicated appearance than the short-period records, which are somewhat oscillatory, with predominant frequencies of about one hertz, equivalent to wavelengths of several kilometres. The wavelengths are much greater than the source dimension of less than 1 Km. (Chapter 4) and the complicated waveforms observed on the short-period seismograms are presumably caused by structural effects between E.R.P.M. and PRE.

I decided to model long-period seismograms at PRE for mine tremors near E.R.P.M. by comparing observed seismograms with theoretical seismograms for generalised point sources buried in a half-space. Theoretical seismograms were generated using a computer program written by Johnson (1974). I then determined five out of six components of the moment tensor for four seismic events near E.R.P.M. The sixth component, corresponding to dip-slip fault striking N-S unfortunately cannot be easily constrained for E.R.P.M. events recorded at PRE. The observed and theoretical seismograms were similar in appearance, and the similarity was improved when phase velocity dispersion predicted using a simple two-layered model was applied to the theoretical seismograms. The moment tensors were consistent with normal faulting and provided further data to support

the empirical relationship between seismic moment, Mo (in dyne-cm), and magnitude, log Mo = 17,7 + 1,2 M which is determined in Chapter 4. The seismic moments of tremors at E.R.P.M. can now alsc be determined directly from the peak-to-peak amplitude of L-Pz at Pretoria.

Investigation of fresh exposures of shear zones associated with seismic events is a unique aspect of studying seismic events in deep-level gold mines. One particular exposure, consisting of two shear zones in the Western Claims pillar area of E.R.P.M. has been the subject of a number of studies (Ortlepp, 1978; Gay and Ortlepp, 1979 and McGarr et al 1979a & b). The finely comminuted rock, or fault gouge, which fills mining-induced shear zones is very similar to gouge formed under conditions of triaxial compression in the laboratory. This similarity is investigated in the final Chapter (Chapter 6). It is shown that the crushing energy, defined as the work done during formation of a shear zone divided by the total surface area of gouge particles, has a value of about 4×10^5 ergs/cm^2 for both sets of gouge. This result might be applicable to natural faults under certain conditions.

In summary, some new investigations of mine tremors were undertaken and have led to a better understanding of their mechanics. The results of these studies have provided the means of quantitatively relating mine tremors to the state of stress, mining activity and rock properties and have demonstrated the high degree of similarity between mine-induced events and natural earthquakes. Thus, most, if not all, of the findings for the mechanics of mine tremors can be applied directly to tectonic earthquakes.

CHAPTER 2.

Location of E.R.P.M. Seismic events, 1976 - 1978.

INTRODUCTION:

Since mine tremors on the Witwatersrand were first located from seismic recordings by Gane et al (1946), a number of studies have been undertaken to define the relationship between mining and seismicity. The most important step in these studies has been the determination of accurate hypocentral locations.

The first underground array of seismometers was installed in E.R.P.M. by Cook (1962, 1963). He determined locations using a string analogue, a device consisting of a scaled model of the seismometer array from which locations were obtained by drawing strings from the seismometer positions to a common point such that P-wave travel times were brought back to a common origin time. Cook found that the tremors were located within 80m of active mine faces. The analogue location device is slow to use and the results are susceptible to subjective bias.

McGarr et al (1975) described the results of seismic locations over a more extensive area of E.R.P.M. than that covered by Cook (1962). We located the tremors with a computer programme which minimised the sum of the squares of the time residuals of P-wave arrival times (calculated arrival times minus observed arrival times). Almost all the tremors in a region of the mine in which locations were accurate to within 20m in plan and 30m in elevation (depth below surface) located between the reef plane and 150m in the hangingwall. Some 160 events were located for this study.

During 1975 and 1976 improvements were made to the electronics of the record and replay tape record systems following designs by R.W.E. Green of the Bernard Price Institute (B.P.I.)Wits University. An array of ten HS 1 and H S J vertical component geophones was laid out, using some of the previous geophones and cabling. The array was centred around the Chamber of Mines Experimental crosscut in the Hercules section of

E.R.P.M. This crosscut was being developed to test haulage support systems under severe stress conditions and to monitor conditions in the focal regions of mine tremors.

This Chapter describes a Fortran IV computer programme "SMSLOC" listed in Appendix A2 which was used for locating more than 2 000 seismic events which occurred in E.R.P.M. Locations were based on reliable P - and S - wave arrival times between August 1976 and August 1978. Most records were read by clerks at the Chamber of Mines Mining Research Laboratories.

The conventional tape record and replay system which has been used at E.R.P.M. resulted in special problems in interpreting the records, such as cross-talk, that create additional problems of misidentifying arrival times. The computer programme "SMSLOC" was written to incorporate several features which assisted us in getting the best locations for P and S-wave arrival times with the minimum amount of record re-reading.

This enabled us to build up a complete data set of (generally) reliable locations without rereading the records at the B.P.I. or resorting to computerised methods to reject incorrect arrival times. Automatic procedures for rejecting incorrect arrival times have to be used with caution, especially if the solution is not strongly overdetermined. One incorrect arrival out of twelve could probably be identified with a reasonable degree of certainty.

INSTRUMENTATION.

Signals from H S J and H S 1 vertical component geophones were amplified by a factor of about 200 by battery-powered amplifiers and transmitted along cables underground to a tape deck centrally situated on 68 level in the Hercules section of E.R.P.M. at a depth of about 2,8 Km. below surface. 40 Channels of data could be recorded continuously onto 25,4 mm magnetic tape moving at 25,4 mm/sec past two 20 track tape heads 40 mm apart. The data were recorded using A M mode and A C bias. Timing was provided by a digital clock which wrote time signals onto two channels. Replay took place at the B.P.I. at about 150 mm/sec, or six times the record speed, using a tape deck similar to the record deck.

Paper records of 24 channels of data were obtained on an oscillograph recorder using paper 200 mm. wide, running at 500 mm/sec, equivalent to about 90 mm/field second. Seismic events could easily be identified by listening to a seismic channel on a loudspeaker. An eight-track head was placed 150 mm ahead of the two replay heads and the signals from four geophones were analysed by an event discrimination circuit. This circuit monitored the envelopes of the four signals and if the levels exceeded preset levels on at least two channels, a paper record was written. This event detector worked very well and only events of special interest were replayed by hand.

The recording and replay electronic circuits were similar to those used in the B.P.I. portable seismic recording system (Green, 1973). The overall frequency response of the entire system was flat over a wider range of frequencies than the original seismic system installed by Cook (1962), with 3 db points at about 10 and 250 Hz. Data from most geophones were recorded at two levels of gain, separated by a

factor of about 16. High-gain traces exhibited very clear P-wave arrivals while S-wave arrivals were often very clear on the low gain traces. Because data from only six to eight geophones were generally being recorded, it was decided to use the most distinct S-wave arrivals to provide additional data for obtaining locations.

OBSERVATIONS.

Although the seismograms were generally of better quality than those obtained from the previous seismic array at E.R.P.M., great care was still required to avoid choosing erroneous arrival times. A number of factors led to difficulties in choosing arrivals.

(1) Overlapping traces. The average spacing between adjacent traces on the paper records was 8 mm. To obtain a good signal-to-noise ratio, the traces were allowed to have maximum amplitudes of up to 40 mm. The resulting trace overlapping sometimes made it difficult to follow individual traces.

(2) Geophone Orientation. All the geophones used for the location array were vertical component geophones. When a seismic event occurred at the same depth as the geophone, the angle of incidence was such that P-wave amplitudes were quite small. Records from a geophone situated at the end of the 73 level Chamber of Mines crosscut often exhibited P-wave amplitudes that were so small that S waves were sometimes misidentified as P-waves.

(3) Multiple events. During blasting time, which lasted for about twenty minutes each workday afternoon at about 1600 hours, the rate of occurrence of tremors was considerably greater than during the rest of the day and events were often superimposed on one another on the records. Sometimes a blast itself would appear to trigger a seismic event almost immediately, causing a multiple event. The kilogram of explosives set off in each hole wrote records for at most one or two geophones.

Several of the largest events were difficult to locate accurately because they immediately followed, and were presumably triggered by, a smaller seismic event.

(4) Source Orientation. The double couple source, which has been shown to describe E.R.P.M. seismic sources (Chapter 3 and Diering, 1978), radiates very low amplitudes along directions close to the nodal

planes for P and S waves. Non-least time arrivals might be picked as the first arrival for geophones close to the nodal planes.

(5) Cable Cross-Talk. Transmission of signals from the amplifier at the geophone to the recording room took place along armoured telephone cables or blasting cables. A small amount of cross-talk would sometimes be visible between two signals which had been transmitted along the same multi-pair cable.

(6) Record and replay head effects: Cross-talk between adjacent channels sometimes occurred due to the close spacing (0,6 mm) between adjacent channels. An event large enough to result in saturation of most of the high-gain channels would result in cross-talk on several channels and could give the impression, because of the low frequency appearance, that a large distant seismic event had occurred. Large signals also caused saturation of the write heads and a small low-frequency precursor was sometimes visible before the P-wave arrivals.

Because of the large number of events which wrote seismograms with a good signal-to-noise ratio, up to 300/month, and because of the shortage of skilled manpower, most of the seismograms were read and the events located by clerical staff at the Chamber of Mines Mining Research Laboratories. Locations on this basis often resulted in greater location errors due to incorrectly picked arrivals. The two clerks involved had both had previous experience of reading seismograms, but further training was required. The location programme was designed to assist them and to help reduce the number of spurious arrival times used for the final location.

COMPUTER LOCATION PROGRAM.

Between August, 1976 and February, 1977, the computer program for locating E.R.P.M. Seismic events, "SMSLOC" was written and improved. In contrast to previous programs used for locating mine tremors, S-wave arrivals as well as P-wave arrivals could be used. It was decided to feed the data into the computer (the Wits. University I.B.M. model 370) using standard (80 column) computer cards. Due to the considerations discussed above, a number of features was built into the computer program to assist the person reading the records to get a "feel" for the best arrivals. Seidel's method of successive iterations was used to obtain a least-squares fit by minimising a weighted sum of the squares of the time residuals.

Input data required for the locations were : -

(1) The geophone position, in mine coordinates.

(2) The velocity structure between the source and the geophones. At E.R.P.M. we used a different constant velocity for every event to each individual geophone. Mine-wide velocities of 6,1 Km/sec for P waves and 3,8 Km/sec for S waves were used for locating seismic events outside the array of seismometers

(3) Time residuals associated with each geophone. For the tape system at E.R.P.M., head-skew corrections were applied to correct for errors in the alignment of the record and replay heads.

(4) The paper speed of the hard copy records, expressed in mm/Sec.

and

(5) Arrival times of individual phases at each geophone, expressed in mm. from a common timing line.

Items (1), (2), and (3) were constant for every location. One data card was used for data appropriate for each geophone : ten data cards were required for these data.

The date, time of the event and information (4) and (5) were punched

onto one data card for each event. 12 columns of alphanumeric characters were used to describe the date and time of the event. 4 columns were required for the paper speed which was generally about 90 mm/sec., but which sometimes exceeded 100mm/sec. P and S arrivals were read to an accuracy of 0,1 mm from one of the common time lines written onto the records by a flashing light. Three columns of data were sufficient to describe each individual arrival time. Each data card was therefore punched as follows : -

Event title (3A 4)	12 columns
Paper speed (F4.1)	4 columns
3 columns each (F3.1) for two phases for 10 geophones	60 columns
Total	76 columns.

(3A 4), (F4.1) and (F3.1) refer to "FORTRAN" format.

An example of a data card and the corresponding computer printout follows : -

```
22 APR 0854
************
  9 , TO =  11.     244.     380.

X = 22462., Y = 12013., Z = 3065., T =   5., ERROR =  33.

 8 ARRIVALS        2       5       7       8       9      10      11      19
RESIDUALS          3.     -7.     -4.      6.      1.      1.      0.      5.
DISTANCE        2048.    678.    622.    541.   1439.    495.    645.   1439.

RELOCATE WITHOUT DOUBTFUL ARRIVAL  2

X = 22403., Y = 12114., Z = 3295., T =  21., ERROR =  23.

 7 ARRIVALS       -2       5       7       8       9      10      11      19
RESIDUALS         30.     -5.     -1.      2.      3.      0.      5.     -2.
DISTANCE        2175.    602.    547.    425.   1356.    403.    605.   1356.

RELOCATE WITHOUT DOUBTFUL ARRIVAL 19

X = 22401., Y = 12113., Z = 3304., T =  21., ERROR =  28.

 6 ARRIVALS       -2       5       7       8       9      10      11     -19
RESIDUALS         31.     -5.     -1.      1.      2.      1.      6.     -3.
DISTANCE        2174.    602.    545.    423.   1352.    403.    605.   1352.
```

The problems mentioned in the previous section resulted in many incorrect arrivals being chosen as P- or S-wave arrivals. For example, S-wave arrivals or noise due to cross-talk were often mistaken for P-wave arrivals. To obtain a proper location, the seismogram would have to be reread and the mistake corrected. In many cases, however, an element of doubt would exist as to where a particular arrival should be picked. The correct procedure is normally to avoid arrivals which could cause a location to become unreliable. On the other hand, it is generally desirable to use a greater number of arrival times for each location and the best way to gain experience in picking arrivals is to learn to distinguish correct arrivals from noise.

It was decided to introduce the capability of nominating up to two arrivals as being uncertain. The location programme would determine the best location using all the read arrivals, and then repeat the location without using an arrival marked as uncertain. In the case of two uncertain arrivals, two further locations would be determined, without the uncertain arrival with the largest time residual first, and then without the other uncertain arrival. A P-wave arrival time could be designated as uncertain on the data card by entering the geophone number (1 to 10) in columns 77 and 78 using I2 ("FORTRAN") format. Numbers 11 to 20 were used for uncertain S-wave arrival times. A second uncertain arrival could be indicated by using columns 79 and 80.

Locations which were determined using at least seven arrival times, but which resulted in unusually large closure errors (Page 20) were repeated without the arrival which gave the largest time residual. Closure errors of less than 50 m within the array were considered reasonable. The original records were inspected again and it was generally found that the arrival with greatest time residual had been badly chosen. If seven or eight arrivals had been picked, suspicion was sometimes cast on a perfectly good arrival : it was always essential to check the original records.

Each arrival which was excluded from the location procedure would be tested in the program to see whether the phase might have been mis-identified i.e. whether a P-wave arrival was identified as an S-wave arrival or vice versa.

The process of determining locations with and without certain arrival times meant that a choice then had to be made among as many as four, or even five, separate locations for a single event. Subject to checking arrivals that were considered to be suspect, the "best" location was considered to be that which resulted in the smallest closure error. For similar closure errors, the location with more arrivals was preferred. The distance between two locations in such cases is a very good indication of the relative location accuracy. In most cases, the relative location accuracy was better than 50m.

The process of determining locations using different combinations of arrival times meant that the location programme had an interactive character about it that encouraged people who used it to experiment with choosing arrivals and to get the best "feel" for choosing arrivals which might otherwise have been passed off as noise.

Seismic Velocities in E.R.P.M.

Thirty seismic events occurring during August and September, 1976 with at least nine clear (P and S) arrivals were located using a constant P velocity of 6,0 km/sec. and a constant S velocity of 3,8 Km/sec. These velocities were typical of those determined from previous data at E.R.P.M. (McGarr et al, 1975 and McGarr, 1974). The closure error, an error estimate based on the sum of the squares of the time residuals was less than 60 m for these locations. The time residuals were then plotted against hypocentral distances for each event and it was found that some phases were consistently slower, while others were consistently faster than the assumed velocity. These differences were then expressed a a constant velocity to each geophone and the locations were repeated. Although the locations did not move by more than 50 m in most cases, the closure errors dropped by about half to less than 30 m.

A velocity model consisting of a different constant velocity from all the seismic events to each geophone was then used for all subsequent locations. The P velocities ranged from 6,1 Km/sec for ray-paths through hangingwall quartzites to 5,8 Km/sec for ray-paths through footwall quartzites or for relatively short ray-paths through a higher proportion of fractured rock. These velocities agreed closely with velocities determined from calibration blasts which were undertaken for the previous seismic array at E.R.P.M. Higher velocities in the hangingwall rocks are consistent with the observation by McGarr et al (1975) that the hangingwall quartzites had a higher Young's modulus than the footwall quartzites.

The importance of using reliable values for velocities can be demonstrated by considering the range of velocities encountered when a calibration blast is monitored. A range of 5,8 Km/sec to 6,1 Km/sec is equivalent to a range of 5 percent or 50 m over a path length of 1 Km.

If the source region is not surrounded by geophones in every direction, this range could result in arrors of more than 5 percent of typical path lengths.

A calibration blast was set off in a crosscut off the 75 East Hercules footwall drive 160m from the experimental crosscut in Fig. A2, on the 27th April, 1978. 25 Kg. of explosives ("Dynagel") were set off simultaneously and should have written records for all eight geophones operating at the time. However, the tamping was very poor, and the resulting seismic event had a Richter local magnitude of about -1.1 and only 5 P-wave arrivals and 2 S-wave arrivals were detected.

The calibration blast resulted in substantial S-wave amplitudes because the poor tamping resulted in considerable asymmetry in the source function and because the surrounding rock was in a complex stress field due to the overlying excavation. Locations based on several records of the same event were 48 m west, 17 m south and 19 m above the true location of the blast with a scatter of about 5 m.

These data could have been used to improve locations in the vicinity of the calibration blast by joint hypocentral determinations of the location of one or more seismic events nearby with a greater number of clear arrivals. These data could then have been used to perform joint hypocentral determinations for more accurate absolute locations of all the events in the vicinity of the calibration blast. We felt that the data from the calibration blast was insufficient to justify this procedure and instead all locations were moved 48 m east, 17 m north and 19 m downwards in an attempt to correct for systematic errors.

RESULTS:

Locations of mine tremors which occurred between the H and K sections of E.R.P.M. during December, 1976 to February, 1977 are presented in Figure A1 of the Appendix. The size of each symbol indicates the magnitude. The magnitude scale was based on the coda duration measured at two geophones site some 500 m north-east of Figure A1 and was drawn up as an extension of the local magnitude scale based on measurements of records from the WWSSN station at PRE (Chapter 4).

Tremors originated near all the actively advancing faces, generally between 50 m behind to 100 m ahead of the face and between the reef plane and 100 m in the hanging-wall, in agreement with McGarr et al (1975) who presented some previous data for the East Hercules (H) region. The location in the lower part of the West K longwall (bottom right of Fig. A1) plotted below reef. This location was outside the array of seismometers and the locations were subject to larger errors.

The areas of the Hercules region immediately west and east of the 73L crosscut were quiet and active respectively compared to the seismicity along the west K longwall. The low seismicity on the faces immediately to the west of the crosscut was even more marked than it appears in Fig. A1 because the face advance there was much greater than that in West K and the seismicity per area mined was therefore much lower. The lower level of seismicity is qualitative support for the results of McGarr and Wiebols (1977) who showed that safety pillars reduce seismicity in proportion to the reduction in energy release rate, or amount of elastic convergence between the hanging-wall and foot-wall.

The high level of seismicity just east of the crosscut probably

correlated with the dip dyke which separates H and K. I relocated all the events in this cluster by joint hypocentral determinations using one of the events as the master event. The relative locations were then accurate to better than 20 m and the extent of the clustering shrunk somewhat so that the locations were then in a region with dimensions of about 100 m in each direction. In contrast, the stable fracturing which occurs continuously in front of an advancing face has a vertical extent of up to about 30 m, 15 m in each direction (Cook et al, 1966). Violent fractures can therefore extend further from an advancing face that non-violent fractures.

During 1977 three Sacks - Everton volumetric strainmeters were installed in the Chamber of Mines crosscut. McGarr et al (1978) found that coseismic strain steps were in good agreement with strain steps predicted by the double-couple point source representation of earthquakes. Reliable locations were required for this investigation and the distance between the strainmeters and the seismic events appeared to have been determined with an accuracy of better than 50 m.

LOCATION ALGORITHM

The location algorithm in the program "SMSLOC" minimised the weighted sum of the squares of the time residuals for seismic events in a medium such that the P and S velocities to each individual geophone remain constant. An iteration procedure based on Seidel's method (Appendix A1) is used.

Take Xi, Yi and Zi as the X, Y, and Z co-ordinates of the i-th geophone (i = 1,10 in "SMSLOC"),

and Xo, Yo and Zo as the hypocentre of the seismic event,

Therefore $Di = ((Xi - Xo)^2 + (Yi - Yo)^2 + (Zi - Zo)^2)^{1/2}$ is the distance between the event and the i-th geophone.

Take Tci = the arrival time of the P(Tpi) or S(Tsi) phase at the i-th geophone,

To = the origin time of the event,

and Vci = the average (constant) P (Vpi) or S (Vsi) velocity between (Xo, Yo, Zo) and (Xi, Yi, Zi).

The distance residual, Rci, associated with each arrival time was defined as the product of the time residual and the average velocity:

Rpi = Di - Vpi(Tpi - To) for P waves and

Rsi = Di - Vsi (Tsi - To) for S waves.

The programme "SMSLOC" reduced the weighted sum of the squares of the distance residuals, Ro, to a minimum.

$$Ro = \sum_{\text{all arrival times}} Ki^2(Rpi^2 + Rsi^2)$$

The following weighting function was used:-

$$Ki = 1\,000/(600\ m + Di)$$

This weighting function was chosen so that likely uncertainties in the accuracy with which arrivals were read and uncertainties due to velocity variations were given equal weight. 600 m is the distance at which a P-wave reading error of 1 m sec is equivalent to a velocity error of one percent (for P-waves).

Seidel's method uses Rci and it's partial differential with respect to each of the four unknowns, Xo, Yo, Zo and To :-

$$\frac{\partial Rci}{\partial Xo} = Xo/Di$$

$$\frac{\partial Rci}{\partial Yo} = Yo/Di$$

$$\frac{\partial Rci}{\partial Zo} = Zo/Di$$

and

$$\frac{\partial Rci}{\partial To} = Vci$$

A set of four linear equations were then set up and solved in a manner described in Appendix A1. The solution gave values which were used to improve an initial guess location until the location converged.

A closure error, on estimate of the internal co sistency of the solution was defined as

$$\text{Error} = \left(\frac{1}{N-4} \sum_{i=1}^{N} Rci^2\right)^{\frac{1}{2}}$$

where N is the number of arrivals used for the location.

The first guess value did not affect the final location but the number of iterations required to find the final location was reduced if the first guess was close to the final location. The first guess was, therefore, taken close to the geophone which registered the earliest arrival. A solution was considered to have converged when the movement between successive iterations was less than a metre. Poor data would often lead to divergence, in which the solution ran away, or persistent large oscillations. A damping factor which became smaller as the number of iterations increased was applied to reduce these oscillations. The resulting location would only be used as a guide for re-evaluating the arrival times chosen originally.

CHAPTER 3.

Focal Mechanism Solutions.

INTRODUCTION:

This chapter presents focal mechanism solutions of five seismic events which occurred at the East Rand Proprietary Mines (E.R.P.M.) during February and March, 1972. These events were chosen from the events for which source mechanisms are determined in Chapter 4. The method used was the same as that described by Spottiswoode et al (1971), except that S-wave polarisations at a surface station at E.R.P.M. and at the World-Wide Standardised Seismograph Network (WWSSN) station at Pretoria (PRE) were also used.

Hypocentral locations were obtained using the array of 10 vertical component geophones in E.R.P.M., described by McGarr et al (1975), using an earlier version of the computer program described in the previous chapter. P-wave arrivals at a vertical array of five three-component sets of seismometers in the Cinderella vertical shaft at E.R.P.M. were also used. Portable seismic recording systems (Green, 1973) were used at the surface station and in the vertical array.

Rock fails in the vicinity of the workings in deep-level gold mines both violently and non-violently : Violent failure results in mine tremors (e.g. McGarr, 1971) and is characterised by considerable energy release. Many shear zones, or Type 2 failures (McGarr, 1971 b) filled with highly comminuted rock have been observed at E.R.P.M. Some of these shear zones, or burst zones, have been correlated directly with seismic events and with underground damage (Spottiswoode et al, 1971; Ortlepp, 1978). They are, in fact, very recent fault zones. It will be shown in chapter 6 that the formation of these shear zones is an important factor in the energy balance at E.R.P.M.

Burst zones observed at E.R.P.M. have generally been found to be parallel to the edges of the enlarging tabular excavations. Generally, they are parallel to the advancing faces, but they have also been observed to be parallel to abutments remaining at the edges of advancing faces. Shear displacements have been measured wherever possible and have always indicated normal faulting consistent with convergence of the stopes. Ortlepp (1978) described observations made in a series of raises (tunnels) developed along two intersecting burst zones from 40 m below the stoping at the Western Claims Pillar area of E.R.P.M. up to the stoping above. The greatest measured shear displacement of 100 mm or more was about 15 m below the reef horizon and about 30 m ahead of the face at the time the shear zone formed.

McGarr et al (1975) found that the centre of seismicity in the East Hercules region of E.R.P.M. was about 60 m above the advancing faces. Events located up to 100 m in the hangingwall. Focal mechanism solutions sample the pattern of failure of a much larger region than is possible using underground observations alone. Data from focal mechanism solutions complement in situ observations of burst zones.

OBSERVATIONS

The initial directions of P-wave motion were read from seismograms written by eight geophones of the underground array of seismometers and five geophones of the vertical array of seismometers. P and S first motions at a portable station on the surface of E.R.P.M. and at the short-period records at PRE were also read. The levels of gain of both the underground array of seismometers and the vertical array of seismometers were so high that the directions of motion of the S waves could not be clearly distinguished as they were lost in the saturated and/or overlapping coda of the P waves for events with magnitude greater than 1.
As all the geophones of the underground array of seismometers were sensitive to vertical ground motion only, and therefore wrote ambiguous first motion P-waves at near-horizontal angles, arrivals within 10° of the horizontal were considered unreliable.

First motions were plotted using an equal-angle stereographic projection of the focal sphere, a small imaginary sphere around the hypocentre. Upper hemisphere projections were used. First motions which should plot in the lower hemisphere were plotted at their antipodes in the upper hemisphere because first motions are caused by stresses at a point and all physically plausible point sources possess central symmetry.

Ray paths were assumed to be straight to the underground and surface geophones at E.R.P.M. The angle of emergence for ray paths to PRE (about 54 Km. due North of E.R.P.M.) was taken as 74° using an average P-wave velocity of 5,95 Km/sec. at E.R.P.M. (McGarr et al, 1975) and a crustal velocity, P_1, of 6,18 Km/sec (Gane et al, 1956). Ray paths for S waves were assumed to be the same as for P waves. Because S waves are contaminated by the coda of the P waves, only very clear S arrivals were used to determine S-wave polarisation. The vertically polarised S-wave (SV) at PRE was only used if the first motion on both the radial

(North - South) and vertical components were clear and in the same sense. Because PRE is virtually due North of E.R.P.M., the horizontal components are oriented so that essentially pure SV is observed on the vertical and N-S components and SH only the E-W component.

P-wave compressions and rarefactions were separated as far as possible on the stereographic projections by two orthogonal planes - the P-wave nodal planes. The centres of rarefaction quadrants define the compressional, or P, axis and the centres of the compressional quadrants define the tensional, or T, axis. The intermediate, or B, axis lies on the intersection of the nodal planes. S-wave polarisations also constrain the fault-plane solutions : S-wave first motions diverge from the P axis and converge on the T axis and are perpendicular to the P-wave nodal planes. The B axis is a null axis for S as well as for P.

Events analysed in this chapter are listed in Table 1 and their locations are plotted in plan relative to the mine workings in Figure 1. Event locations were accurate to about 20 m in plan and about 30 m in elevation (McGarr et al, 1975).

Fault-plane solutions of events 1 and 2 are shown in Figure 2. The events located about 50 m behind the 75 - 77 East Hercules longwall, 60 m apart in plan and 150 m apart in elevation. Both events have fault-plane solutions consistent with normal faulting although there is one inconsistent arrival for the event on 3 February at 1410. First motions could not be read at PRE for the event on 8 February at 1814 because it was too small. (M_L = 1,1).

Fault-plane solutions of events 3 and 4 are shown in Figure 3. They located about 40 m apart ahead of the 73 East G face and close to 73 West H face, which stopped advancing during 1969 after mining up to the edge of a dyke. All the first motions of these two events are consistent with the proposed fault-plane solutions.

The event on 23 March at 1629 (event 5) occurred near the bottom of the 73 - 74 East Hercules longwall, which was about 150 m ahead of the 75 - 77 East Hercules longwall at the time. The fault-plane solution (figure 4) is also appropriate for a normal fault although there is an appreciable component of strike-slip motion.

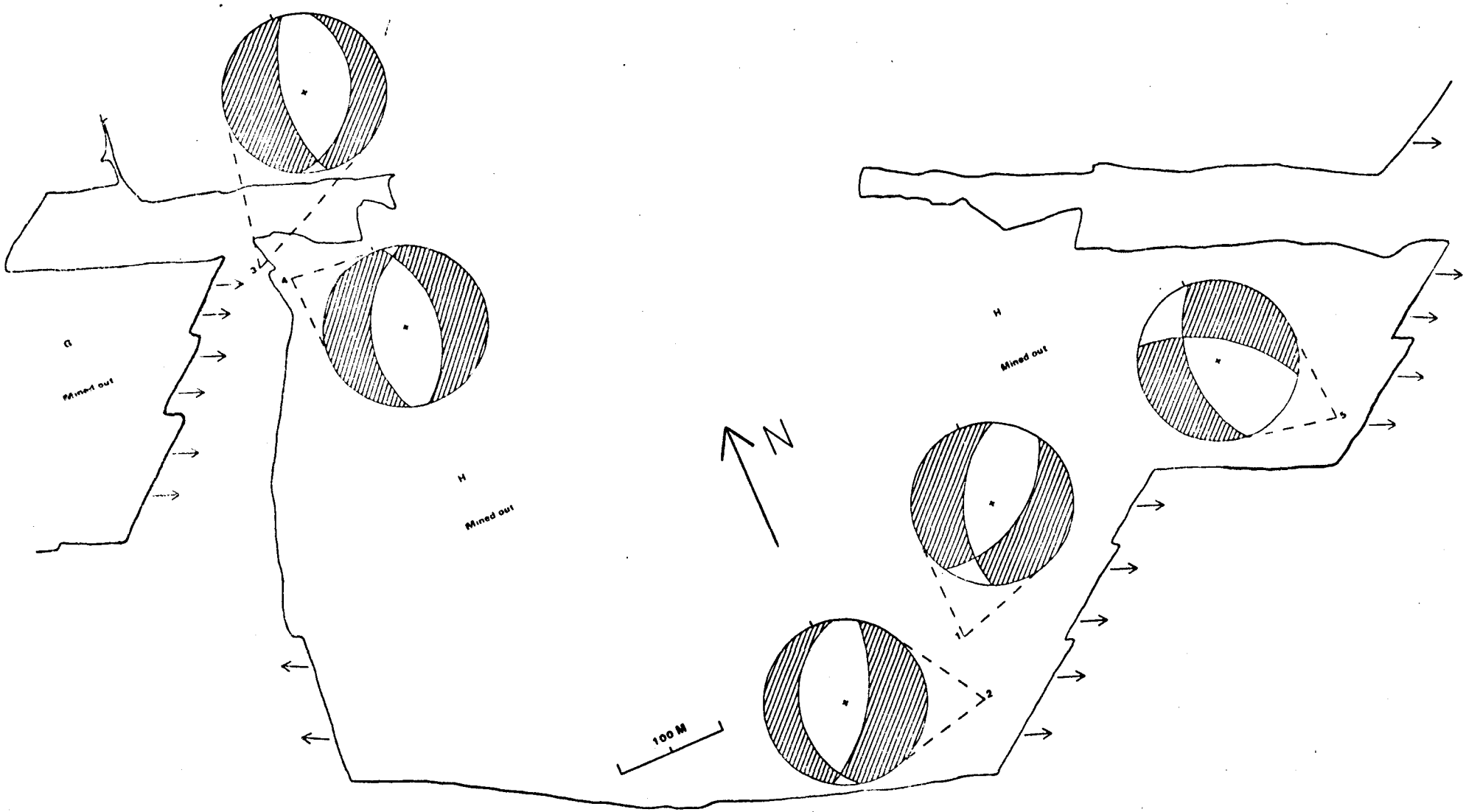

Figure 1. Map of the East G and H stopes of E.R.P.M. with the face positions during March, 1972. Arrows indicate the direction of face advance for faces being mined at the time. Five seismic events are plotted together with their source mechanisms. Hatching indicates quadrants of compressional first motions.

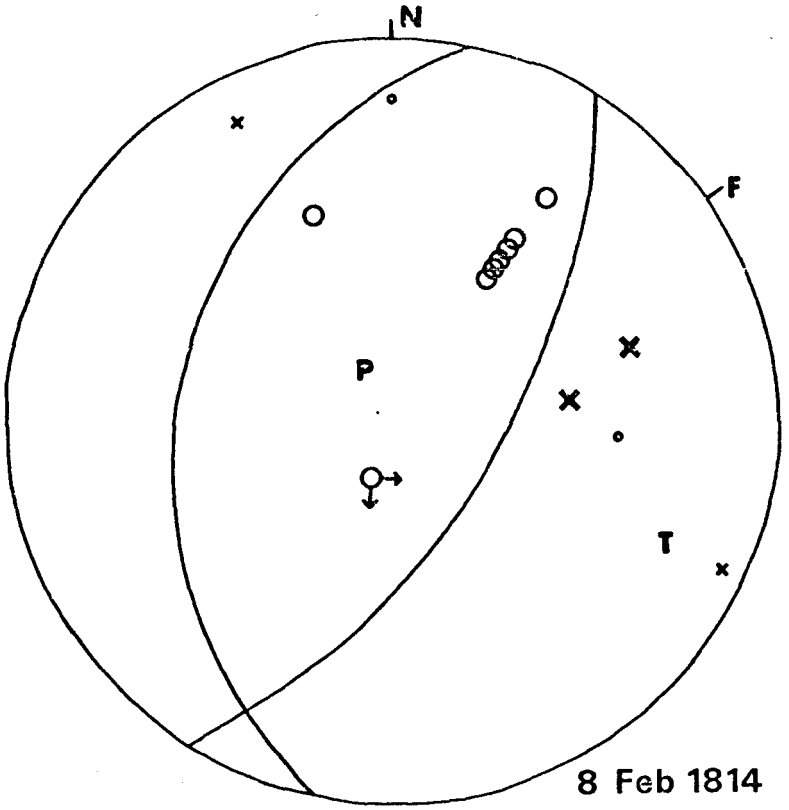

2.

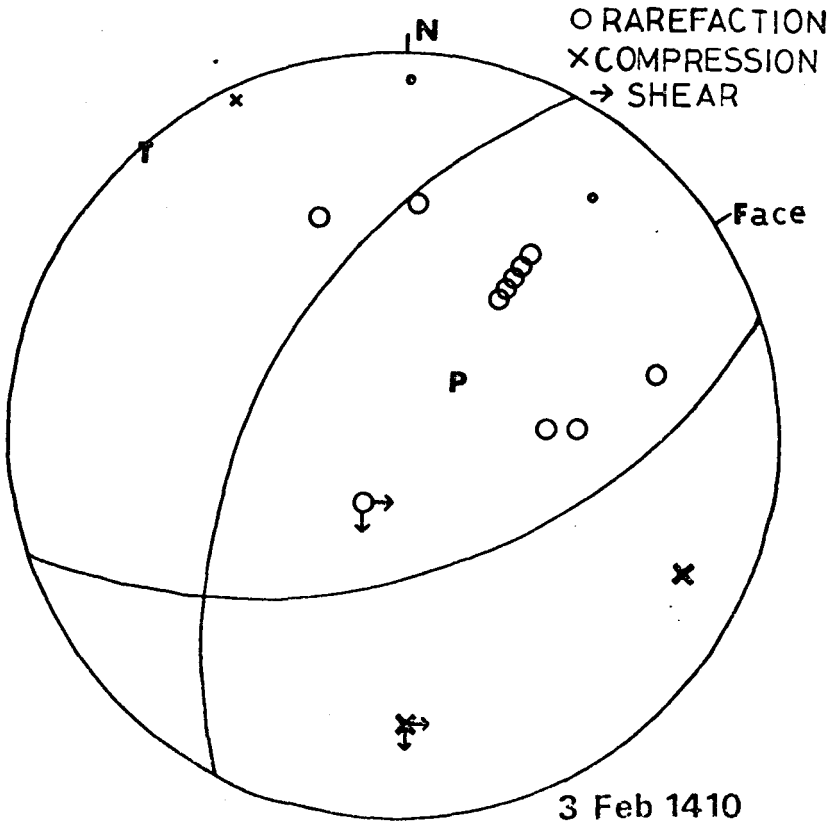

1.

Figure 2. Fault-plane solutions of events 1 and 2 on 3 February and 8 February, 1972.

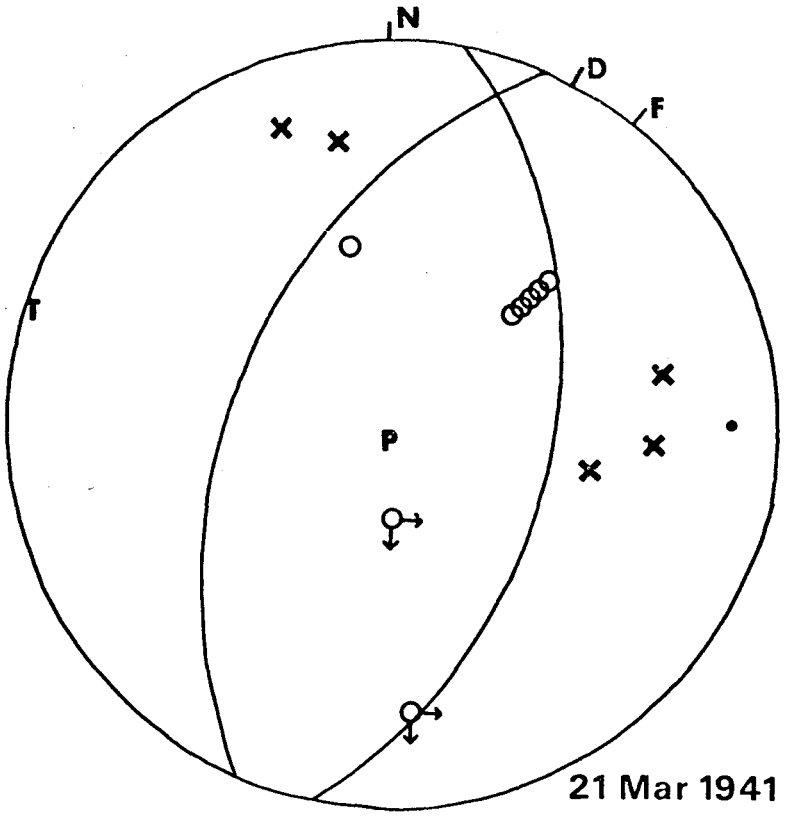

4.

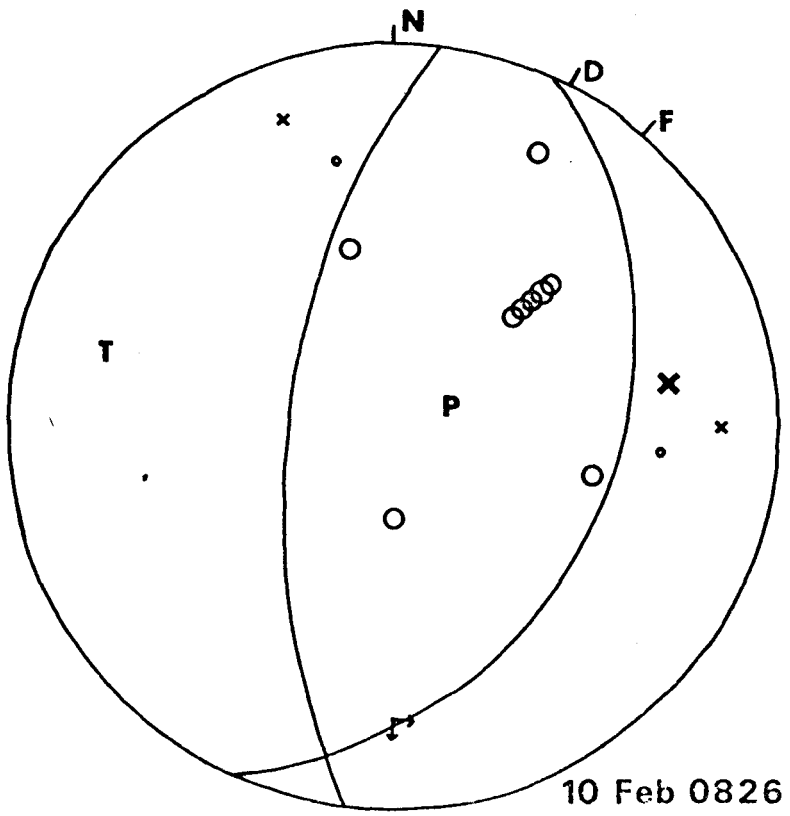

3.

Figure 3. Fault-plane solutions of events 3 and 4 on 10 February and 21 March, 1972, D marks the strike of the nearby dyke. Other symbols are the same as in Figure 2.

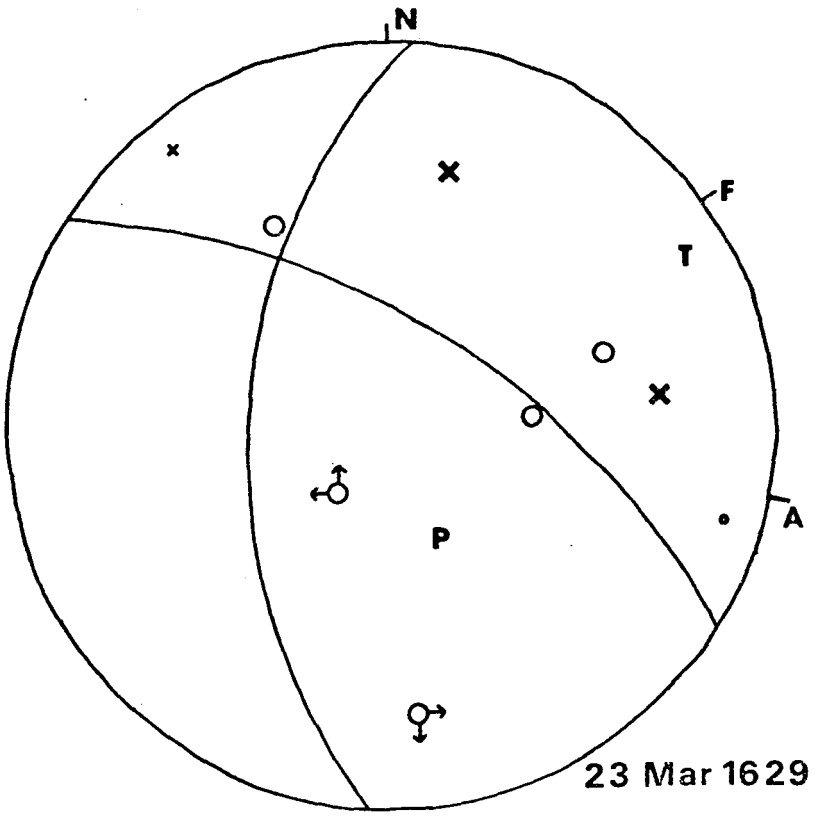

Figure 4. Fault-plane solution of event 5 on 23 March, 1972. A marks the strike of the 74 E H South abutment. Other symbols are the same as in Figure 2.

INTERPRETATION.

Fault-plane solutions of shallow crustal earthquakes are correlated with active tectonic faults when the hypocentre falls on a known fault or the earthquake causes a significant surface break. One of the orthogonal planes defined by the fault-plane solution is always found to be parallel to the fault plane and the normal to the other plane, the auxiliary plane, is the slip vector. The distribution of aftershocks can also be used to determine which of the two nodal planes was actually the fault plane (e.g. McGarr and Green, 1972).

In the absence of an observable fault, or sufficient aftershock data, it will not, in general, be clear which plane represents the fault plane and failure in a volume of rock, rather than shear failure on a specific plane, is a more generalised way to interpret the seismic source. The P axis is the direction of maximum reduction in compression stress in the volume of failure and the T axis represents the direction of maximum increase in stress. Shear failure of rock samples in the laboratory under conditions of triaxial compression normally takes place at an angle of about 30° to the maximum compressive stress or 15° to the direction of greatest shear stress (e.g. chapter 3). The P and T axes are therefore not necessarily parallel to the maximum and minimum stress axes before failure occurred.

DISCUSSION

The events on 3 and 8 February (figure 1 and 2) both have fault-plane solutions consistent with failure on fault planes parallel to the advancing 75 - 77 East Hercules longwall. Both nodal planes in each case are nearly parallel to the advancing longwall. The planes marked A are the preferred direction of failure. They are consistent with Type 2 failure in th hanging-wall McGarr (1971 b). Although neither of the P-wave nodal planes of the event on 23 March at 1629 strikes parallel to the closest advancing face, 74 East Hercules, one nodal plane is semi-parallel to the nearby South abutment of the 74 East Hercules face. As burst zones have been observed to strike parallel to abutments at E.R.P.M. it is quite possible that the 23 March event was associated with failure adjacent to this abutment.

The nodal planes of the events on 10 February and 21 March all strike nearly parallel to the nearest advancing face, 73 East G. However, they strike more nearly parallel to the dyke between G and H. As this dyke had a history of bursts associated with it, it is possible that these two events occurred in this dyke in response to increasing stress due to the advancing East G faces.

The P axes of all five fault-plane solutions presented here are within 20° of the vertical, in agreement with the results of Spottiswoode et al (1971). The maximum principal stress of the ambient state of stress in the Witwatersrand system is also approximately vertical and approximately equal to the pressure due to the weight of the overburden (Gay, 1975). E.R.P.M. seismic events have the effect of releasing the maximum principal stress locally. Because the average overburden pressure due to gravity over a large area must remain the same, this stress release also has the effect of increasing the vertical stress elsewhere. Theoretical calculations of stress condition near advancing faces show that the maximum principle stress is close to the vertical and peaks quite sharply just ahead of the face position (e.g. McGarr, 1971 a).

This peak can therefore be reduced and smoothed out through stress release accompanying seismic events.

About 70 percent of all the P-wave arrivals from the five events considered here were dilational (Table 1), a finding consistent with previous studies by Joughin (1966) at the Harmony gold mine and Hallbauer (1967) at the Western Deep Levels mine. They both found that 70 to 80 percent of the first motions they observed were dilational. High proportions of dilations are consistent with source mechanics involving normal faulting in all three cases; the geophone layout was similar in the three cases. Firstly, more than half of the geophones were within 60° of the vertical of the focal sphere, that is in the upper quarter of the focal sphere and generally within a dilational quadrant of the fault-plane solution of a normal fault. Secondly, first-motion arrivals which would plot within 10° of the horizontal on the focal sphere were excluded from the first motion plots because these geophones were vertical component instruments. For the case of normal faulting, these instruments would register more compressional than dilational first motions. The two effects combined to give a greater proportion of dilational arrivals for these three studies than the average of 50 percent expected for random sampling of double-couple sources.

Inconsistent arrivals as observed for events 1 and 5 can be attributed to a number of effects. Velocity variations at the source can lead to inconsistent data. McNally and McEvilly (1977) found that a group of fault-plane solutions of earthquakes on the San Andreas fault indicated velocity contrasts of 15 percent in the source region. The location error of E.R.P.M. events of up to 30 m in elevation and up to 20 m in plan (McGarr et al, 1975) could cause errors in the direction of the ray paths of up to 4° for typical hypocentral distances of 500 m or more.

The frequency response of instrumentation used for location purposes is generally chosen to extend up to the highest frequencies which can be conveniently transferred to hard copy records because the ultimate limit to location accuracy is the time resolution on the seismograms. For the underground array in E.R.P.M. during 1972, the highest frequency observed was about 200 Hz. The corresponding linear dimension of the source which this data sampled was therefore approximately β/200 Hz = 20 m, where β is the shear-wave velocity. This is considerably smaller than the linear dimension of about 200 m which is associated with the source of a tremor with magnitudes of about 2 (chapter 4). Long-period instrumentation gives a more reliable measure of the total failure process (Sykes, 1967) and the PRE first motions, with predominant frequencies less than 5 Hz, were therefore given more emphasis relative to first motions from the underground array when they were incompatible.

Diering (1978) performed a moment-tensor inversion for two E.R.P.M. seismic events, calculating all six components of the moment tensor from records obtained from the underground array of seismometers during 1977. He found that they were in good agreement with sources consistent with normal faulting : the component of volumetric strain changes was small and the P, B and T axes had amplitudes and orientations appropriate for normal faulting. While this method requires sophisticated and detailed analysis of the seismograms, it is particularly applicable to mine tremors because uncomplicated waveforms of both P and S waves can be observed at many different directions from the source. Uncomplicated waveforms imply that structural details along the ray paths do not obscure the record of the failure history of the fracture.

CHAPTER 4.

SOURCE PARAMETERS.

ABSTRACT

Spectra of ground displacement of P and S waves were measured for 24 tremors using records from a seismograph station on the surface of the East Rand Proprietary Mines near Johannesburg, South Africa. The tremors occurred in close proximity to mining at depths of the order of 3,2 km below the station and had magnitudes ranging from about 0 to 3. Ground displacement due to P and S waves is, to a first approximation, a unidirectional pulse of the order of 0,1 to 0,2 sec in width, although considerable complexity is often present in the wave forms. The corresponding spectra of displacement amplitude appear to be flat at low frequencies and generally diminish according to f^{-3} at high frequencies, where f is frequency. Analysis of the spectra using the model of Brune for S waves and its extension for P waves by Trifunac suggests source dimensions ranging from about 50 to 500 m and stress drops ranging from about 5 to 50 bars. Moments estimated from the low-frequency limits of the spectra vary from 10^{18} to 10^{21} dyne-cm. Seismic energies calculated from the records of ground velocity are in good agreement with log E = 11,8 + 1,5 M originally developed by Gutenberg and Richter for surface-wave magnitudes.

The mine tremors appear to be highly similar to natural crustal earthquakes with regard to stress drops, the relationship between moment and magnitude, and the relationship between size and magnitude. Underground observations of damage caused by the larger tremors indicate that the actual rupture process is highly complex, consisting of many discrete failures; these observations cannot be fitted by a simple dislocation model.

INTRODUCTION

Studies of body-wave spectra from natural earthquakes have been used to estimate source parameters such as seismic moment, mean displacement, extent of faulting and mean stress drop associated with rupture (e.g. Wyss and Brune, 1968; Hanks and Wyss, 1972; Berckhemer and Jacob, 1968)

This chapter reports the results of an experimental study of the source parameters of 24 tremors associated with the East Rand Proprietary Mines (ERPM) in Boksburg, Transvaal, South Africa, during 1972. Tremors at ERPM have been the subject of a number of studies including those of Cook (1963) and McGarr (1971). Cook first established the very close relationship between tremor occurrence and mining. McGarr discussed some of the physics underlying the generation of seismic events in Witwatersrand gold mines and presented evidence that they are the results of shear failure across normal faults.

Measurements of ground velocity for these events were made using a seismograph station located on the surface of the mine about 1 km south and 3 km above the hypocentral regions as seen in Figure 5. (Hypocenters of the events were located to within about 35 m of uncertainty using an underground array of 10 geophones distributed about the source region (McGarr et al., 1975). The events were all located in close proximity to active mine faces and so were almost certainly triggered by mining.

Spectra of displacement amplitude for earthquakes, as measured in the far-field, are found to attain a constant value at low frequencies (e.g. Berckhemer and Jacob, 1968; Wyss and Brune, 1968). The low-frequency limit is proportional to M_o, the seismic moment (Keilis-Borok, 1960; Aki, 1966). At high frequencies, the spectra diminish generally as $f^{-\gamma}$, where γ is typically observed to be about 2 (e.g. Wyss and Hanks, 1972). The corner frequency is defined by the intersection of the high- and low-frequency asymptotes. Corner frequencies have been related to earthquake source dimensions in a number of ways (e.g. Savage, 1972; Brune, 1970, 1971) but in all cases the corner frequency is inversely proportional to the source dimension. Although the source model of Brune (1970) is appropriate for shear-wave spectra only, it has since been extended by Hanks and Wyss (1972) and Trifunac (1972) to compressional-wave spectra.

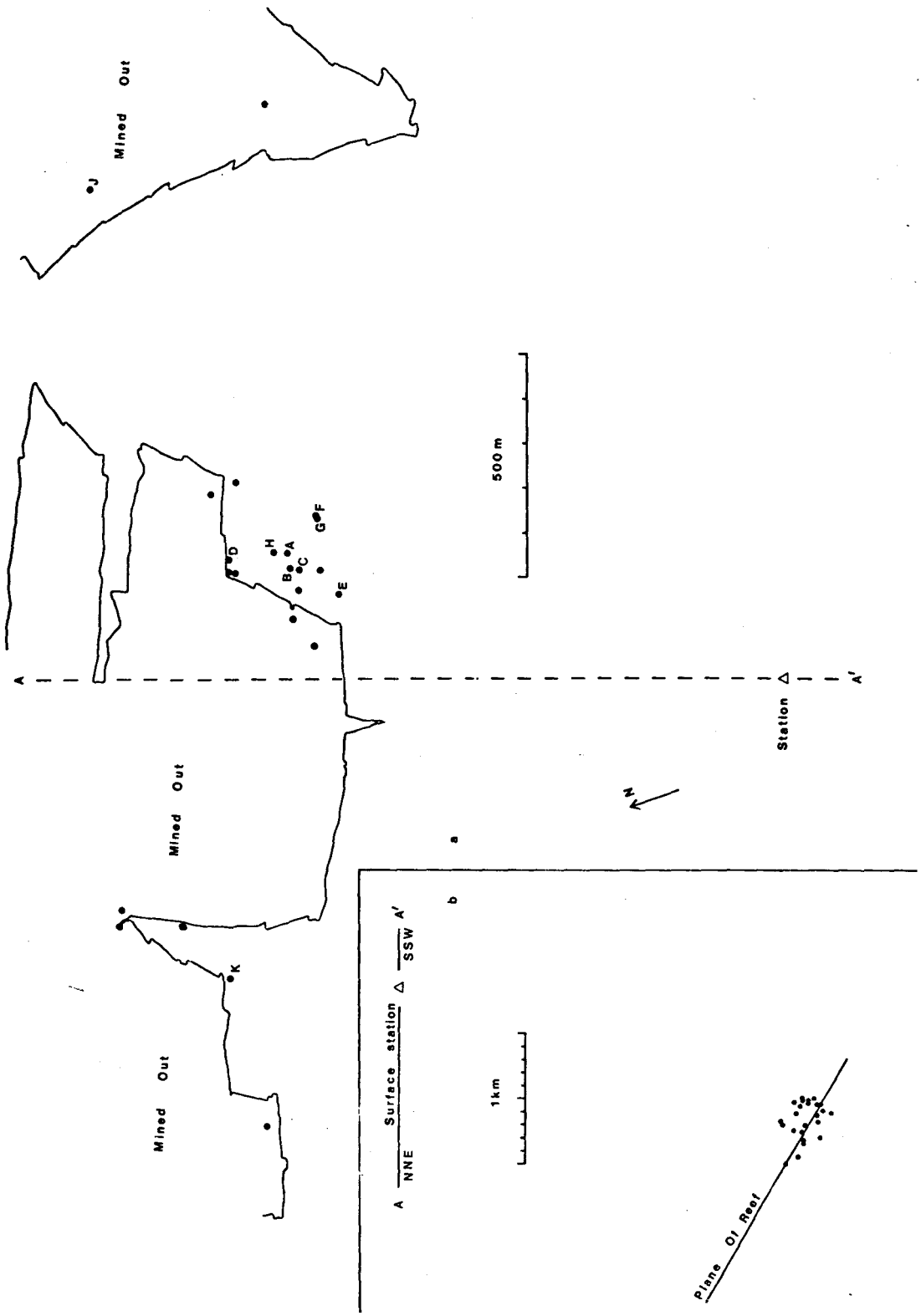

Figure 5. (a) Plan view of part of ERPM showing face on November, 1972, event location and seismograph station. 10 events are labelled. A for November 2, 1150A, B for November 2, 1150B,C for August 22, 1021,D for February 4, 2250,E for November 21, 0005,F for November 21, 0020A, G for November 21, 0020B, H for November 2, 2007,J for February 8, 1855, and K for February 4, 1537. (South African Standard Time is used throughout). (b) Section across strike, projected onto A - A'.

INSTRUMENTATION

The instrumentation used in the seismograph station that provided the basic data of this study has been described by Green (1973). Signals from Electrotech EV 17 and EV 17H seismometers, critically damped, were recorded at two levels of gain in the AM mode on 13-mm magnetic tape running at about 2 mm/sec. The horizontal seismometers were oriented N-S and E-W. Two additional channels were used for timing: a crystal clock produced a time code on one channel and radio time from station WWV was recorded on the other.

Seismic events were replayed from the tapes onto hardcopy records using a loudspeaker for detection of events. Events of particular interest were prepared for computer analysis by generating a digital tape from the analog tape. The carrier frequency of the clock signal was used to maintain a constant digitization rate of 320 samples per second. The relative response of the entire system to ground velocity is shown in Figure 6; peak response to velocity was at about 20 Hz. The experimental calibration values were found to fit very closely an analytic function of the form.

$$Y \sin(2\pi f) = \frac{BfX \sin(2\pi f + \delta)}{(f^2 + f_L 2)^{\frac{1}{2}} (f^2 + f_H 2)^{\frac{1}{2}}} \qquad (4.1)$$

Where
- Y is output amplitude
- X is ground velocity
- f is frequency
- B is constant of channel and gain setting
- $\delta(\omega)$ is the phase lead
- f_L and f_H have values of 8 and 50 Hz, respectively.

Equation (4.1) was used to derive true ground velocity from the digitized records.

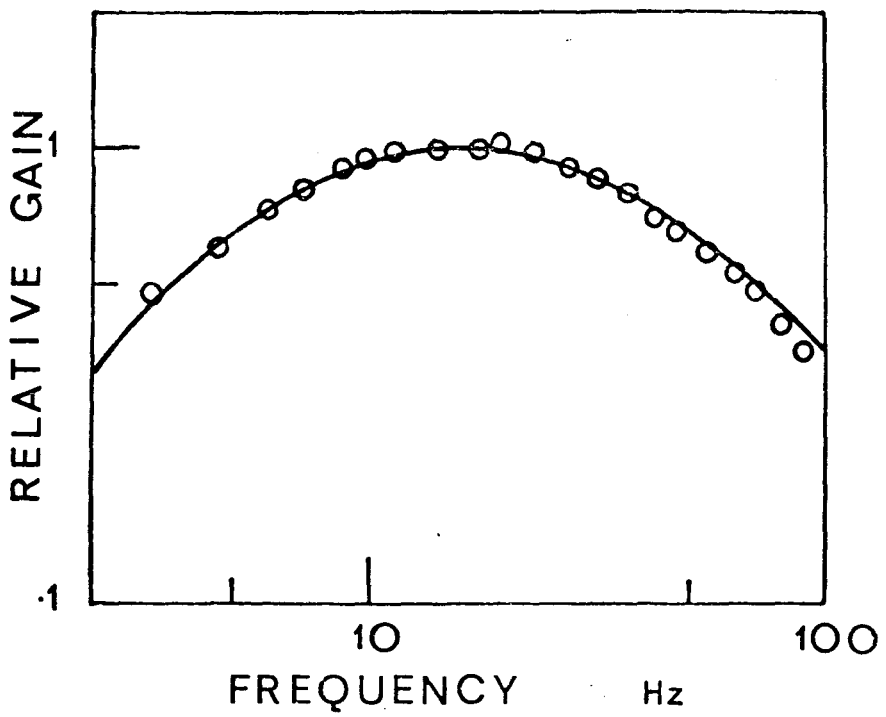

Figure 6. Velocity response of seismograph system. (Vertical scale is arbitrary.) Equation (1) is a fit to observed values.

The underground seismic array used to locate the seismic events of this study was similar to that described by Cook (1963). It consisted of 10 geophones distributed throughout a region about $2\frac{1}{2}$ km in extent and ranged in depth from about 1,9 to 3,4 km below surface. The underground array has been described in more detail by McGarr et al (1975).

MAGNITUDE DETERMINATIONS

The most suitable records for magnitude determinations of tremors at E.R.P.M. were written at the World-Wide Standardised Seismograph station at Pretoria (PRE) 50 Km. north of E.R.P.M.

The seismic waves of largest amplitude from tremors at ERPM as written on the short-period seismograms at PRE are S-waves or more usually Rayleigh waves and have an apparent frequency of about 1 Hz. Magnitudes were calculated from seismograms written at PRE using $M^{PRE} = \text{Log } (A_{PR}\ G_{WA}/G_{PR}) - \log A_o$; where A_{PR} is the maximum amplitude at PRE, in millimeters, $G_{WA} = 2800$ and $G_{PRE} = 50{,}000$

are the maximum gains at the Wood-Anderson and Pretoria short-period seismographs, respectively, and $- \log A_o = 2,6$ for a distance of 50 km (Richter, 1958, p. 342).

As a check on this procedure, I converted two PRE seismograms into Wood-Anderson seismograms by digitizing the signals at a rate of 10 samples per second, correcting for the amplitude and phase in the frequency domain for the PRE and Wood-Anderson responses, and finally calculating synthetic Wood-Anderson seismograms. Local magnitudes, M_L calculated from the synthetic seismograms were 0,2 lower than M^{PRE}. Although displacements at frequencies above 5 Hz are not very noticeable on the Pretoria records, they were filtered out by the crude digitization process and so the calculated M_L is probably slightly too low.

Magnitudes were also calculated for events recorded at the local station using a method devised by Eaton et al. (1970 p. 1162) for a field seismograph system similar to that used for this study. Although the response of the system (Figure 2) was slightly different from that of Eaton et al. (1970) and their distance dependence was uncertain for hypocentral distances less than 30 km, the local station magnitudes, $M^{S.D.}$, generally differed from M^{PRE} by less than 0,5.

TRANSMISSION OF SEISMIC WAVES

To reduce the analysis of body waves to that for a source in an infinite, homogeneous, isotropic and lossless medium, it was necessary to account for the velocity structure, attenuation and scattering along the ray path and for the effect of the free surface. ERPM hanging-wall quartzites which the ray path traversed are massive in appearance, with very low porosity, and vary little in their elastic properties (McGarr et al. 1975).

Between the hypocenters and the seismograph station, the rock is predominantly quartzites of the Witwatersrand system overlain by

a thin (~300 m) layer of Ventersdorp lava. As seen in Figure 5 the ray paths from the hypocenters to the station was nearly perpendicular to the reef, and therefore to the strata. Effects of refraction and shear wave birefringence were therefore, unimportant, so straight ray paths were assumed.

I tested the effects of attenuation by using the underground array; it was found that the duration of the first half-cycle did not depend on hypocentral distance over a range of 4 km. A causal operator (Carpenter, 1966) was applied to various signals that resembled the first cycle of the seismograms. A Q of 200 increased the duration of the first half-cycle by 50 per cent over 3 km, an effect that would have been noticed on the seismograms, indicating that Q has a minimum value of 200. It will be seen that a value as low as 200 would be unimportant in this study.

The horizontal and vertical components of the P phase at the surface station were very similar, especially for the first 0.15 sec, indicating that P waves were not scattered significantly within about 1 km of the station.

In summary, it appears that changes in the body-wave signals introduced during transmission can be safely neglected.

The effect of the free surface was removed by using coefficients presented by Gutenberg (1944) for a Poisson's ratio of 0.25. SH motion is doubled at the free surface. At the typical angle of incidence of 24°, the vertical component of ground motion of P waves and the horizontal component of SV waves were enhanced by a factor of 1,8; in the range of 20° to 30° this factor is insensitive to small changes in either the angle of incidence or Poisson's ratio.

GROUND DISPLACEMENT

Ground displacement was derived from seismograms by correcting for instrument response and the effect of the free surface. Seismograms that provided the basic data for five of the events of this study are

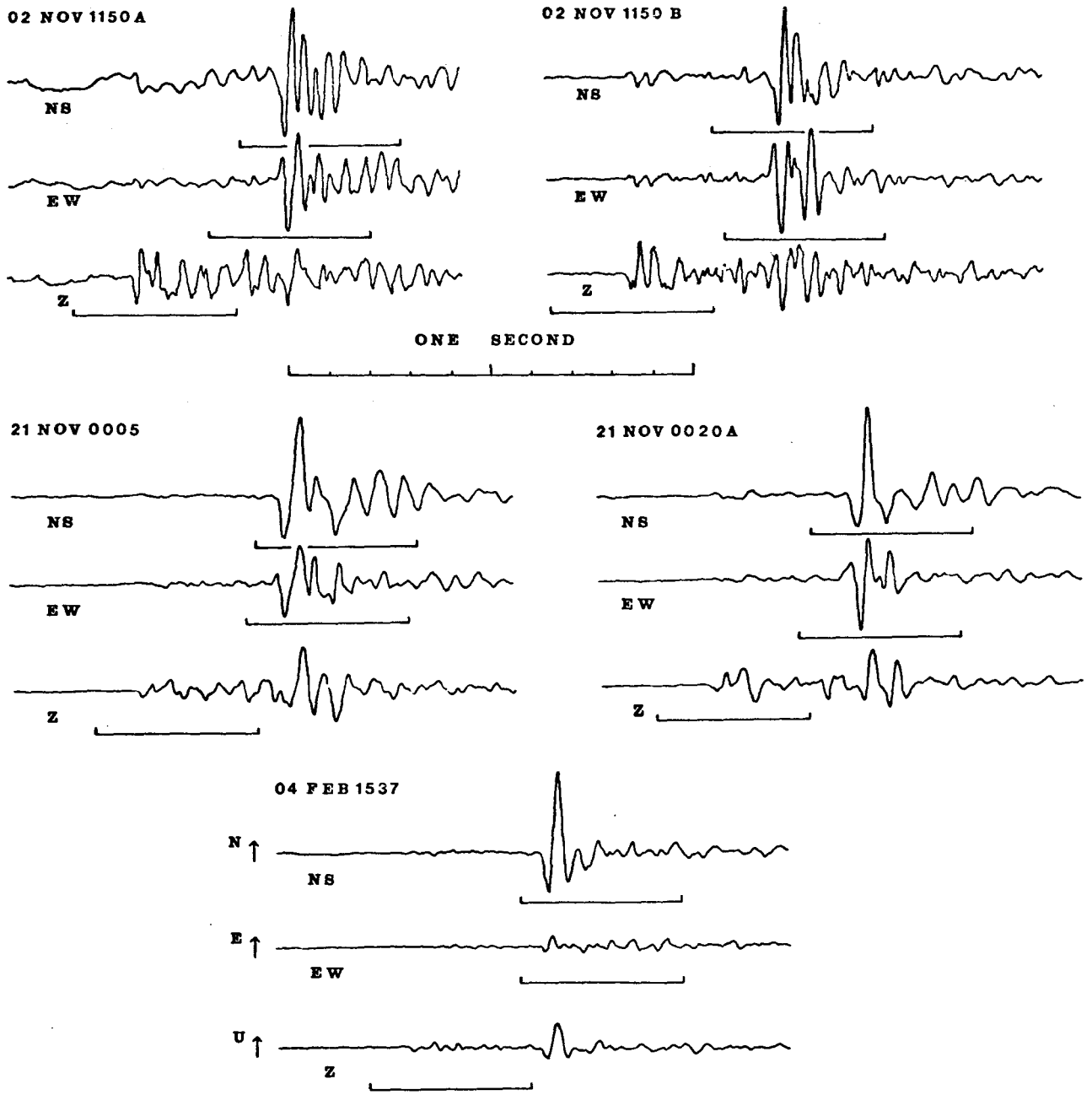

Figure 7. Vertical and two horizontal seismograms of five of the events. The time scale of the two events on November 2, at 1150 is continuous, with the relative gain of A ten times that of B. Time windows used for calculating P (Z), S (NS) and S (EW) spectra and displacements are indicated.

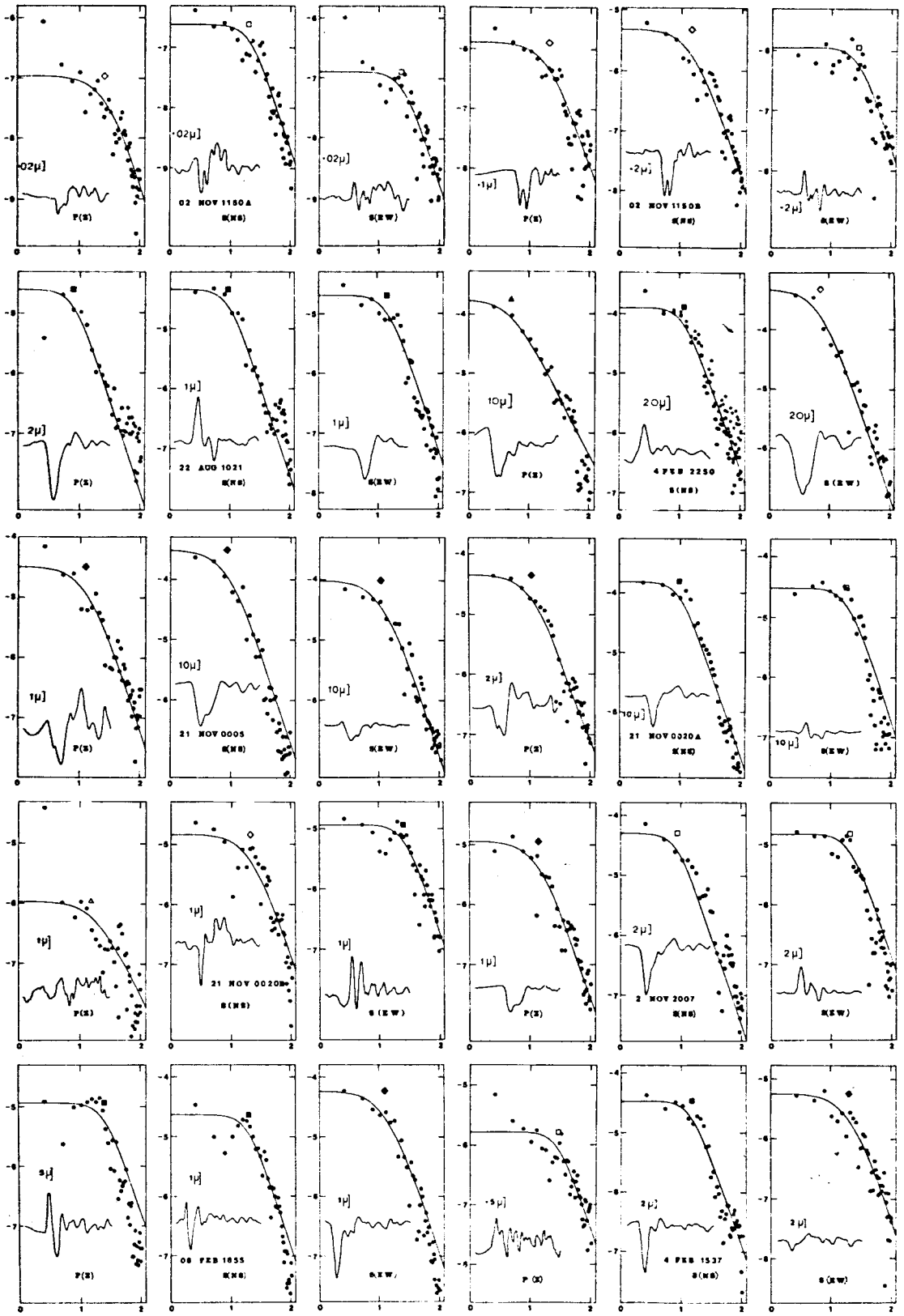

Figure 8. Spectra and displacement for 10 events. The horizontal axis is log-frequency (Hz) and the vertical axis is log displacement spectral density (cm-sec). Our interpretation according to equation 3 is shown. △ is used for (3a) at ($f_0 \Omega$ (0)), □ for (3b) and ◇ for (3c). Hollow symbols are used when the theoretical fit is poor. The effect of $Q = 200$ is shown for the S (NS) spectral component of the event on February 4, at 2250.

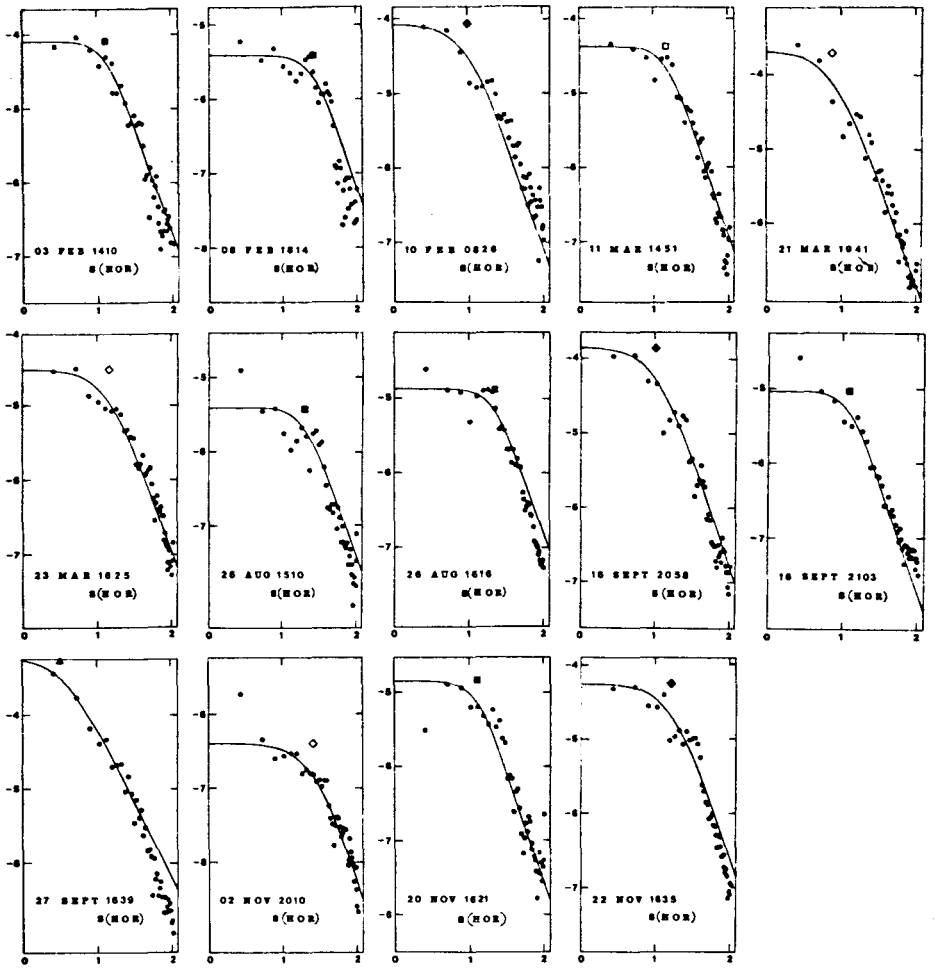

Figure 9. Shear wave spectra of the 14 events not specifically discussed in the text. Symbols are explained in Figure 8.

shown in Figure 7; time windows used for analysis of ground displacement are indicated beneath each trace. P waves were analyzed using records of the vertical component of ground motion and the horizontal components provided the data for analysis of shear waves.

Although the vertical component of the P wave is a well-defined phase for most events, it is occasionally somewhat diffuse. For example, the foreshock of the event on November 2nd at 1150 has a P wave that continues into the S wave; phases such as this are not amenable to the analysis of this chapter.

Figure 8 shows earth displacement and corresponding spectra for three components of ground motion of 10 seismic events. The seismograms of displacement were analyzed using time windows with a duration of 0,4 sec. Longer windows were found to be unnecessary as nearly all of the displacement of a particular phase occurs well within 0,4 sec. From the viewpoint of defining spectra at low frequency there was no point to longer time windows because the instrument response to displacement is low even at 2,5 Hz, the fundamental frequency of the windows used here. For cases where the spectral displacement at 2,5 Hz was markedly different from that at 5 Hz, the spectrum was arbitrarily assumed to be flat below 5 Hz for purposes of computing the displacement (e.g. the P phase for the event on August 22nd at 1021).

The event of February 4th at 2250 was the largest of the tremors studied here with a magnitude of about 3. The P wave was largely an impulse with a width of about 0,13 sec and in the downward direction (Figure 8). The two components of the shear wave were also unidirectional impulses although the pulse on the N-S component has a much narrower width. The spectra for this event appeared to flatten at the low frequencies but the time window was too short for a low-frequency plateau to be well-defined. At high frequencies the spectra for this event showed a power-law decay, f^{-3} for the shear waves and f^{-2} for P.

The spectrum of the N-S component of S was also computed for the case of Q = 200; the corrected values are shown by stars in the figure. We see the effect of a Q as low as 200 as not being likely to be important.

The event of November 21st at 0005 had a magnitude of 2,5 and occurred near the event of February 4th at 2250 (Figure 5). The S-wave components were unidirectional impulses (Figure 8) but the P wave appeared to have been very complex; the spectrum of P showed considerable structure at low frequencies. For S, a low-frequency plateau was defined. The event of November 21st at 0020A was probably an aftershock of that at 0005. This event had a magnitude of 2,0 and occurred about 140 m from the main shock (Figure 5). Both body phases were reasonably well represented as unidirectional pulses.

The event of November 21st 0020B occurred 7 sec. after that of 0020A and was much smaller, with a magnitude of 0,8. The signal-to-noise ratio for P was very poor, mostly because of the coda of the previous event and so the displacement signal and spectra are of poor quality. The S/N ratio for S was somewhat better and we see that the displacement consisted of narrow pulses about 0,05 sec in width with corresponding high-frequency energy in the spectra.

The tremors on November 2nd at 1150 occurred within 1 sec of each other (Figure 7); the event 1150A occurred first and was much smaller. Magnitudes for the two events were -0,2 and + 0,9 for 1150A and 1150B respectively; they were located within 50 m of each other (Figure 5). The wave forms for this pair of events were remarkably similar although the codas of the phases of 1150A are somewhat larger compared to the initial pulses than for 1150B.

Later, on November 2nd, an event of magnitude 2 occurred at 2007, locating about 40 m from the event at 1150B. The displacement signals were all unidirectional pulses, to a good approximation and the spectra

showed very little complexity.

The event of August 22nd at 1021 was located about 55 m southwest of the event of November 22nd 1150B and had a magnitude of 1,8 (Figure 5). The body-wave displacements were largely unidirectional and the low-frequency asymptote of the S-wave spectra was quite well-defined.

The event of February 8th at 1855 occurred near some mining to the east of the events previously discussed (Figure 5); its magnitude was 1.6. The P wave and the N-S component of S were complex, each trace showing considerable displacement in both directions; the E-W component pf S was considerably simpler.

Finally, the event of February 4th 1537 occurred well to the west of the other events (Figure 5) and had a magnitude of 1,5. Although both components of S could be well represented as unidirectional pulses, the coda of P was comparable in amplitude to the initial pulse of the phase. The fault-plane solution for this event (unpublished data) indicated that one of the P-wave nodal planes nearly passed through the seismograph station.

In general, the seismograms of earth displacement of Figure 8 showed a considerable variation in wave form even for events occurring within a region 100 m in extent. Many of the signals consisted of one or two unidirectional pulses and others show more complexity.

SEISMIC ENERGY

Perret (1972) has shown that for equidirectional radiation and for $r \gg c/\omega$ (where r is hypocentral distance, c is seismic wave velocity and ω is angular frequency), the seismic energy radiated by the source in the form of P or S waves is

$$E_c = 4\pi \rho c r^2 \int v_c^2 \, dt \qquad (4.2)$$

where $c = \alpha$ or β, the compressional or shear velocity, respectively,

TABLE 1.

Seismic Energies and Magnitudes.

Event	M^{PRE}	$M^{S.D.}$	Energy ($X10^{12}$ ergs)			Ep/Es
			P(Z)	S (NS)	S(EW)	
3 Feb. 1410	2,0	1,7	40	470	70	0,07
4 Feb. 1537	1,55	1,5	3,6	800	22	0,004
4 Feb. 2250	2,9	2,1	420	1000	1700	0,15
8 Feb. 1814	1,1	1,2	0,9	3,6	7,6	0,08
8 Feb. 1855	-	1,6	22	36	38	0,30
10 Feb. 0826	2,3	1,7	72	130	56	0,38
11 Mar. 1451	-	1,7	12	210	11	0,05
21 Mar. 1951	2,9	2,2	180	470	72	0,33
23 Mar. 1625	(1,9)	1,9	60	38	22	1,00
22 Aug. 1021	-	1,8	17	74	38	0,15
26 Aug. 1510	-	1,2	3,8	2,2	1,3	1,07
26 Aug. 1616	-	1,8	4,4	67	13	0,06
16 Sep. 2058	2,8	2,2	320	270	110	0,84
16 Sep. 2103	-	2,0	2,0	4,0	1,3	0,38
27 Sep. 1639	2,8	2,3	75	190	640	0,12
2 Nov. 1150A	-	-0,2	0,008	0,02	0,01	0,27
2 Nov. 1150B	-	0,9	0,55	1,5	1,2	0,21
2 Nov. 2007	1,9	2,0	11	8,4	6,1	0,76
2 Nov. 2010	-	0,2	0,007	0,04	0,02	0,13
20 Nov. 1621	-	1,5	3,6	17	5	0,16
21 Nov. 0005	2,5	2,4	72	1200	310	0,05
21 Nov. 0020A	2,0	2,3	130	1000	380	0,09
21 Nov. 0020B	-	0,8	0,54	0,67	0,87	0,35
22 Nov. 1635	(2,2)	1,9	180	150	150	0,62

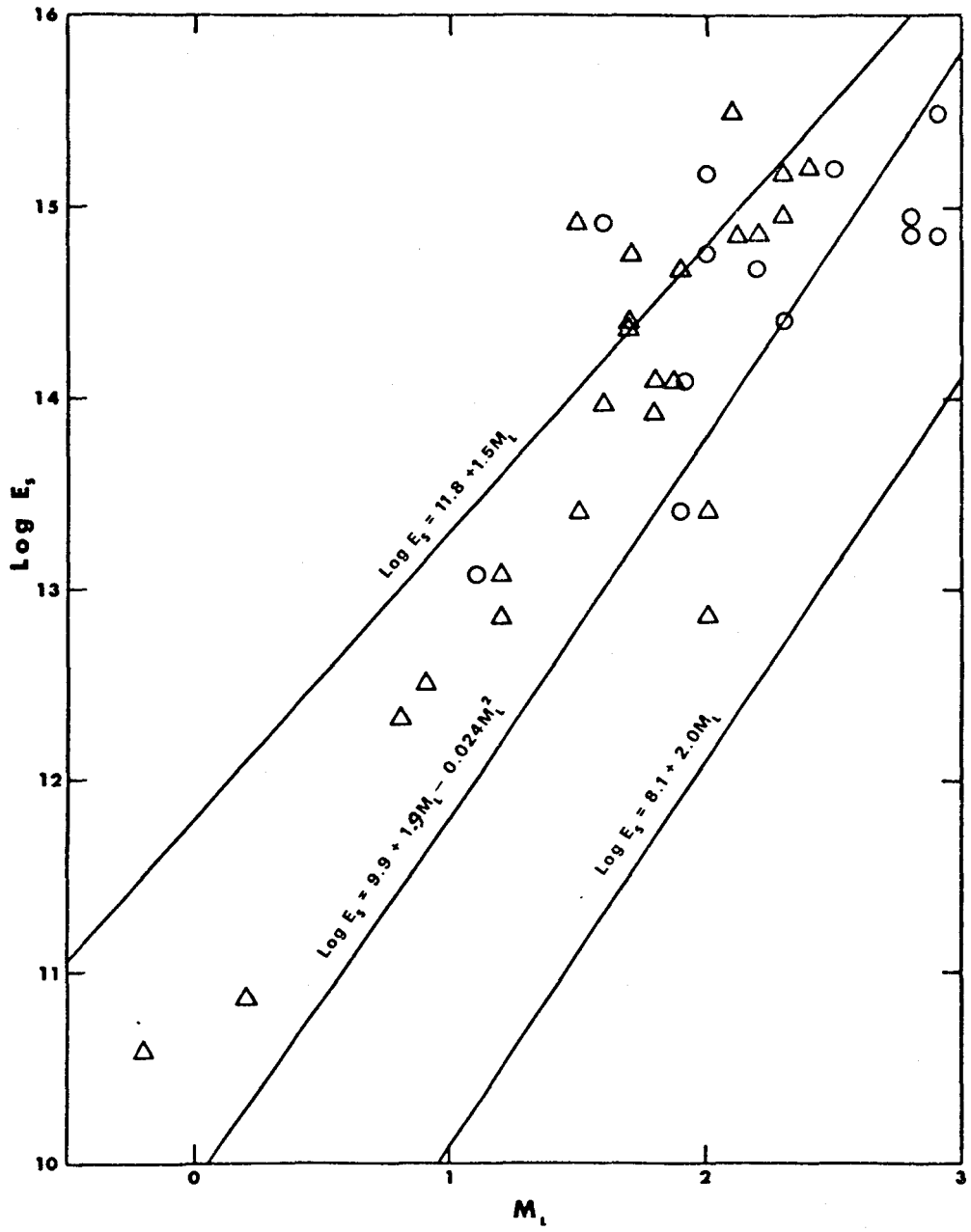

Figure 10. Total seismic energy as a function of magnitude. Triangles are used for M from PRE, and magnitude deduced from seismograms recorded by the local station are indicated by circles.

depending on the phase; ρ is the density and v_c is the ground velocity of the P or S wave; the integration is performed over a time window 0,4 sec. long around the phase. In this study, the largest value of c/ω occurs for c = 6 km/sec and $\omega = 2\pi f = 15{,}7$ sec^{-1} or $c/\omega = 0{,}38$ km r, for all events reported here, is greater than 3 km. so the condition $r \gg c/\omega$ is satisfied.

The condition that the radiation be equidirectional is not satisfied. In principle, it is possible to account for the effect of the radiation pattern. In practice, however, this has been found to be an intractable procedure so in this chapter it is assumed that the seismograph station was in a region of average radiation for both phases.

Energies for P and S waves computed using (4.2) are presented in Table 1 along with magnitude information for the 24 events studied in this Chapter. Times are South African Standard Time. Two magnitudes determined from the Pretoria records were uncertain and are given in parentheses. In Figure 10, the total seismic energy for each event is shown as a function of magnitude. The relationship of Gutenberg and Richter (1956), log E = 11,8 + 1,5 M derived for surface-wave magnitudes of large shallow earthquakes, provides a reasonably good fit to the data of Figure 10. Log E = 9,9 + 1,9 M - 0,024 M^2 (Richter, 1958, p.366) fits the data somewhat less well, while the data are not consistent with Log E = 8,1 + 2,0 M from Thatcher and Hanks (1973).

The last column of Table 1 gives the ratio of P - to S-wave energy for each event. The median value of Ep/Es as in Table 1 is 0,18.

ANALYSIS OF SPECTRA

For purposes of interpretation, each spectrum of this study was trial-fitted by one of the three following functions

$$\Omega^{A}(f) = \frac{\Omega^{A}(0)}{1 + (f/f_o^{A})^2} \qquad \text{(A)}$$

$$\Omega^{B}(f) = \frac{\Omega^{B}(0)}{1 + (f/f_o^{B})^3} \qquad \text{(B)} \qquad (4.3)$$

$$\Omega^{C}(f) = \frac{\Omega^{C}(0)}{(1 + (f/f_o^{C})^2)^{3/2}} \qquad \text{(C)}$$

where $\Omega(f)$ is the spectrum of ground displacement.

Most models of the seismic source predict spectra similar in shape to (A) or (C) with the shape of (A) being somewhat more common (e.g. Brune, 1970; Aki, 1967; Berckhemer and Jacob, 1968). Radiated displacement having the time dependence $te^{-t/\tau}$ yields an amplitude spectrum of shape (A) where τ is a time constant; a time dependence of $t^2e^{-t/\tau}$ corresponds to (C) (Savage, 1972). The spectrum (B) does not correspond to any existing models of the seismic source but has been used here because it fits many of the spectra of this study more closely than either (A) or (C); the function $t^2/(1 + t^4)$ corresponds to a spectrum similar to (B). All of these functions of time are understood to be 0 for $t < 0$.

Two criteria were used to fit one of the functions (4.3) to a particular spectrum. The function was required to provide a good fit to the experimental points and the seismic energy deduced from the analytical function had to be in agreement with that calculated using equation (4.2). Each spectral shape of equation (4.3) defines $\Omega(0)$, the low-frequency asymptote, and f_o, the corner frequency. $\Omega(0)$ for a number of spectra in this study are poorly defined because of an inadequate instrument response at frequencies less than 5 Hz.

Values of $\Omega(0)$ and f_o for these spectra should accordingly be considered as minimum and maximum estimates, respectively.

Hanks and Wyss (1972) have shown that (4.2) is equivalent to

$$E_c = 2\, r^2 c K \Omega^2(0) f_o^3 \qquad (4.4)$$

where K depends on the high-frequency asymptote only; thus, energy calculated from (4.4) was required to be in agreement with that calculated from (4.2) in fitting one of the functions of equation (4.3) to the data.

As can be seen in Figures 8 and 9 the fits of (4.3) to the data are entirely adequate. It is of interest to note that none of the experimental spectra suggests an intermediate region between the low- and high-frequency regions for which the spectrum decays according to f^{-1}; according to Brune (1970) such an intermediate region would be indicative of a fractional stress drop.

Shear-wave spectra of ground displacement were calculated from spectra of the two horizontal components of S using $\Omega^2_{HOR}(f) = \Omega^2_{NS}(f) + \Omega^2_{EW}(f)$. These spectra are shown in Figure 9 for the 14 events not shown in Figure 4. Equations (3) were generally found to fit the S_{HOR} spectra better than the spectra of the two S components taken separately, even when the corner frequencies were not the same.

Table 2 summarizes the analysis of the spectra. We see that most of the spectra were best fitted with functions having a high-frequency asymptote proportional to f^{-3}. According to Savage (1972) this argues for a far-field displacement that initially increases quadratically with time.

For phases with corner frequencies of about 10Hz or less the low-frequency asymptote is poorly defined and so in these cases a region of intermediate decay might not be obvious. $\Omega(0)$ is well established for phases with higher corner frequencies, however, and for these cases it is clear that there are no regions of fall-off parallel to f^{-1} in the

spectra (Figures 8 and 14).

INTERPRETATION

Spectral plateaus and corner frequencies for the tremors of this study are listed in Table 2. These quantities have then been used to deduce seismic moment, source dimension, and stress drop for each event using the model of Brune (1970 and 1971). Brune's model was chosen, primarily, because it has received considerable attention in the recent literature on earthquake source parameters and has become, to some extent, a standard for comparison (e.g. Hanks and Wyss, 1972; Trifunac, 1972 a,b).

The seismic moment, M_o, is related to the low-frequency limit of the spectrum of ground displacement by

$$M_o = \frac{\Omega(0)}{R^c(\theta,\phi,r)} \qquad (4.5)$$

where $R^{\alpha}(\theta,\phi,r) = f(\theta,\phi)/(4\pi\alpha^3\rho r)$ for P waves and $R(\theta,\phi,r) = g(\theta,\phi)/(4\pi\beta^3\rho r)$ for S waves. The functions $f(\theta,\phi)$ and $g(\theta,\phi)$ were given by Haskell (1964) for two types of shear faulting.

To relate $\Omega(0)$ to M_o, it is necessary to correct for the effect of the radiation pattern. Although fault-plane solutions of five of the events studied in this chapter are presented in Chapter 1, I decided to make average rather than specific radiation corrections. There are two reasons for adopting this approach. First, the radiation factors are highly sensitive to changes in the orientation of the P-wave nodal planes so any small error in the fault-plane solution might result in a more significant error in the radiation correction. Second, there is some evidence that the radiation pattern is not generally uniform for the entire rupture process of a tremor; in particular, the two components of the S-wave ground motion often have substantially different wave forms (Figures 7 and 8). In the situation reported, scattering, refraction and shear-wave birefringence do not adequately account for these differences.

Median values for radiation factors for a double-couple source were determined from values of $f(\theta,\phi)$ and $g(\theta,\phi)$ calculated for 1 000 points randomly distributed on the focal sphere. The median value of $f(\theta,\phi)$ is 0.39 and for $g(\theta,\phi)$ is 0.57; this result is the same for both types of shear faulting considered by Haskell (1964).

The moments listed in Table 2 were calculated using equation (4.5) with

$$\alpha = 5{,}9 \text{ km/sec}$$

$$\beta = 3{,}8 \text{ km/sec}$$

$$\rho = 2{,}7 \text{ gm/cm}^3$$

$$r = 3{,}3 \text{ km}$$

An average P-wave velocity α was determined using P waves from two large chemical explosions recorded by the underground seismic array (McGarr et al, 1975). McGarr (1974) found that S-wave velocities in E.R.P.M. are close to 3,8 Km/sec. For the events of this study the focal distance, r, varied by less than 10 per cent from 3.3 km.

Brune (1970, 1971) presented a model of the seismic source in which the fault is represented as a circular area. The radius of the fault, r_o is related to the corner frequency by

$$f_o = 2.34\beta/(2\pi r_o)$$

for S waves and

$$f_o = 1.97\alpha/(2\pi r_o) \qquad (4.6)$$

for P waves using the extension of Brune's theory by Trifunac (1972a)

The average displacement, $\bar{u}_d$, is given by Aki (1966)

$$\bar{u}_d = M_o/\pi r_o^2 \mu \qquad (4.7)$$

where the modulus of rigidity, $\mu = \beta^2\rho \simeq 3{,}9 \times 10^{11}$ dyne/cm^2.
The stress drop across the fault plane at the time of rupture is given by Brune (1971).

$$\Delta\sigma = (7/16)\, M_o/r_o^3 \qquad (4.8)$$

Moments, source radii, stress drops and average displacements inferred from P and S waves of the tremors reported here are listed in Table 2.

TABLE 2.

Source Parameters from P and S Spectra. Parameters from P-wave Spectra are given First for Each Event.

Event		Spectral Fit	$\Omega(0)$ (10^{-4} cm-sec)	f_o (Hz)	M_o (10^{20} dyne-cm)	r_o (m)	$\Delta\sigma$ (bars)	$\bar{u}_d$ (cm)
3 Feb.	1410	C	0.25	12	1.4	150.	17.	0.7
		B	0.85	12.5	0.92	110.	28.	0.58
4 Feb.	1537	B*	0.016	30	0.09	60.	18.	0.29
		B	0.35	15.8	.38	90.	23.	.38
4 Feb.	2250	A	1.6	5.2	8.8	350.	9.	0.85
		A	6.7	4.1	7.2	345.	7.	.50
8 Feb.	1814	B	0.016	19.	0.09	95.	4.4	0.11
		B	0.045	25.	.049	55.	11.	.12
8 Feb.	1855	B*	0.12	22.	0.68	105.	25.	0.65
		B	0.18	18.	.19	80.	17.	.26
10 Feb.	0826	A	0.5	6.5	2.8	280.	5.5	0.42
		C	0.9	10.	1.0	140.	15.	.40
11 Mar.	1451	B*	0.06	18.	0.33	100.	15.	0.39
		B	0.42	14.5	.45	100.	22.	.39
21 Mar.	1941	A	1.2	4.8	6.5	385.	5.2	0.5
		C*	2.0	8.0	2.21	175.	16.	.56
23 Mar.	1625	B*	0.22	13.	1.3	140.	20.	0.75
		C	0.33	14.	.36	100.	14.	.28
22 Aug.	1021	B	0.28	8.4	1.6	220.	7.	0.27
		B	0.55	12.	.59	120	15.	.35
26 Aug.	1510	C	0.08	14.	0.44	130.	8.8	0.31
		B	0.04	18.5	.043	75.	4.	.06
26 Aug.	1616	B	0.035	19.	0.2	95.	10.	0.26
		B	0.15	21.5	.16	65.	23.	.30
16 Sept	2058	B	1.3	7.	7.	260.	18.	1.3
		C	1.4	10.	1.5	140.	22.	.62
16 Sept	2103	C	0.04	15.6	0.22	120.	6.1	0.2
		B	0.09	11.5	.10	125.	2.3	.05
27 Sept	1639	A*	0.9	4.4	5.	410.	3.2	0.36
		A	5.3	3.0	5.7	470.	2.2	.21
2 Nov.	1150A	B*	0.001	22.	0.006	80.	0.5	0.011
		C	0.003	24.	.003	60.	0.65	.01
2 Nov.	1150B	C	0.014	20.	0.075	90.	4.5	0.11
		C	0.047	18.	.05	80.	4.3	.07
2 Nov.	2007	C	0.11	14.	0.6	130.	12.	0.42
		C	0.5	13.5	.54	105.	19.	.40
2 Nov.	2010	A*	0.001	16.	0.006	110.	0.2	0.005
		C	0.004	26.	.004	55.	1.1	.01

Table 2 - continued.

Event	Spectral Fit	$\Omega(0)$ (10^{-4} cm-sec)	f_o (Hz)	M_o (10^{20} dyne-cm)	r_o (m)	$\Delta\sigma$ (bars)	$\bar{u}_d$ (cm)
20 Nov. 1621	C	0.04	18.	0.22	100.	9.3	0.26
	C	0.15	16.	.16	90.	9.5	.17
21 Nov. 0005	C	0.32	12.5	1.8	145.	25.	1.
	B	2.5	8.2	2.7	175.	22.	.74
21 Nov. 0020A	C	0.45	11.5	2.5	160.	27.	1.1
	B	1.2	13.	1.3	110.	43.	.89
21 Nov. 0020B	C*	0.012	23.	0.07	80.	5.7	0.11
	B*	0.021	20.	.023	70.	2.8	.04
22 Nov. 1635	A	1.3	4.4	6.9	410.	43.	0.47
	C	0.55	16.5	.59	85.	10.	.66

* $\Omega(0)$ and f_o are less reliably determined.

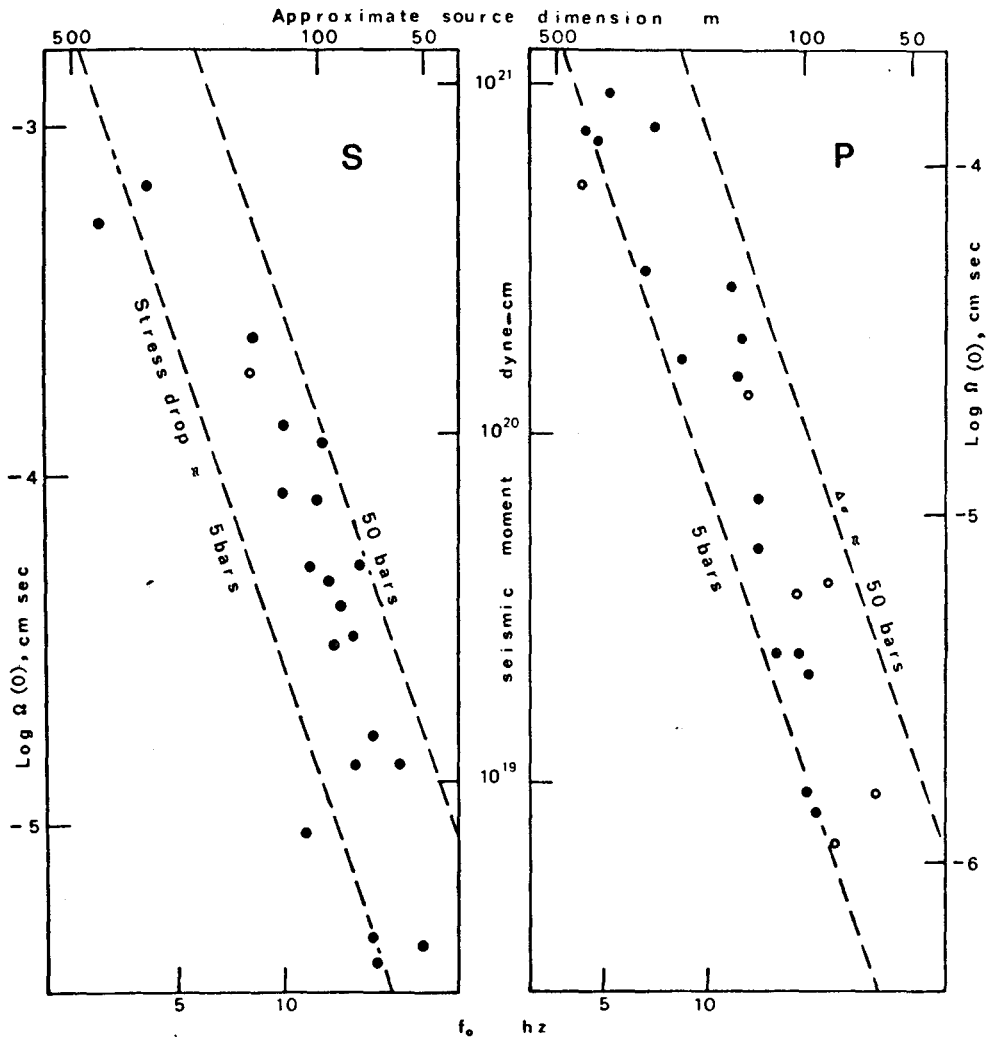

Figure 11. Ω (0) as a function of f_0 or M_0 as a function of r_0 for P and S waves.

Figure 11 is an $\Omega(0)$- f_o diagram for the mine tremors; this type of diagram has been used by Thatcher (1972) and Hanks and Thatcher (1972). On this diagram, lines of slope -3 are contours of equal stress drop. Brune's theory, as extended by Trifunac (1972a) was used to define the contours of equal stress drop in Figure 11. We see that nearly all of the data for mine tremors are between the contours of 5 and 50 bars. For comparison, most corresponding data for earthquakes in the southern California region are in the range of 1 to 100 bars (Thatcher, 1972; Thatcher and Hanks, 1973). Thus, stress drops for mine tremors at ERPM are in the range found for crustal earthquakes.

Sizes of mine tremors are compared with earthquake dimensions in Figure 12; the earthquake data are from Liebermann and Pomeroy (1970). The dimensions of the mine tremors were taken as $L = 2r_o$ (Table 2). The dimensions of the mine tremors are seen to be in good agreement with the empirical relationship of Wyss and Brune (1968) between local magnitude and fault dimension.

$$M = 1,9 \log L - 6,7$$

where L is the fault dimension in centimeters.

The relationship between moment and local magnitude for shocks at ERPM is shown in Figure 13; the moments in the figure were calculated from $M_o = (M_o(P) + 2.M_o(S))/3$ where $M_o(P)$ is deduced from the P wave and $M_o(S)$ from the S wave. The best empirical fit to the data is $\log M_o = 17,7 + 1,2\ M$, where M_o is in dyne-centimeters. The slope of 1,2 depends considerably on M_o for two events with magnitudes of about 0; these events had marginal signal-to-noise ratios as analyzed here and so these two points in Figure 3 should not be given as much emphasis as the other data.

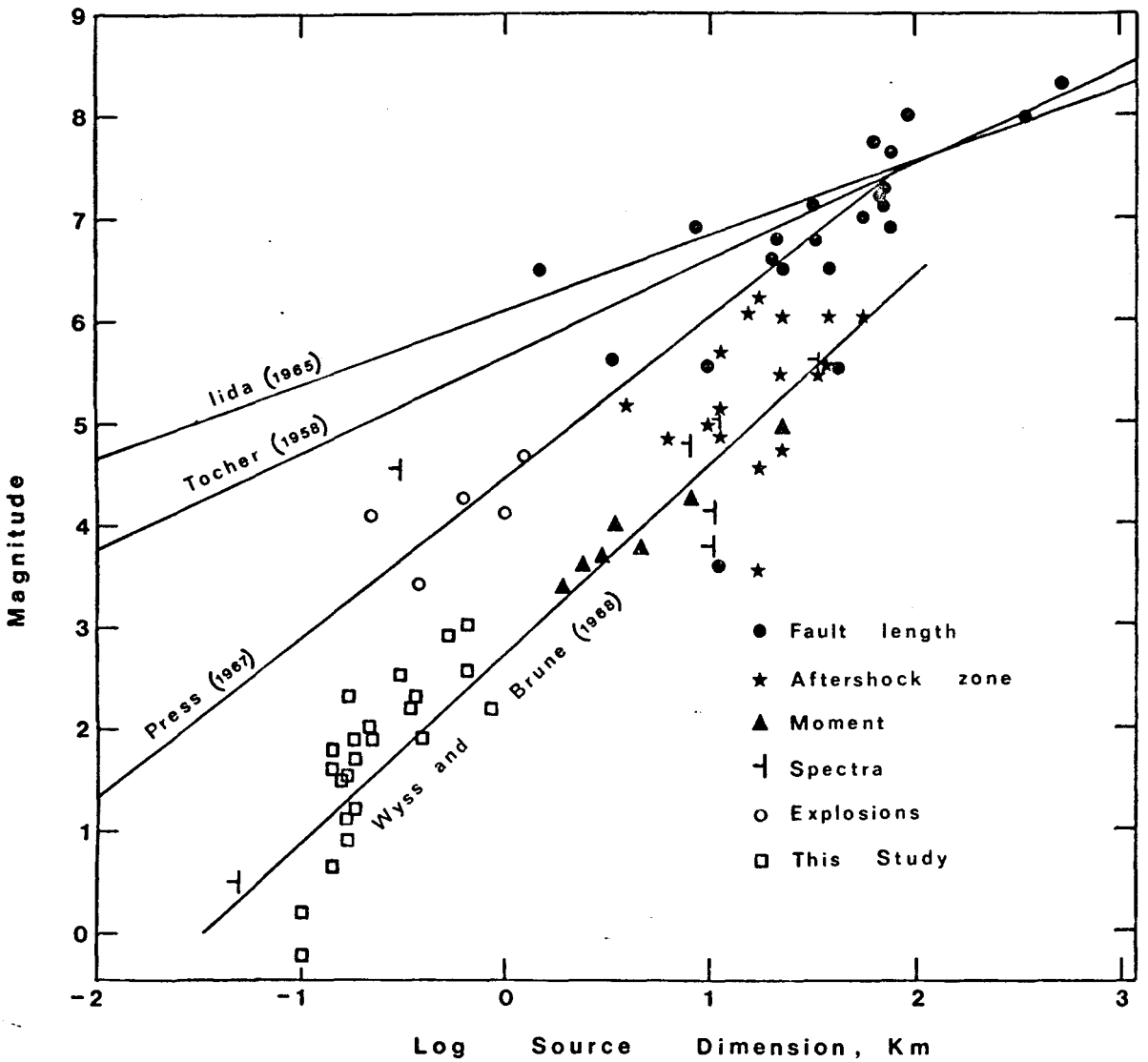

Figure 12. Magnitude as a function of fault dimension. Earthquake data and empirical relationships from Liebermann and Pomeroy (1970).

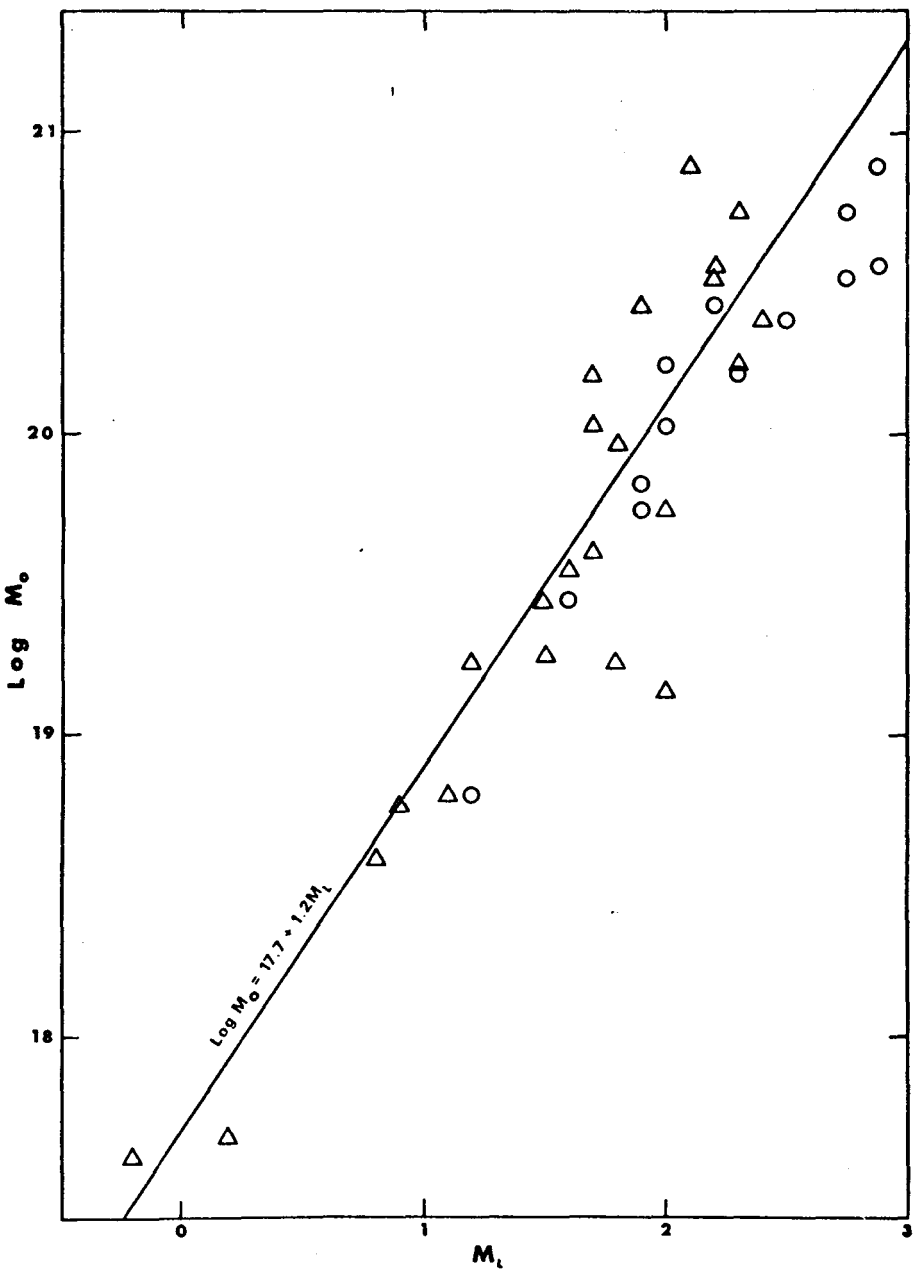

Figure 13. Moment as a function of magnitude. Symbols are explained in Figure 10.

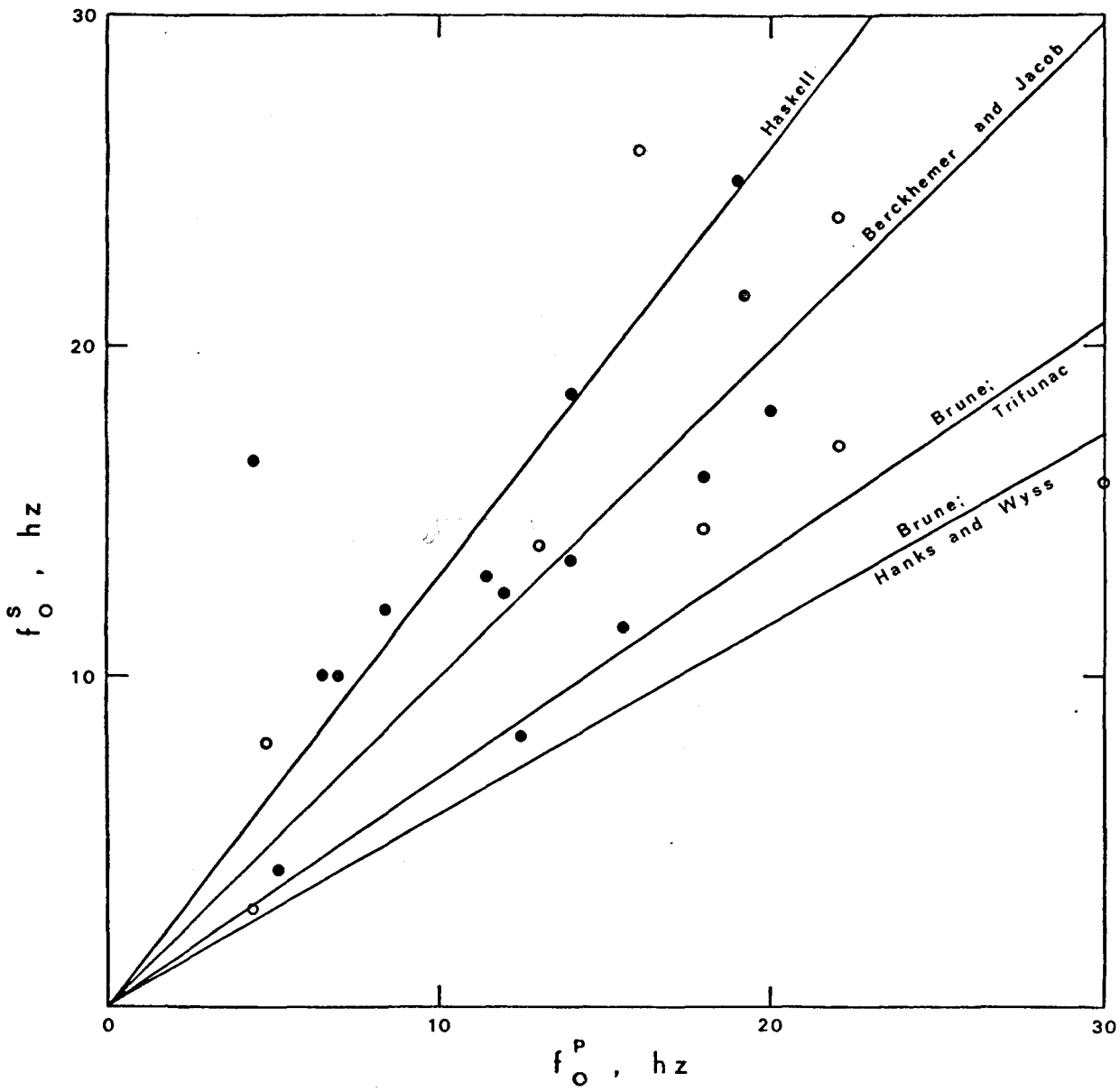

Figure 14. f_o^p as a function of f_o^s. Hollow symbols are used when f_o^p or f_o^s is considered to be less reliably determined. Theoretical results of Berckhemer and Jacob (1968); Haskell (1964) and Brune (1970) as extended by Hanks and Wyss (1972) and Trifunac (1972a) are included for comparison.

The relationship of P- to S-wave corner frequencies is somewhat irregular as indicated in Figure 14. The data appear to be distributed about the line $f_o^P = f_o^S$, but the scatter is so great that it probably is not useful to draw any conclusions from Figure 14 except for the negative conclusion that f_o^P is not simply related to f_o^S. Molnar et al. (1973) reviewed similar sets of data for earthquakes and also found considerable scatter in the diagrams of f_o^S as a function of f_o^P; however, their data suggest that f_o^S is generally somewhat lower than f_o^P.

APPARENT STRESS

A simple fault model, in which displacement across a shear fault is halted by frictional forces in excess of the final shear stress, was considered by Savage and Wood (1971). They showed that the apparent stress should be less than one half the stress drop, or $\xi = 2\eta\bar{\sigma}/\Delta\sigma < 1$ where η is the seismic efficiency, and $\bar{\tau}$ is the mean shear stress acting during failure. Wyss and Brune (1968) showed that the apparent stress, $\eta\bar{\sigma} = \mu E_s/M_o$, where E_s is the seismic energy. Therefore $\xi = 2\mu E_s/M_o\Delta\sigma$.

When body-wave spectra are used to determine E_s, M_o and $\Delta\sigma$, ξ is a constant related to the spectral shape that agrees best with the observed spectrum. For S-wave spectra, ξ is 0.1, 0.2, and 0.5 for equations (4.3A), (4.3B) and (4.3C) respectively. Apparent stress values are less than 4 bars, with a median value of 1 bar. Seismic efficiency of ERPM seismic events is discussed in more detail in chapter 6.

DISCUSSION

The analysis of seismic spectra of mine tremors in the magnitude range 0 to 3 indicates that these events have dimensions ranging from about 50 to 500 m. In a number of cases, the total extent of underground damage corresponding to a particular tremor has been documented. For example, the event of February 4th at 2250

(Table 2, Figure 5) caused severe damage in at least four widely separated regions distributed over about ½ km of the mine. Each "rockburst" was of the order of 5 to 20 m in extent; the most seriously damaged region was closest to the focus of this event. In between these regions of violent damage the mine was virtually unaffected. The total extent of the underground damage for this event is in good agreement with the size of the event deduced from the spectra of ground displacement as interpreted using Brune's theory (Table 2). Observations of underground damage, however, suggest that this event consisted of a series of widely separated and intense ruptures. Brune (1970) indicated that the displacement spectrum for an earthquake consisting of a complex series of ruptures should decay as f^{-1} for frequencies in an intermediate range extending upward from the corner frequency. The spectra for the event of February 4th at 2250 (Figure 8) do not show any such effect. This discrepancy between observations of the tremors at ERPM and Brune's theory remains unexplained.

The best documented case of a burst fracture in a deep-level gold mine has been that of a pair of intersecting fractures in the Western Claims Pillar area of ERPM. Gay and Ortlepp (1978) mapped about 75m of exploratory raises developed to expose these fractures and mapped the fracturing in detail. Ortlepp (1978) correlated the burst fractures with underground damage and with seismic events recorded at PRE. Samples of fault gouge collected from this fracture system have yielded information on driving stress (Chapter 6).

McGarr et al (1979a) showed that these underground observations fit a source model with both source dimension (r_o) and seismic moment (M_o) about one order of magnitude smaller than the values expected from the seismic data using the relationships presented in Figures 12 and 13. As this apparent discrepancy is too great to be explained by errors in interpreting the seismic data, the fracturing must have extended, continuously or discontinuously, much farther than was observed

underground. Furthermore, the shear displacement was observed to increase from a value too small to measure (less than about 2 cm) in the vicinity of the mined-out area to a maximum of 10 cm 20 m below the mined-out area.

Figure 3 of McGarr (1971) shows an unusually large and extensive burst fracture that was associated with an event of magnitude 3,0. The dimension of this fracture was of the order of 40 m and the violent crushing of support in the near vicinity of the fracture indicated shear displacements of 30 to 50 cm. The stress drop across this fracture can be estimated from where W is the dimension of one side of a square fault plane (Chinnery, 1969). For W = 40 m and $\bar{u}_d$ = 30 cm, $\Delta\sigma$ is about 2,2 kb, in good agreement with the results of triaxial tests on quartzite at low confining stress. The overall dimension of this event, inferred from Figure 12 is about 800 m and so the fracture that outcropped in the mine workings did not account for much of the total extent of the tremor. From Figure 13 we see that the moment for an event of magnitude 3 is about $1,5 \times 10^{21}$ dyne-cm. The moment estimated for the outcropping fracture from its dimension and displacement is about $1,5 \times 10^{20}$ dyne-cm or 10 per cent of the total moment of the tremor.

Thus, the visible damage of the tremor accounts for only a small part of the total shear failure that must have occurred for an event of this size. Most of the seismic strain release undoubtedly occurred in the solid rock, well away from the workings. This tremor appears to have been due to a number of separate ruptures, one of which outcropped into the workings causing much damage.

Generally, the total extent of underground damage seems to agree with the total extent of the focal region deduced from the seismic spectra; each region of continuous damage, however, rarely exceeds 20m in extent. Stress drops estimated for burst fractures that outcrop into the workings are typically of the order of 1 kb or higher.

All displacements measured to date have indicated normal faulting consistent with stope convergence. On yet a larger scale, the pattern of isolated rockbursts attributed to a single tremor does not, in general, suggest a planar failure region. The four regions damaged during the event of February 4 at 2250 were not distributed along a plane, and the areas between these rockbursts were unaffected. (Underground damage reports were supplied by W.D. Ortlepp).

The seismic spectra of this study indicate that the peak in the spectrum of seismic energy, for events in the magnitude range 2 to 3, occurs between 5 and 15 Hz. This is in good agreement with the observation by Cook (1963) that most of the seismic energy of the larger tremors is radiated at about 10 Hz. Furthermore, the suggestion by Cook that he might have grossly underestimated energies in the larger tremors of his study is confirmed by the results of this paper. Cook's seismic recording equipment was only responsive to frequencies between 15 and 150 Hz.

Stress drops for events at ERPM are somewhat greater than those estimated by Smith et al. (1974) for seismic events occurring in the vicinity of coal mines in eastern Utah. Using analysis similar to that of this paper, they inferred stress drops ranging from 0.2 to 9.6 bars. Source radii for the coal mine tremors are in the same range as those for the tremors at ERPM but the moments are typically one to two orders of magnitude less, resulting in much lower stress drops for the coal mine tremors.

Both sets of stress drops, however, are within the range of stress drops observed for natural earthquakes.

The far-field measurements reported here indicate that mine tremors are highly similar, if not identical, to natural crustal earthquakes. This result is important because the source regions of mine tremors are far more accessible, as a consequence of the deep mining, than source regions of tectonic shocks. Furthermore, the rapid strain changes in the rock resulting from mining induce such a high level of seismicity that tremors of magnitude 2 and larger are recorded at least once per week in a region of the order of 1 Km in extent in the areas of ERPM that are currently being mined. Thus, the deep gold mines provide a convenient means of studying earthquake source processes at close hand.

CHAPTER 5.

Seismic moments and source orientation from PRE.

ABSTRACT.

Seismic events occurring near E.R.P.M. with magnitudes greater than 3,0 write simple looking records on the long-period seismograms at PRE, about 54 km to the North. Observed seismograms from four seismic events occurring near E.R.P.M. during 1975 were analysed by calculating theoretical seismograms from generalised point sources with no net forces and no net torques. Synthetic seismograms calculated for sources that consist primarily of N - S striking normal faults give a reasonable fit to the observed seismograms. Agreement is improved if account is taken of Rayleigh-wave dispersion due to a surface layer 1 Km. thick with a Rayleigh-wave velocity 10% less than that of the underlying material. Inferred seismic moments are in good agreement with the empirical relationship $\log M_o = 17,7 + 1,2\ M$ determined previously, where M_o is the seismic moment in dyne-cm and M is the local magnitude.

INTRODUCTION.

The source mechanisms of shallow crustal earthquakes can be determined by fitting synthetic seismograms to observed seismograms (e.g. Johnson and McEvilly, 1974; Langston, 1976). Although source mechanisms are ideally determined by analysing seismograms written at a number of stations, strong constraints can be placed on the source mechanism by studying seismograms from a single station. Fault-plane solutions and moment - tensor determinations of E.R.P.M. seismic events using short-period data indicate that E.R.P.M. events have mechanisms consistent with normal faulting (Chapter 3 and Diering, 1978).

In this chapter, five out of six components of the moment tensor of four large seismic events occurring near E.R.P.M. during 1975 were determined by fitting synthetic seismograms to observed seismograms written by the long-period components at PRE. The peak amplitudes of each of 5 phases (P, diffracted sP, SV, SH and Rayleigh) were used to control the fit. Synthetic seismograms were written using a computer program developed by Johnson (1974 and 1976, written communication) for point sources in a homogeneous half-space.

Gane et al (1956) used mine tremors to determine P and S structure along a traverse northward from the Witwatersrand and found that crustal velocities were constant at 5,99 km/sec for P and 3,55 Km/sec for S out to Moho crossover at about 150 Km. The ray paths between E.R.P.M. and PRE traverse Archaean granites and well-consolidated Precambrian sediments of the Pretoria Witwatersrand and Ventersdorp systems. The homogeneous half-space approximation assumed by Johnson's computer program is a reasonable approximation for the velocity structure between E.R.P.M. and PRE, because velocities in the sediments are similar to those in the basement granite.

Because there was no location network of seismometers at E.R.P.M. during 1975, the events considered here were not precisely located. The similarity with known E.R.P.M. events indicated that they originated near E.R.P.M. It is reasonably certain that they occurred at hypocentral depths of about 3 Km. as it has been shown (e.g. Cook, 1963; McGarr et al, 1975) that the tremors in the vicinity of E.R.P.M. are all closely associated with current mining; most of the mining at E.R.P.M. during 1975 was carried out at depths of about 3 Km.

I chose data from 1975 because the recording speed of 30 mm/minute was twice as fast as before and after 1975 and allowed reasonable time discrimination of data from mine tremors. The slower paper speed of 15 mm/minute was generally preferred as it reduced the amount of trace overlap when large teleseisms occurred.

TABLE 3.

Times and magnitudes of four large seismic events occurring near E.R.P.M. during 1975. (South African Standard Time).

	Time.	M_L
26 June	1029	3,5
3 July	0559	3,6
3 July	0644	3,4
29 August	1359	3,5

OBSERVATIONS.

Seismic events located near E.R.P.M. (e.g. Chapter 4) write records on the PRE short-period seismograms with S - P intervals of 6,1 to 6,4 seconds and with the amplitides of the E - W component of the P - wave less than 20 percent of the amplitudes of the N - S component of the P-wave. The first motion of the larger events indicatesa southerly azimuth. Four seismic events which occurred during 1975 near E.R.P.M., according to these criteria, and which wrote clear seismograms on the long-period components at PRE, were chosen for this study. Table 3 lists the times and magnitudes of these events. The original records were hand digitised at a sampling rate of about 3 samples/second and (small) corrections were made for the skewing effect of the recording drum. Microseismic noise with periods varying from about 5 Hz to 8 Hz was present. The predominant period of the noise in the vicinity of each event recording was measured and sine waves with the corresponding period was generated and subtracted from the digital data in an attempt to minimise the noise. For purposes of presentation and analysis, these data were interpolated to a sampling rate of 10 samples/second.

Although noise, mostly long-period, is still present in the seismograms, shown in Figure 15, a number of phases clearly exceed the noise level: maxima and minima corresponding to P, diffracted sP, S and Rayleigh waves are indicated. The sP - P time of 0,7 sec. is consistent with the expected focal depth of 3 Km. The sP phase was noticed because the polarity was opposite to that of the P wave and it was identified on the basis of theoretical seismograms (Figure 16). The same separation time has been noticed on PRE short-period records with unusually small P-wave first motions. The four seismic events produced very similar seismograms, indicating similar source mechanisms for all four.

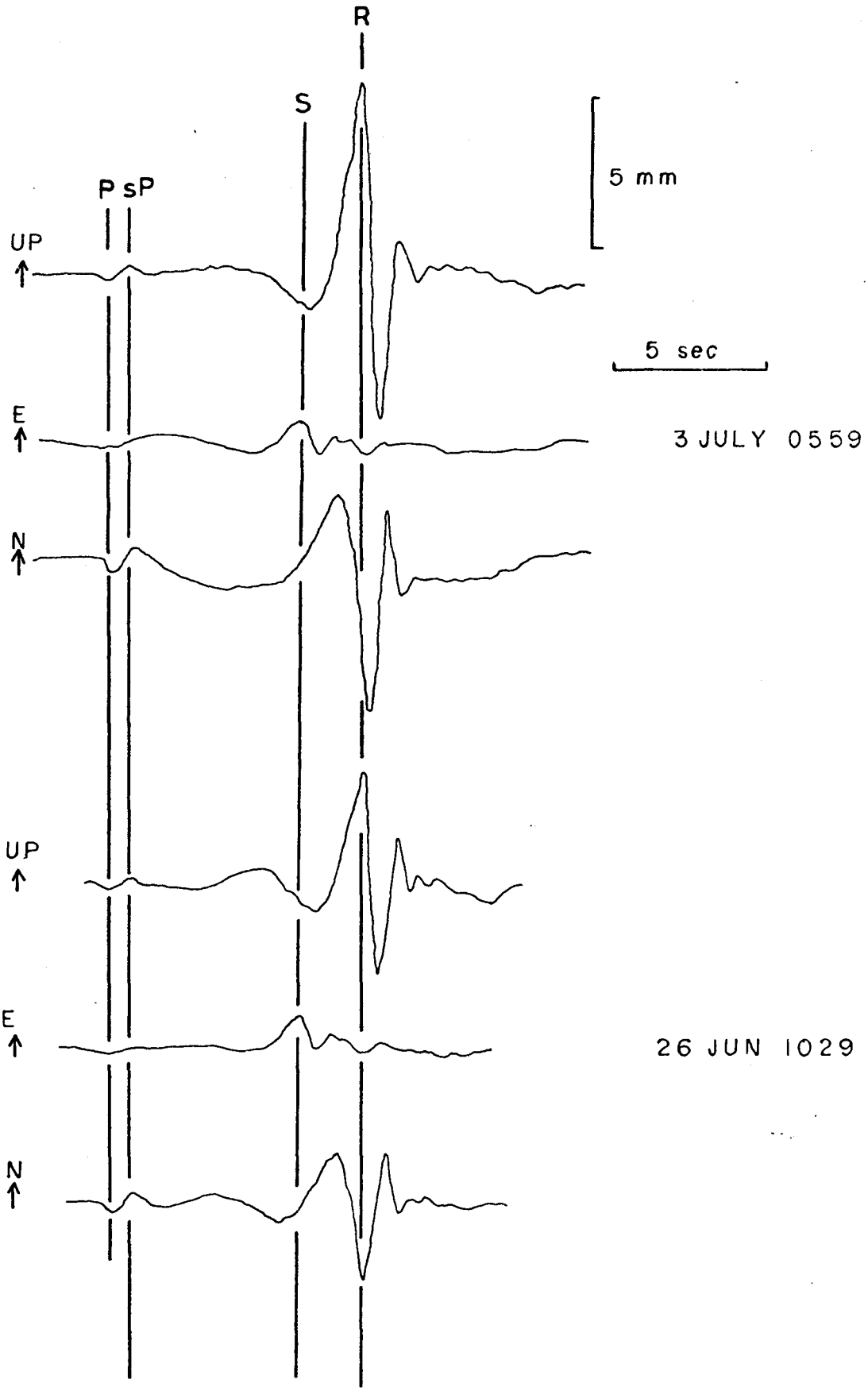

Figure 15. L - P seismograms at PRE from four seismic events occurring near E.R.P.M. during 1975.

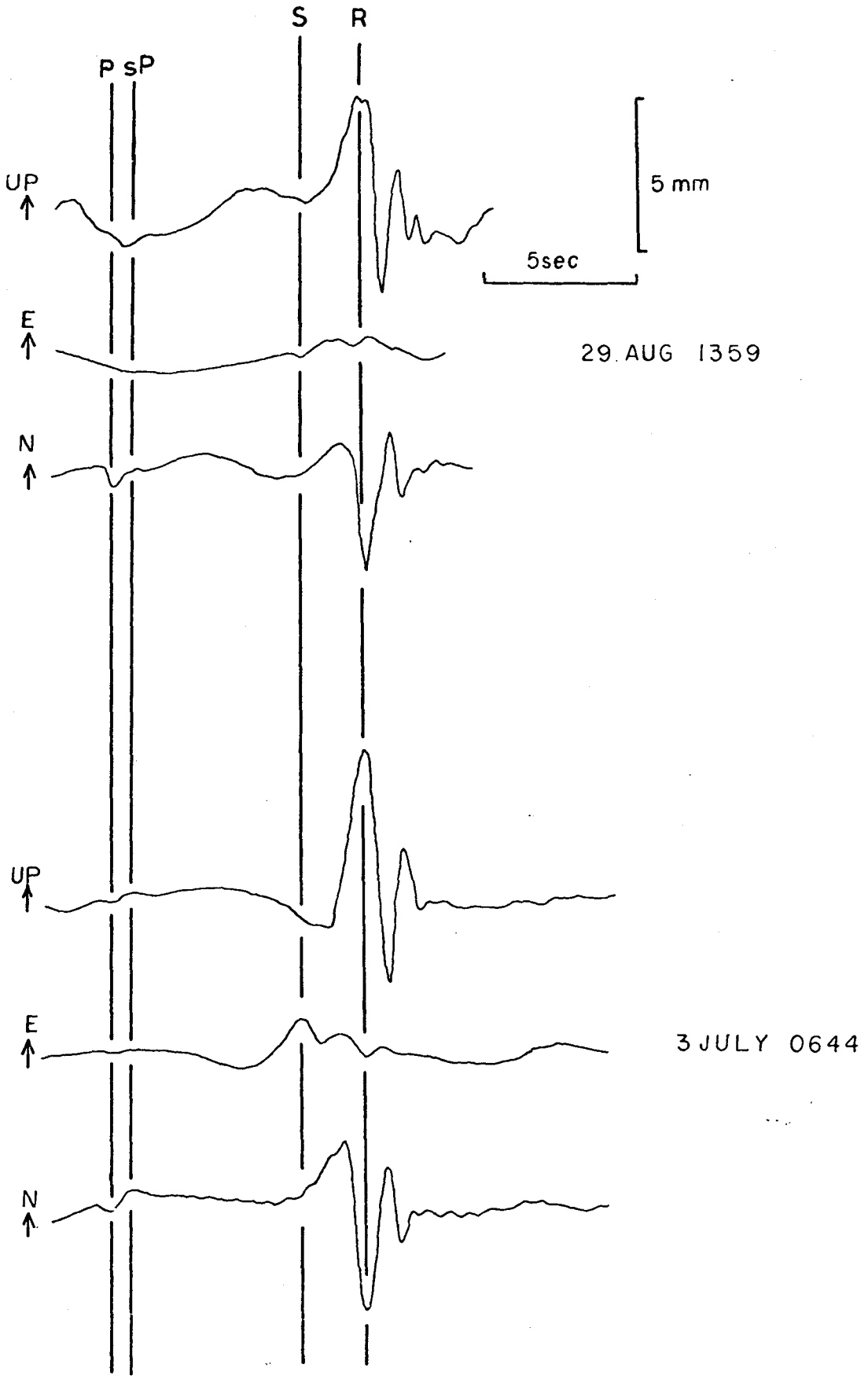

Figure 15 continued.

All phases had the same polarity except for the E - W component on 29 August at 1359. Because the events occurred nearly due south of PRE, the N-S and E-W components closely represented radial and transverse ground motion.

SYNTHETIC SEISMOGRAMS:

Ground motion at PRE due to four "canonical" sources at E.R.P.M. was calculated using a computer program written by Johnson (1974 and 1976, written communication) for a point source buried in a homogeneous half-space. The four sources are pure strike slip, pure dip slip, vertically oriented compensated linear vector dipole (C L V D) (Knopoff and Randall, 1970) and volumetric expansion. The C L V D was chosen because of mathematical convenience and is equivalent to the sum of two normal faults striking at right angles to one another. The first two sources each take on two different orientations: strike slip on N-S and NE-SW striking planes and dip slip on N-S and E-W striking planes. Any source with no net force or torque can be considered as a linear sum of these six sources.

P and S velocities of 5,99 Km/sec and 3,55 Km/sec were used (Gane et al, 1956) and 54,5 Km, 3 Km and 2700 Kg/m^3 were used for the epicentral distance, source depth and density. The predicted S - P time of 6,25 sec is in agreement with times of 6,1 to 6,4 sec. observed on the short-period seismograms at PRE.

Synthetic seismograms for comparison with the records at PRE were calculated by convolving the synthetic ground motion due to a point source by a source function, an attenuation operator and by the impulse response of the PRE long-period system (Appendix A3). A box-car function with a duration of 0,3 second was used for the source function, extrapolated from data presented in Chapter 4. The attenuation operator was the causal Q operator of Carpenter (1966) with $Q = 200$ for S waves. (A minimum estimate Chapter 4).

Both the source function and the Q operator were unimodal and of shorter duration than the predominant periods of the synthetic ground motion and therefore had the effect of smoothing the arrivals out without changing the peak amplitudes significantly. The exact form of the source function and the correction due to attenuation were not important for this study because only peak amplitudes were used.

Synthetic seismograms from the six independent sources used by Johnson (1976, written communication) are shown in Figure 16: traces not shown are zero. Focal mechanism solutions describe each source orientation (see Chapter 3). The dip-slip and strike-slip sources have seismic moments of $3{,}4 \times 10^{21}$ dyne-cm, the C L V D is equivalent to the sum of two normal faults, each with a seismic moment of $1{,}7 \times 10^{21}$ dyne-cm. and the volumetric expansion source represents a volume increase of 10^{10} cm^3.

Four sources radiate radial and vertical motion only because they are symmetrical about the vertical (N-S) plane radial to the source, while the other two (antisymmetrical) sources radiate transverse motion only. The P, diffracted sP, S and Rayleigh-wave amplitudes and the times at which S and Rayleigh-wave peak amplitudes occur differ noticably for seismograms from the four symmetrical sources. North-South striking strike-slip faulting writes seismograms at PRE similar in shape to seismograms from N-S striking dip-slip faulting, but with amplitudes about twenty times greater. The N-S striking dip-slip component cannot be resolved in practice from a single station due North of the source unless the N-S striking strike-slip component is very well constrained.

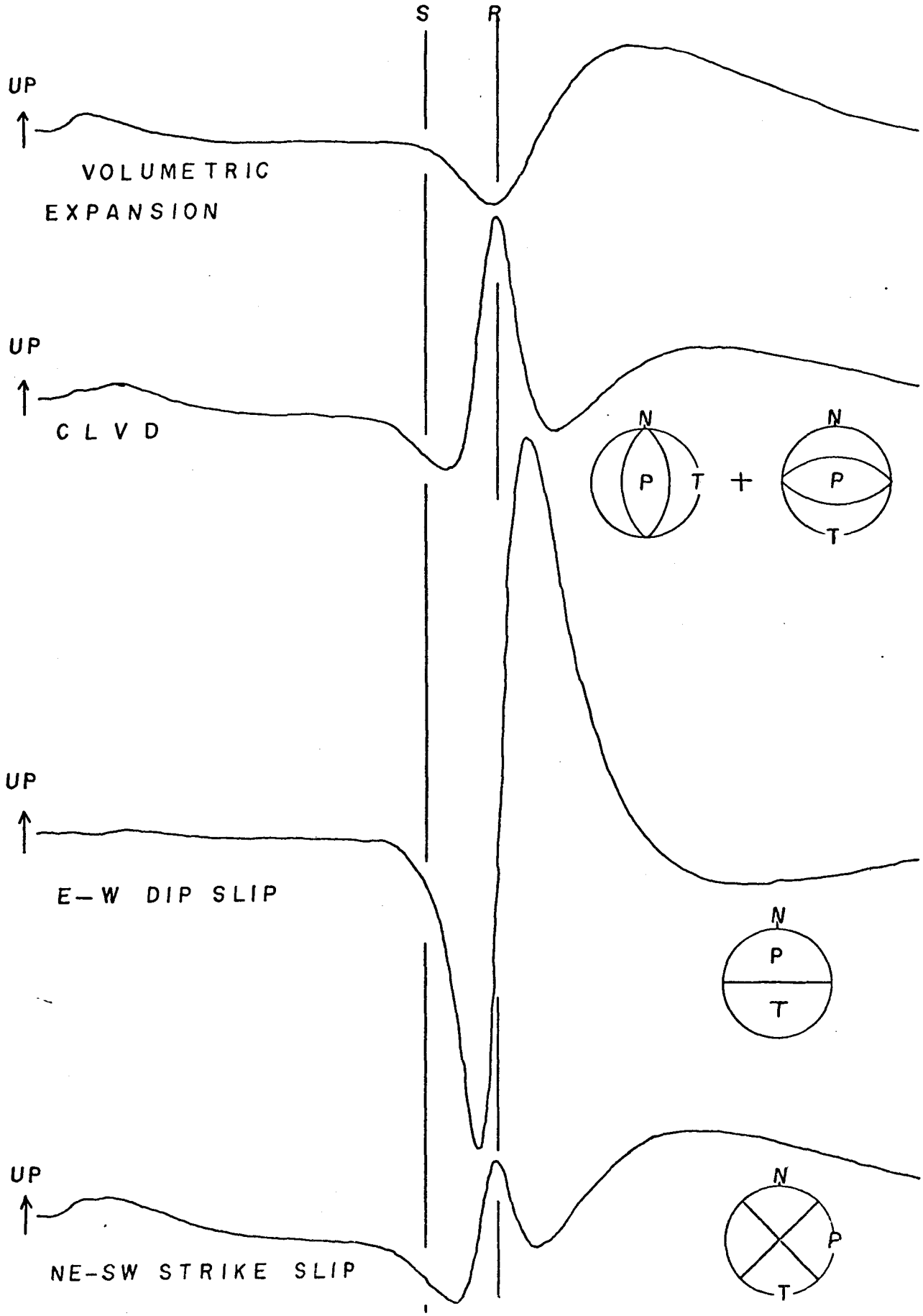

Figure 16. Synthetic seismograms at PRE from four canonical sources in a homogeneous half-space.

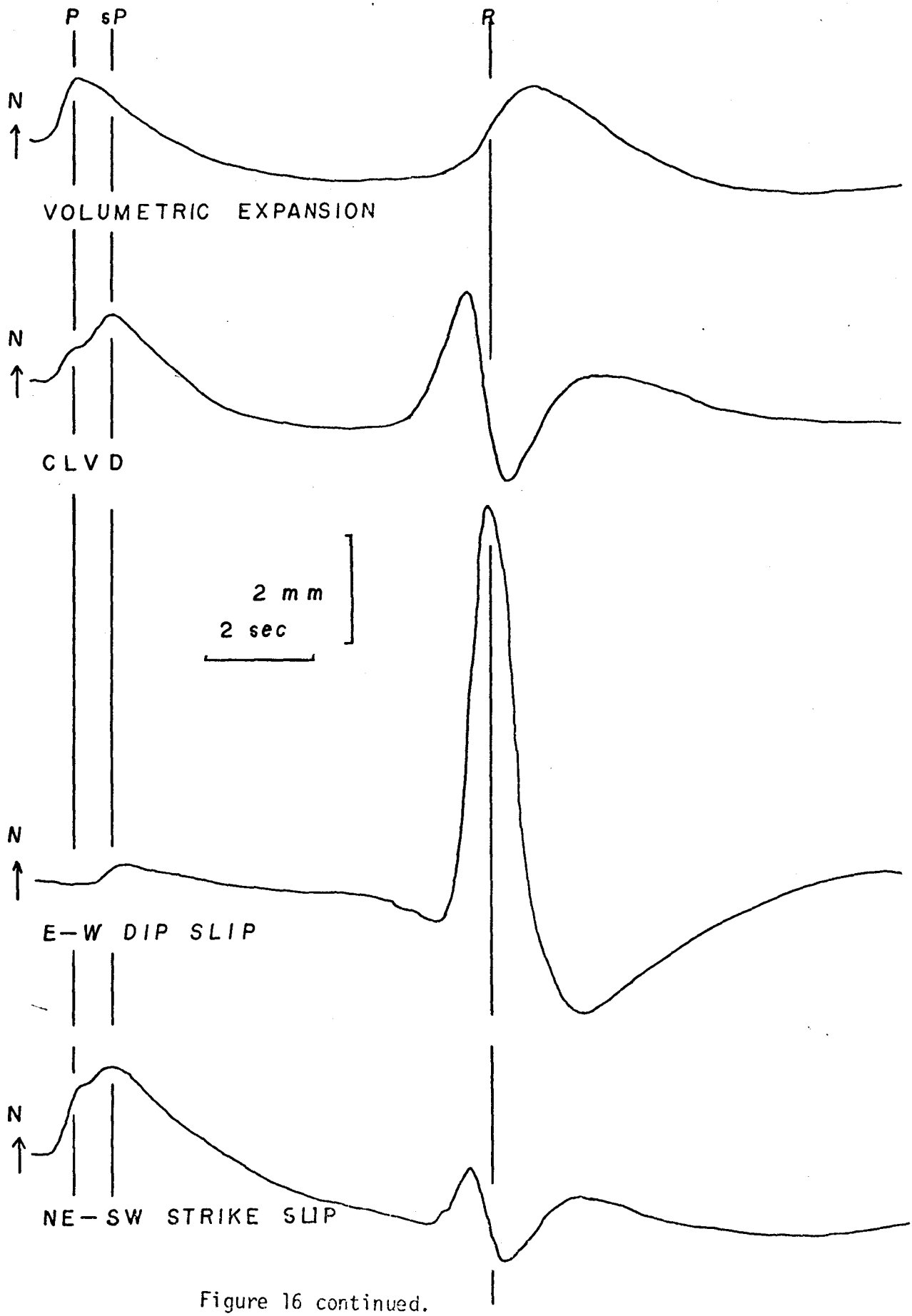

Figure 16 continued.

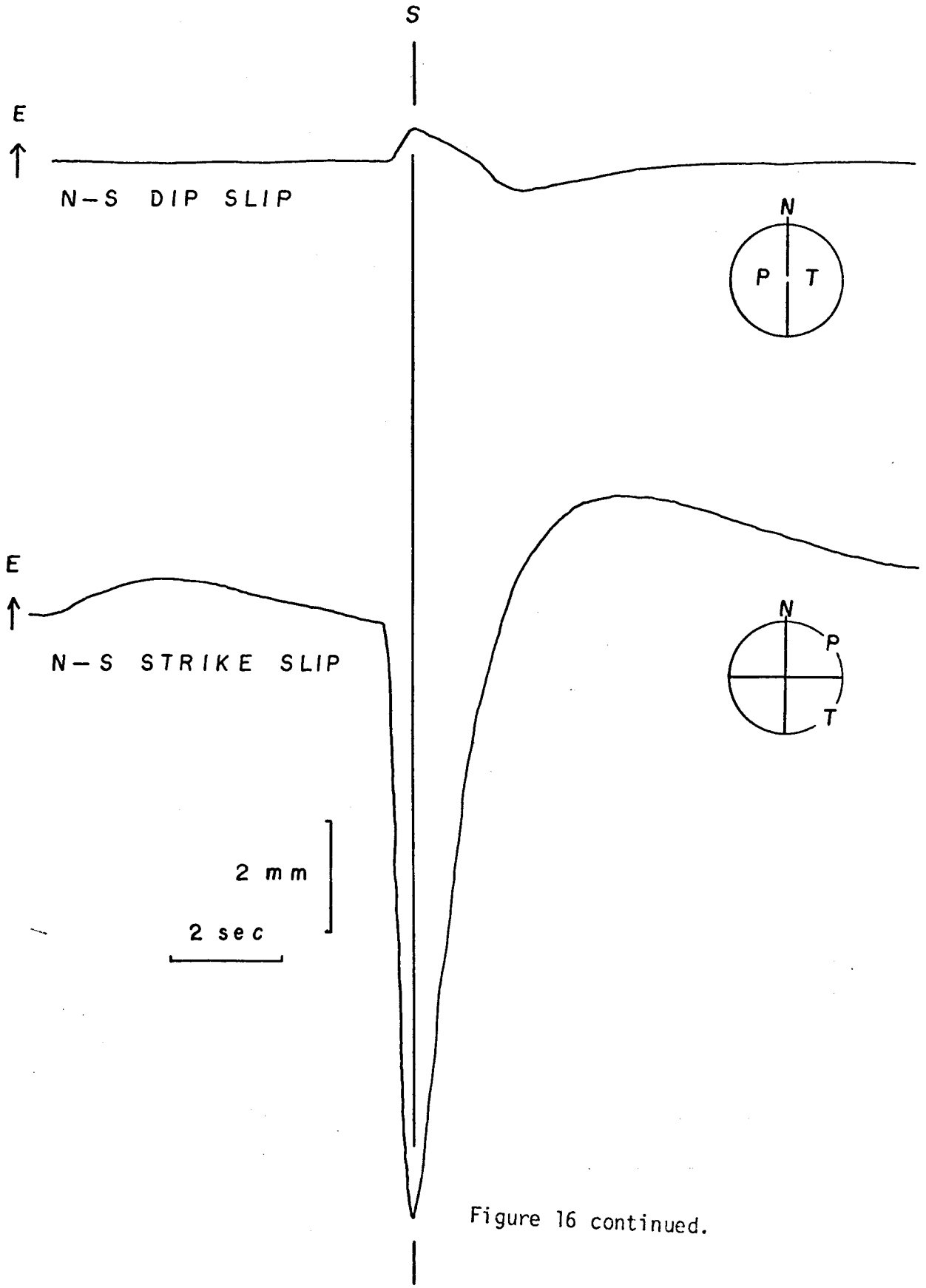

Figure 16 continued.

Synthetic N - S and vertical seismograms consisting of a linear combination of the four symmetrical sources were constructed so that peak amplitudes agreed as closely as possible with peak amplitudes of the observed seismograms in Figure 15. P, diffracted sP and first-swing Rayleigh-wave amplitudes of the N - S components and S and first-swing Rayleigh-wave amplitudes of the vertical components were used to obtain the best fit. An iterative procedure which accounted for the time difference between the peak amplitudes of the seismograms from the four theoretical sources was used to obtain the best agreements between the theoretical and observed amplitudes, for generalised sources and then for sources with no net volume change. Synthetic seismograms are compared to the observed seismograms in Figure 17: Table 4 lists the inferred volume change for the fit which allowed volume change (dashed lines in Figure 17) and the shear components for the fit which excluded volume change (dotted lines in Figure 17). Agreement with the observed seismograms (Figure 17) was reasonable except that Rayleigh waves of the observed seismograms were later and more oscillatory than Rayleigh waves of the theoretical seismograms. It is shown later that Rayleigh wave dispersion can account for part of this discrepancy.

TABLE 4.

Components of sources buried in a homogeneous half-space.

Synthetic seismograms are shown in Figure 17.

Event		Bns	Bne	Dew	C	Mo	V
		x 10^{21} Dyne-cm.					x 10^{10} cm^3
26 June	1029	3,27	-2,48	0,92	1,88	5,9	- 0,58
3 July	0559	2,94	-4,42	0,27	3,65	9,2	- 0,92
3 July	0644	3,92	-3,13	-0,58	2,63	7,6	- 0,49
29 Aug	1359	-0,65	-3,43	-0,07	2,12	5,7	- 0,68
TOTAL		9,48	-13,46	0,54	10,28	28,4	- 2,67

KEY: Bns : N - S striking strike-slip.

Bne : NE - SW " " "

Dew : E - W " dip-slip.

C : Average of N - S and E - W striking normal faults (45° dip) (C L V D).

V : Volumetric expansion.

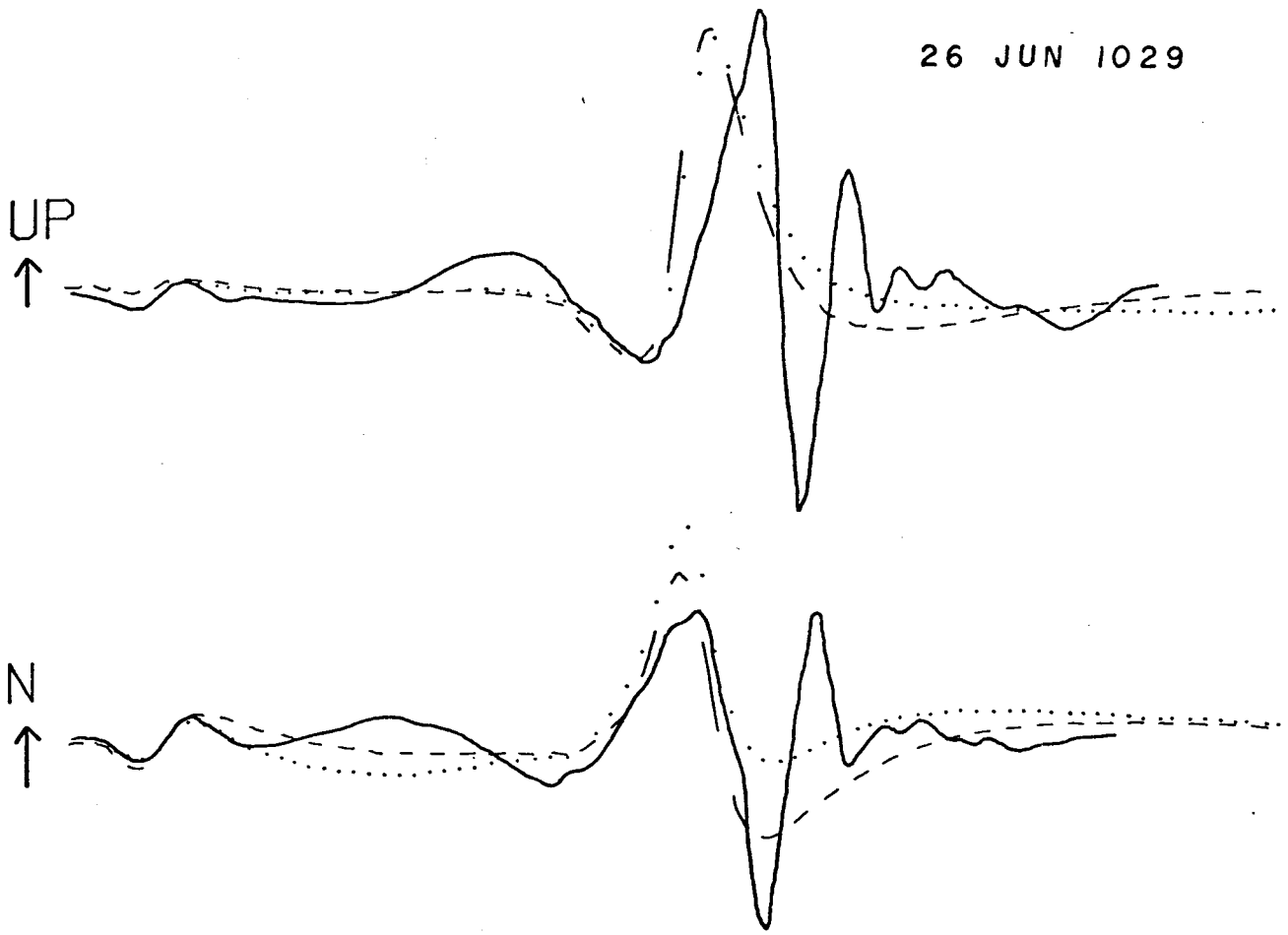

Figure 17. Synthetic seismograms from sources with net volume change (dashed lines) and with no net volume change (dotted lines) compared to observed seismograms.

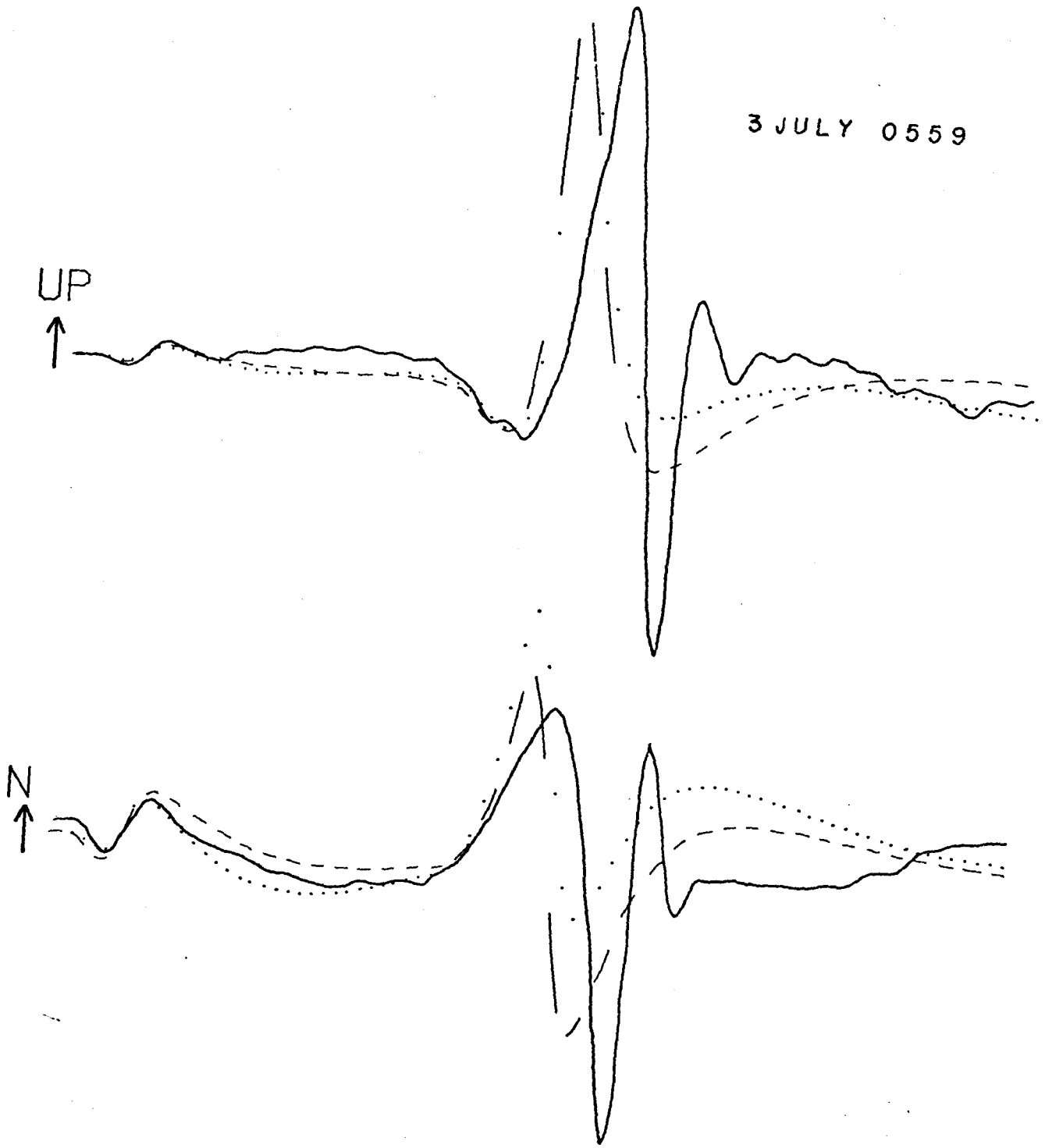

Figure 17 continued.

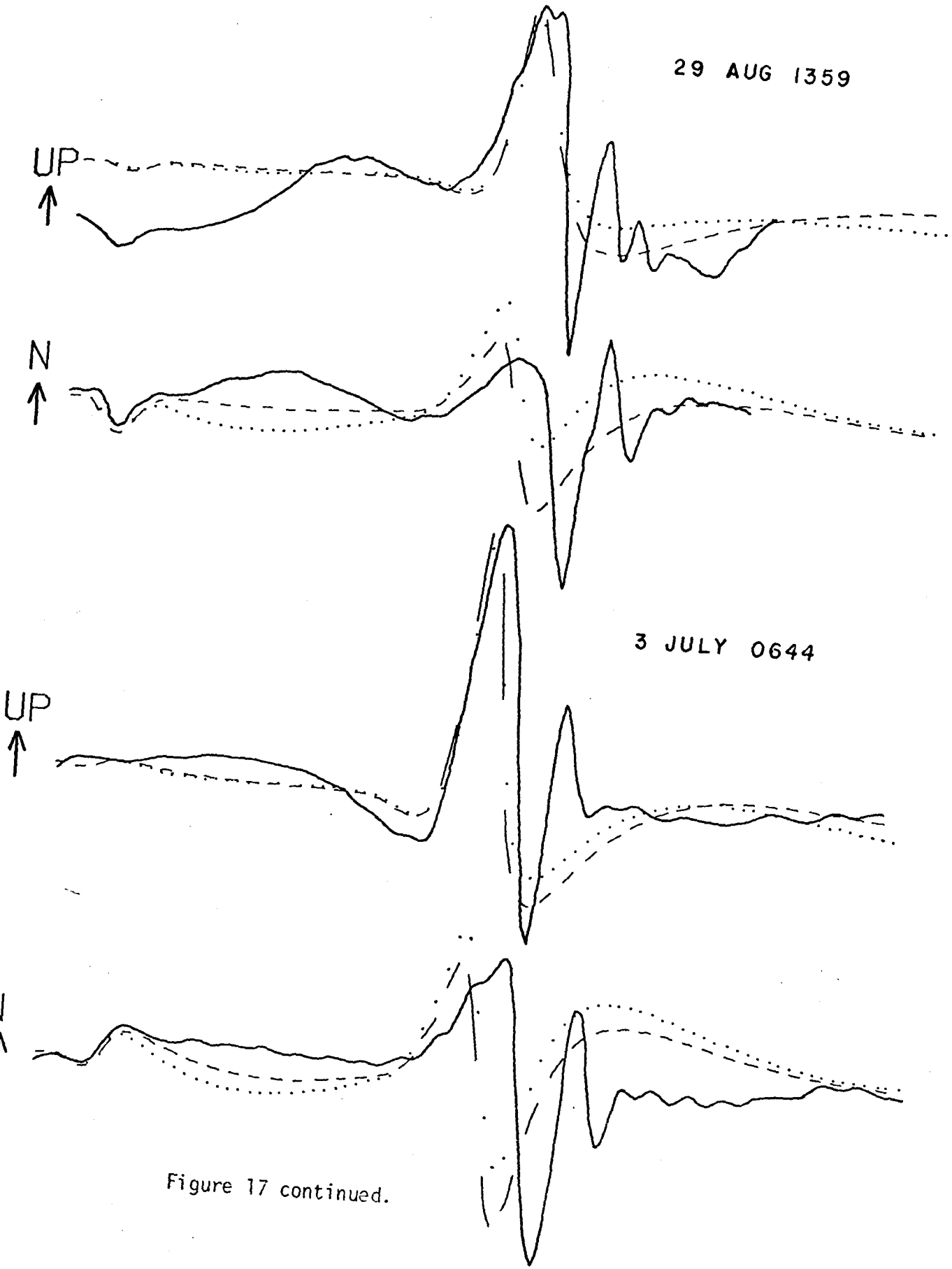

Figure 17 continued.

SEISMIC MOMENTS:

The seismic moment tensor, Moij, for the case of no change in volume, can be expressed in terms of the four "canonical" sources used in this study by

$$Moij = \mu \, \Delta \epsilon_{ij} \, V$$

$$= \begin{matrix} C + Bne & Bns & Dew \\ Bns & C - Bne & - Dns \\ Dew & - Dns & - 2C \end{matrix} \qquad (5.1)$$

where the axes are North, East and Up respectively,

$\Delta \epsilon_{ij}$ is the average strain change over a volume, V, of rock with modulus of rigidity, μ,

Compressive stresses are taken as positive,

Bns, Bne, Dew and C are the components indicated in Tables 4 or 5,

and Dns is the N-S striking dip-slip fault component not determined in this Chapter.

By analogy with the strain energy of distortion, (e.g. Jaeger and Cook, 1969, PP 118 and 33), in which strain energy (a scalar) is expressed in terms of strain (a tensor), the conventional scalar seismic moment, M_o, can be expressed in terms of the seismic moment tensor by

$$M_o^2 = \tfrac{1}{2} \, Moij \; Moij$$

$$= 3 \, C^2 + Bne^2 + Bns^2 + Dns^2 + Dew^2 \qquad (5.2)$$

For unknown Dns and random source orientation,

$$M_o^2 = (3 \, C^2 + Bne^2 + Bns^2 + Dew^2) \times 5/4 \qquad (5.3)$$

RAYLEIGH-WAVE DISPERSION:

Rayleigh-wave dispersion for periods from 0,6 to 3 seconds was estimated for the E.R.P.M. - PRE path by expressing the phase differences between the observed and theoretical Rayleigh-waves shown in Figure 17, as velocity changes. The presence of S waves on the vertical components does not appear to have affected the results, shown in Figure 18.

In Figure 18, these dispersion data are compared to a theoretical dispersion curve due to a superficial layer, 1 km thick, with a shear-wave velocity of 3,2 Km/sec overlying a half-space with a shear-wave velocity of 3,55 Km/sec. The theoretical curve was adopted from Wilson and Baykal (1948). Intuitively, a gradual increase in velocity with depth would result in a dispersion curve in closer agreement with the data. Weathering, jointing and low confining stresses near the surface should cause continuous velocity changes.

The seismic moments listed in Table 5 are, on average, only about 15 percent greater than the seismic moments listed in Table 4. The values are similar because the wavelengths sampled (about 6 Km) are greater than both the source depth and the thickness of the shallow layer of rocks with low velocities (1 Km.)

Fig.18

PHASE VELOCITY DISPERSION

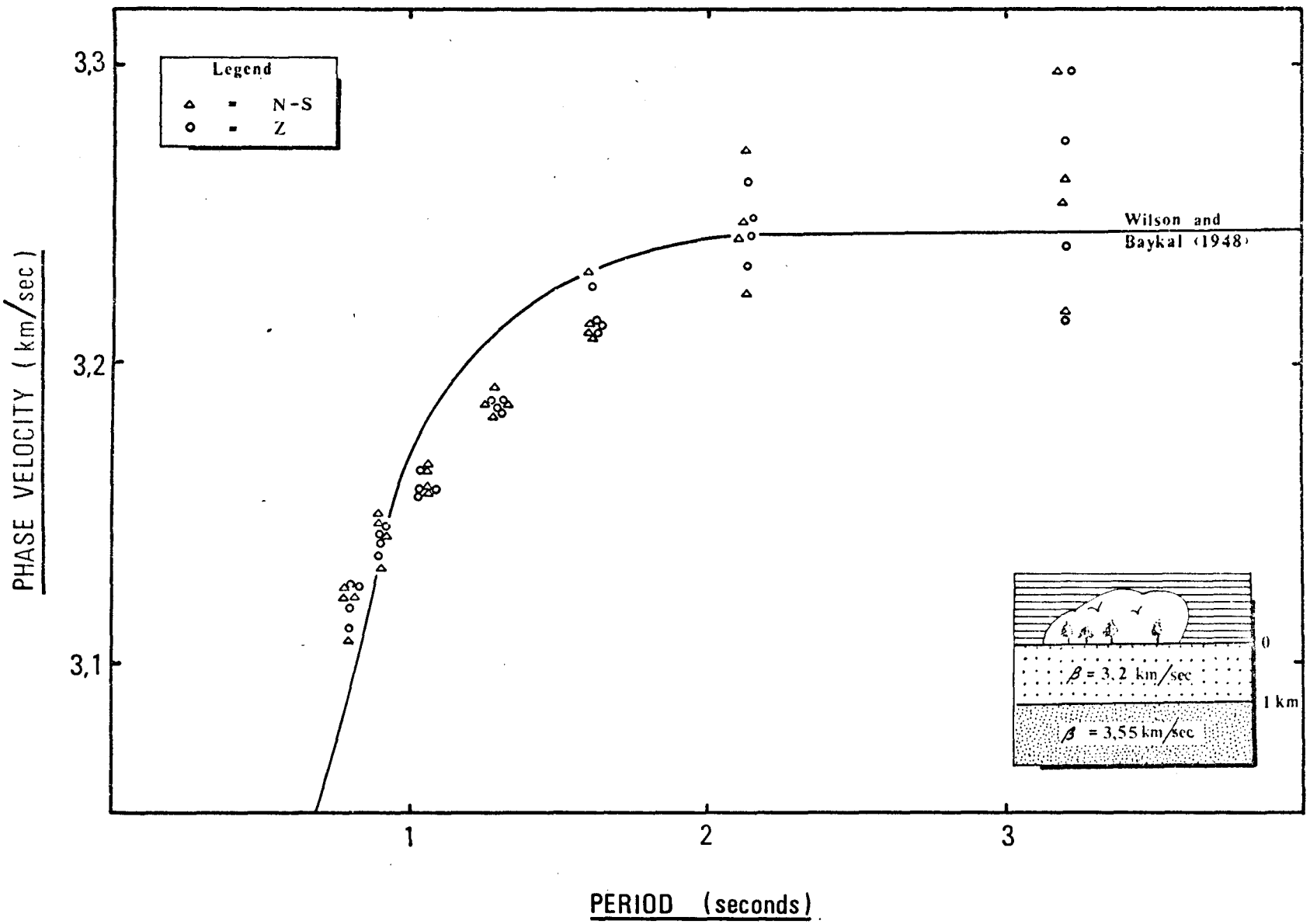

Logie (1951) found S-wave velocities of 3,37 Km/sec. from Witwatersrand tremors to surface stations for epicentral distances of less than 15 Km. Gane et al (1956) noted that a superficial layer 1,3 Km. thick with P and S velocities of 5,40 Km/sec and 3,20 Km/sec respectively would account for P_1 and S_1 intercepts, although there was considerable uncertainty in their data. Båth (1975) found that Rayleigh waves at distances of up to 400 Km. in the Scandinavian shield showed dispersion consistent with a superficial layer about 1 Km. thick with a lower Rayleigh-wave velocity than the underlying material.

The effect of structure on body-wave propagation has not been calculated, but the good agreement between the theoretical and observed seismograms for P and sP phases indicates that long-period body waves are not appreciably affected. In contrast, the more complex appearance of short-period records at PRE is due to structural effects.

Dispersion was applied to the theoretical Rayleigh-waves of Figure 16 using the theoretical dispersion curve shown in Figure 18. The resulting peak amplitudes were then used to determine theoretical seismograms using the method described above. Inferred seismic sources are listed in Table 5 and theoretical seismograms are compared to the observed seismograms in Figure 19. The agreement between theoretical and synthetic seismograms is clearly better than for the case of no dispersion. A small component of volumetric contraction (implosion) (dashed lines in Figure 19) results in a slightly, though not significantly, improved fit.

TABLE 5:

Same as Table 4, except that dispersion shown in Figure 18 has been applied to the Rayleigh-waves. Synthetic seismograms are shown in Figure 17.

Event		Bns	Bne	Dew	C	M_o	V
		X 10^{21} dyne-cm.					x 10^{10} $cm.^3$
26 June	1029	3,27	- 3,09	0,95	2,34	6,9	- 0,39
3 July	0559	2,94	- 2,28	0,31	4,59	9,8	- 0,42
3 July	0644	3,92	- 4,15	-0,71	3,42	9,2	0,02
29 Aug	1359	- 0,65	- 4,18	0	2,67	7,0	- 0,54
TOTAL		9,48	-13,70	0,55	13,02	32,9	- 1,33

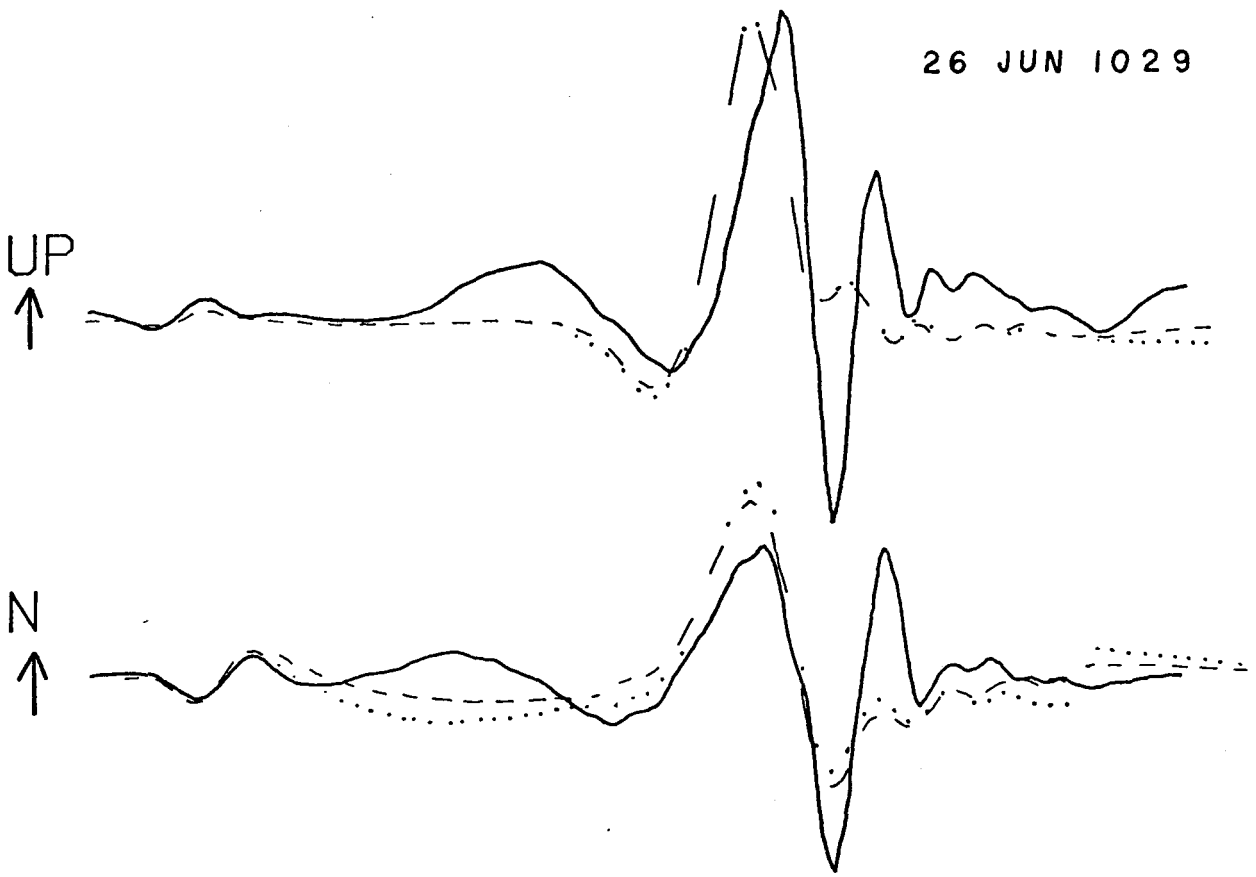

Figure 19. The same as Figure 17, except that dispersion has been applied to the Rayleigh waves.

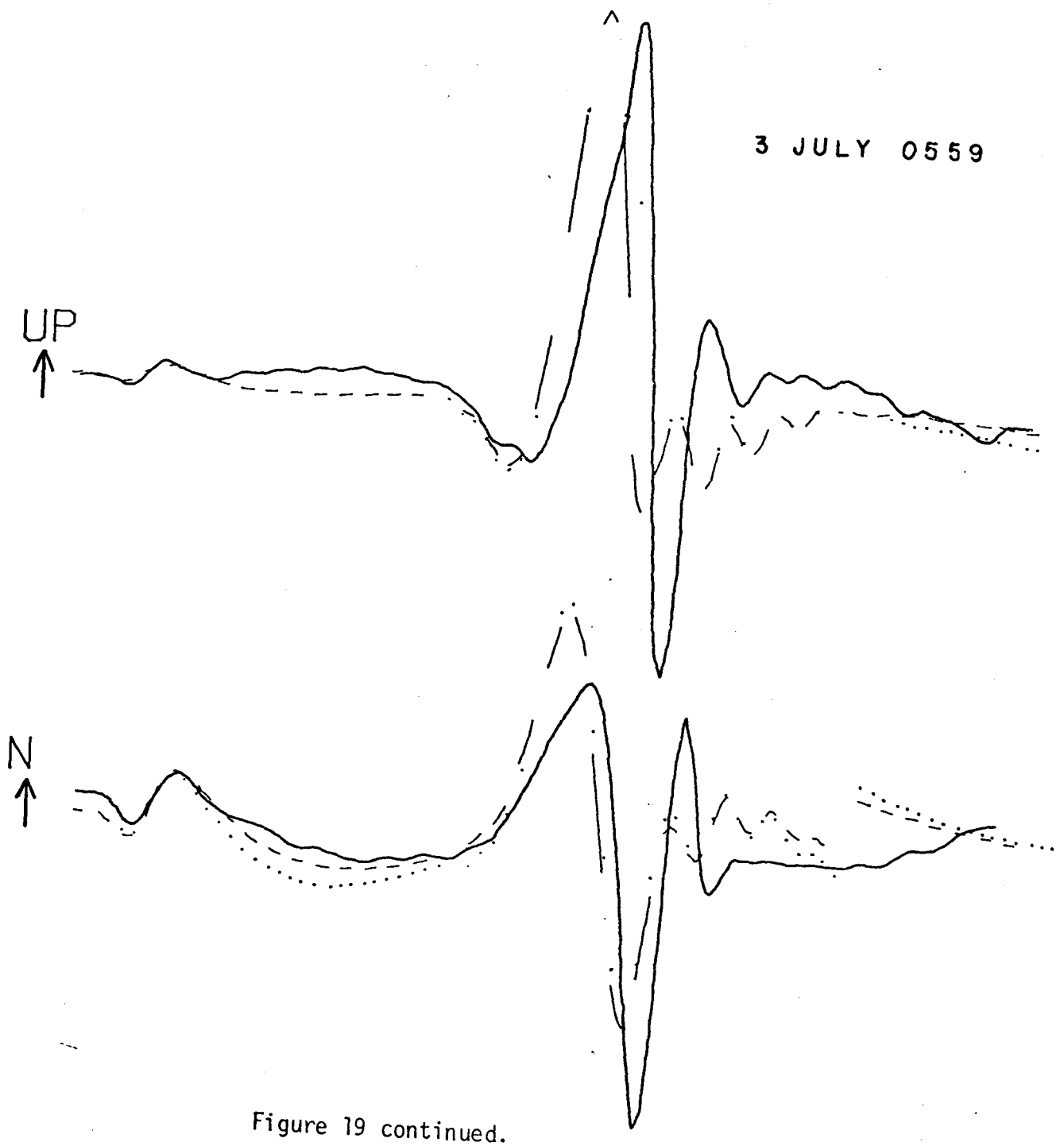

Figure 19 continued.

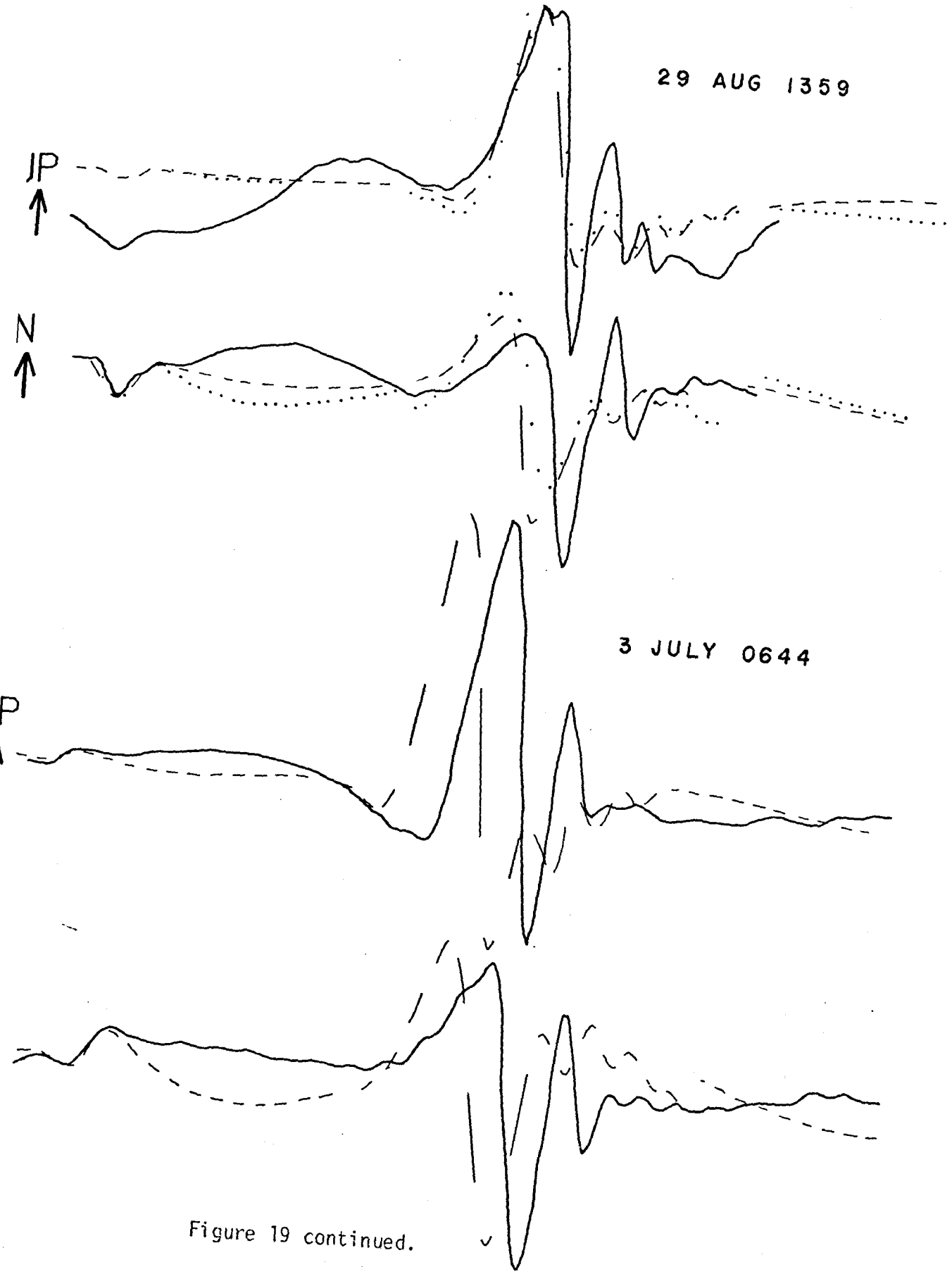

Figure 19 continued.

SOURCE ORIENTATION:

The orientation of the average strain change occurring during seismic events in the vicinity of E.R.P.M. can be estimated by summing the seismic moment tensors presented in Table 5. Equation 5.1 becomes

$$Moij = \begin{matrix} -0{,}68 & 9{,}48 & 0{,}55 \\ 9{,}48 & 26{,}72 & -Dns \\ 0{,}55 & -Dns & -26{,}04 \end{matrix} \times 10^{21} \text{ dyne-cm}$$

For Dns = 0, the principal axes of seismic moments, parallel to the principal axes of strain change, are approximately

M_{o1} = 29,7 x 10^{21} dyne-cm along N 73° E

M_{o2} = − 3,7 x 10^{21} dyne-cm along N 17° W

and M_{o3} = −26,0 x 10^{21} dyne-cm vertically.

Within experimental error, this is equivalent to a normal fault striking N 17° W with a seismic moment of 28 x 10^{21} dyne-cm. Non-zero values of Dns would have the effect of changing the dip angle of fault planes equivalent to this source from 45° to a steeper or shallower dip. Fault-plane solutions of E.R.P.M. seismic events are consistent with fault dip angles between 30° and 70° (chapter 2).

SEISMIC MOMENTS AND MAGNITUDES.

The seismic moments derived from Table 5 using equation (5.2) are shown in Table 6 and compared to the moments calculated from the empirical moment-magnitude relationship suggested in Chapter 4, $\log M_o = 17{,}7 + 1{,}2\ M$.

For the purpose of evaluating equation (5.2), Dns was assumed to be equal to the average of the other shear components. The agreement is well within the error that might be expected from extrapolating the data of Figure 13 to larger magnitudes. Observed peak-to-peak amplitudes of the vertical components are also given in Table 6.

For magnitudes greater than about 3, moments of E.R.P.M. seismic events can be estimated from

$$M_o = 1{,}2 \times 10^{21}\ Az \quad \text{dyne-cm/mm} \qquad (5.3)$$

where Az is the peak-to-peak amplitude of L-Pz in mm. This is a more direct measure of moment than is obtained through a moment-magnitude relationship.

TABLE 6:

Theoretical seismic moments derived from Table 6 and from $\log M_o = 17,7 + 1,2\ M$.

Event	M	Table 5	$10^{17,7 + 1,2\ M}$	Az
		x 10^{21} dyne-cm.		mm.
26 June 1029	3,5	6,9	7,9	9,3
3 July 0559	3,6	9,8	10,5	6,8
3 July 0644	3,4	9,2	6,0	9,3
29 Aug 1359	3,5	7,0	7,9	1,8
TOTAL		32,9	32,3	27,2

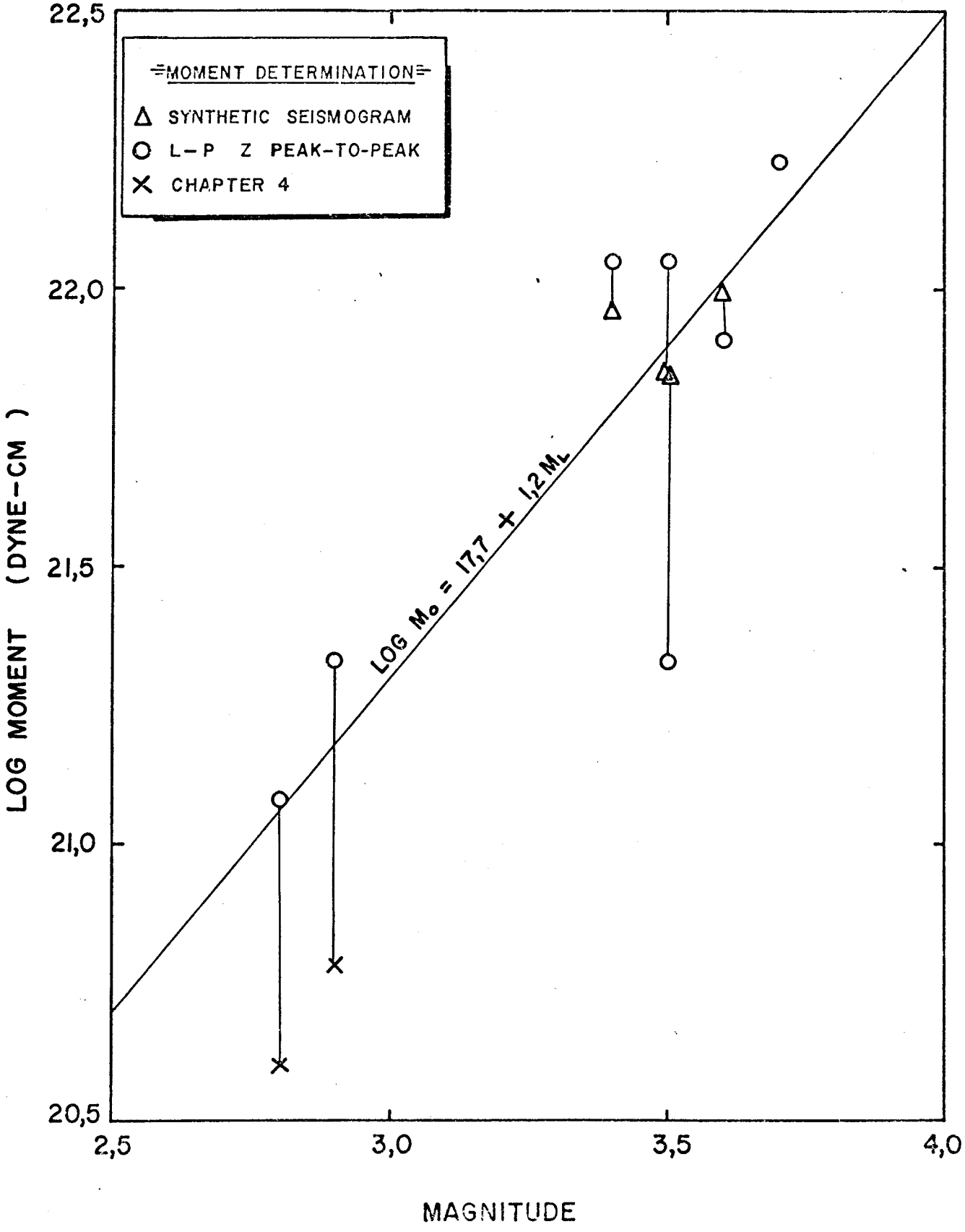

Fig. 20. SEISMIC MOMENT AS A FUNCTION OF MAGNITUDE.

Very small PRE long-period seismograms were identified for two of the events in 1972 for which moments were determined in Chapter 4. The events on 4 February at 2250 (M = 2,9) and 27 September at 1639 (M = 2,8) gave moments of 6 x 10^{20} and 4 x 10^{20} dyne-cm respectively, determined from body-wave data. The seismograms from which these moments were determined were possibly saturated and the moments are therefore minimum estimates: the magnitudes are equivalent to moments of 15 x 10^{20} and 11 x 10^{20} dyne-cm using log Mo = 17,7 + 1,2 M. PRE L - Pz seismograms for these two events had peak-to-peak amplitudes of about 1,8 mm and 1,0 mm respectively. Seismic moments, using equation (5.3) were therefore 22 x 10^{20} and 12 x 10^{20} dyne-cm.

On 21 April 1978 at 08:30 the largest seismic event to have occurred at E.R.P.M. in ten years occurred with a magnitude of 3,7 and wrote a PRE L - Pz seismogram with a peak-to-peak amplitude of 14 mm.

Moment and magnitude data for this Chapter are summarised in Figure 20.

DISCUSSION:

In this Chapter, synthetic seismograms from generalised point sources at E.R.P.M. were found to match observed seismograms on the long-period components at PRE quite closely. The inferred seismic sources have orientations in good agreement with underground observations (McGarr, 1971) and fault-plane solutions (Chapter 3) and seismic moments in excellent agreement with moments derived from spectra of body-waves (Chapter 4.) Only E.R.P.M. seismic events with magnitudes greater than 3, which usually saturate the S - P records, can be used for this type of analysis because of the low gain of the long-period system.

Records from the long-period components were chosen because data at wavelengths of about 5 Km, as observed on the long-period records, are less affected by attenuation, surface weathering, sedimentary cover and topography than the shorter wavelengths observed on the short-period seismograms. The shorter-period seismograms are correspondingly more complex, whereas synthetic short-period seismograms are no more complex than synthetic long-period seismograms for sources buried in a homogeneous half-space.

Although the four events analysed in this chapter occurred in the vicinity of E.R.P.M., no rockburst damage was reported which could have been caused by any of them. (M. Spengler, personal communication, 1976). Similarly, the magnitude 3,7 event which occurred on 21 April, 1978, caused remarkably little damage for its size although it occurred during the day shift when many people were at the faces. In contrast, seismic events with magnitude less than 3 can cause severe damage to the workings and larger events can be even more damaging. Therefore, large events which cause little or no damage must have released strain energy at some distance from active faces.

West faces at E.R.P.M. are generally advanced in longwalls with strike directions varying from N - S in the East to N30°W - S30°E in the West of the mine and could result in normal faulting striking about N17°W, as inferred in this chapter. East faces strike about N60°E in the East and are less common in the West having been stopped when they reached several of the prominent suite of dykes striking N25°E.

Magnitude 3 seismic events occurring near E.R.P.M. write seismograms on the Geological Survey vertical component short-period stations PRY, BLM and KSR. Unfortunately, seismograms from these stations are not as clear as PRE seismograms. First motion polarities were read to see if they could be used to place additional constraints on the source orientation and especially the amplitudes of the N - S striking dip-slip component. Unfortunately, the epicentral distances of 100 to 400 Km. are close to Moho cross-over distances of about 150 Km. (Gane et al 1956) at which the first arrival could be either P or Pn. The angle of incidence was therefore uncertain. The few first-motion polarities which were reasonably clear did not help define the source orientation.

Moments determined in this Chapter are uncertain by a factor of about two. There is no single factor which is susceptible to large errors, but uncertainties in dispersion and velocities, the unconstrained component, digitising and system calibration could each result in uncertainties of about 20% in the determination of the moment.

Short-period and long-period seismometers have recently been installed at the Bernard Price Institute, about 20 Km. West of E.R.P.M. (October, 1978; R. Green, personal communication). The seismograms can be used, together with PRE records, to determine the complete moment tensor of very large E.R.P.M. seismic events.

Chapter 6.

FAULT GOUGE, DRIVING STRESS AND SEISMIC EFFICIENCY.

ABSTRACT

Fault gouge formed in a mining-induced zone of shear failure at a depth of 2 Km. in a deep mine was compared with gouge formed in laboratory samples tested to beyond failure in triaxial compression. The shear stress acting during the formation of the mining-induced zone of shear failure was found to be about 400 bars, determined using two different methods : using a relationship between seismicity and the volume of mining reported by McGarr and from values of the initial stress and stress drop reported by McGarr and others.

The specific crushing energy, or the work done on the gouge zone per unit surface area of gouge particles (determined here from particle-size distributions) was determined as about $3{,}6 \times 10^5$ ergs/cm^2 for gouge from three laboratory samples and about $4{,}5 \times 10^5$ ergs/cm^2 for mining-induced gouge.

The value for driving stress was used together with empirical relationships between seismic energy, seismic moment and magnitude, determined previously, to determine the seismic efficiency, η , of mine tremors as $\log \eta = 0{,}3\ M - 3{,}1$ for seismic events with magnitude, M, between 0 and 3. Resulting efficiencies range from 8×10^{-4} to 6×10^{-3}.

INTRODUCTION

Geodetic and seismic measurements can be used to estimate changes in the stress field due to shallow earthquakes. Absolute measurements of stress, however, can only be made when access to a region is possible. Deep gold mines in South Africa offer access to mining-induced fault zones which are, in effect, fault zones of very recent earthquakes (e.g. Pretorius, 1966; McGarr, 1971; and Ortlepp, 1978) as mine tremors appear to be similar to natural crustal earthquakes (e.g. Spottiswoode and McGarr, 1975).

Mining-induced fault zones consist of crushed rock in a quasi-planar region across which violent shear displacement has occurred. They are similar in appearance to shear zones in laboratory samples that have formed during brittle failure in triaxial compression.

In this paper, fault gouge from laboratory and mining-induced shear zones are compared and in particular, the amount of energy expended per unit surface area of gouge particles called the "crushing energy" is compared. Mining-induced zones of shear failure are ideally suited for comparison with laboratory samples because the stress conditions during their formation are fairly well known and samples of geologically very fresh samples can be obtained. It will be shown that the crushing energy in the two cases is similar, and much greater than the free surface energy. The physical relationship between crushing energy and free surface energy, if any, remains obscure.

The samples of mining-induced gouge were taken from a shear zone exposed in a network of tunnels, or raises, in the E.R.P.M. gold mine. Two intersecting zones were observed and have been documented in some detail by Ortlepp (1978), Gay and Ortlepp (1979) and McGarr *et al* (1979 a and b). Zone "A" was sampled for this study.

Using a cleavage technique designed to minimise energy losses, Brace and Walsh (1962) found values of surface energy ranging from 450 to 1000 ergs/cm^2 for different cleavage planes of quartz. Prentice (1946) loaded cylinders of Witwatersrand quartzite in uniaxial compression to failure and determined a crushing energy of $5{,}5 \times 10^4$ ergs/cm^2. He concluded that the crushing energy was independent of the free-surface area, i.e. that the new surface area was proportional to the work done. Prentice's testing machine, however, was not designed for stiffness, and so he was not able to determine the post-failure energy which might have been important. Bikerman (1970 p.214) pointed out that crushed quartz has a surface layer of amorphous silica with an associated cuticular energy that greatly increases the apparent surface energy. Kanellopoulis and Ball (1975) stated that the large difference between "tensile" surface energy measured on sharp cracks and "compressional" surface energy (crushing energy) required to crush ore in mills must appear as kinetic, thermal and acoustic energy, as well as energy of plastic deformation in the mill.

LABORATORY TESTS.

Three cylindrical samples of E.R.P.M. quartzite, 7,62cm long and 2,54 cm in diameter, were tested to failure and beyond in a stiff triaxial testing machine (Hojem, et al., 1975). In each case a single shear zone at about 30° to the axis of the sample accommodated most of the motion. The confining pressure, σ_r, was exerted by oil through rubber jackets and was kept constant to within a few bars at either 138 bars (sample 20) or 276 bars (samples 21 and 22) by varying the volume of confining fluid manually. 276 bars confining pressure was close to the maximum capability of the testing machine. An axial strain rate of 10^{-5} sec^{-1}, much greater than the ambient strain rate of about 10^{-10} sec^{-1} in E.R.P.M. (McGarr and Green, 1975) was maintained. The strain rate during seismic failure at E.R.P.M. is, of course, much greater and has not been measured. Solid lines in Figure 21 show axial strain, ϵ_1, as a function of axial stress, σ_1, and lateral strain as a function of axial strain.

Samples 21 and 22 followed very nearly the same curves until the confining rubber jacket around sample 21 leaked during the crucial stage of rapid stress drop. Unloading of sample 21 was assumed to occur in the way shown in Figure 21. Average lateral strain $(\epsilon_1 + \epsilon_2)/2$ was determined from the change in the volume of liquid used to hold the confining stress in the load cell constant. Compressive stresses and strains are taken as positive. Dotted lines are the expected unloading, down to zero axial stress, based on an unloading displacement of 0.08mm at the end of the test on sample 22, giving a remnant axial strain, and on a Poisson's ratio of 0.5 for unloading (Hojem et al., 1975), giving a remnant lateral strain. Loading of sample 20 was terminated when the confining rubber jacket leaked.

Figure 21. Variation of axial strain with axial stress and lateral strain for three samples of E.R.P.M. quartzite. Broken lines are inferred values for unloading. (Figure courtesy of C. Heins).

The work done on each sample, W, was calculated from

$$W = V\int \sigma_1 \, d\epsilon_1 + 2\int V\sigma_r \, d\epsilon_r \qquad (1)$$

where V is the volume of the sample. The first term is the work done on the sample by the axial driving piston during the full cycle of loading and unloading. The second term is the work done on the sample by the constant confining pressure and is a negative quantity: about 30% of the work done on the samples by axial compression is spent on lateral expansion against the confining stress. Integration over ϵ_1 is achieved by measuring the area under the stress-strain curve in Figure 21 and over ϵ_r by multiplying the confining stress by the final lateral strain. The energy involved in imposing and releasing the confining stress is less than 1% of W and is not included in the calculations.

Almost all the alteration of brittle rocks caused by failure under conditions of triaxial compression occurs in the zone of shear failure; even before the maximum stress is reached most permanent deformation occurs along the final shear zone (e.g. Hallbauer et al, 1973). Therefore, almost all the work done on the samples is accommodated as resistance, τ, to shear movement, D, over fault area, A :

$$W \approx \int \tau(A) \; D\,(A) \; dA \qquad (2)$$

For triaxial tests, D is a constant over the area of failure and $\bar{\tau}$, the mean driving stress can be written as

$$\bar{\tau} \approx W/AD \qquad (3)$$

The processes at work within shear zones in rock are poorly understood at present and only the particle-size distribution and surface area of gouge particles are investigated in this study and compared to the work done on laboratory and mining-induced shear zones.

$\bar{\tau}$ is called the mean driving stress rather than the mean frictional stress here because the term friction is generally used to describe resistance between two predetermined surfaces. Friction is also often equated with heat production.

DETERMINATION OF CRUSHING ENERGY

The most marked alteration of the samples is the zone of shear failure, where rock is comminuted to form gouge (defined here for convenience as the minus 35 mesh fraction of the shear zone, that is, particles having sizes of less than 0,5mm).

Hallbauer et al (1973) found that the intensity of shear failure under triaxial compression increased as more deformation took place : more gouge was formed as more work was being done on the shear zone.

The crushing energy, G, of gouge is defined here as

$$G = W/MS \qquad (4)$$

where M is the mass of gouge in the sample, and S is the surface area per unit mass. Heat, acoustic energy and deformation outside the shear zone are also energy sinks.

The surface area created in the shear zones was estimated by measuring individual particles of quartz in the gouge to determine the size distribution. This method was chosen in preference to gas absorption, which requires larger quantities of gouge.

Small samples of the gouge were placed in oil on a glass slide, stirred to separate the individual particles and covered with a cover slip. The width of each particle, measured on the calibrated eyepiece of a microscope, was used as a measure of size. Particles were found to vary in size down to less than 5 μm.

To estimate the size distribution, more than 400 particles near a reference line across the slide were counted and measured. At low magnification the width of every particle within a wide strip across the slide was measured, while at intermediate and high magnification every particle within narrower regions adjacent to the same line was measured. As particles of different sizes have similar shapes, the mass of a particle is proportional to the cube of the width, and the (outside) surface area is proportional to the square

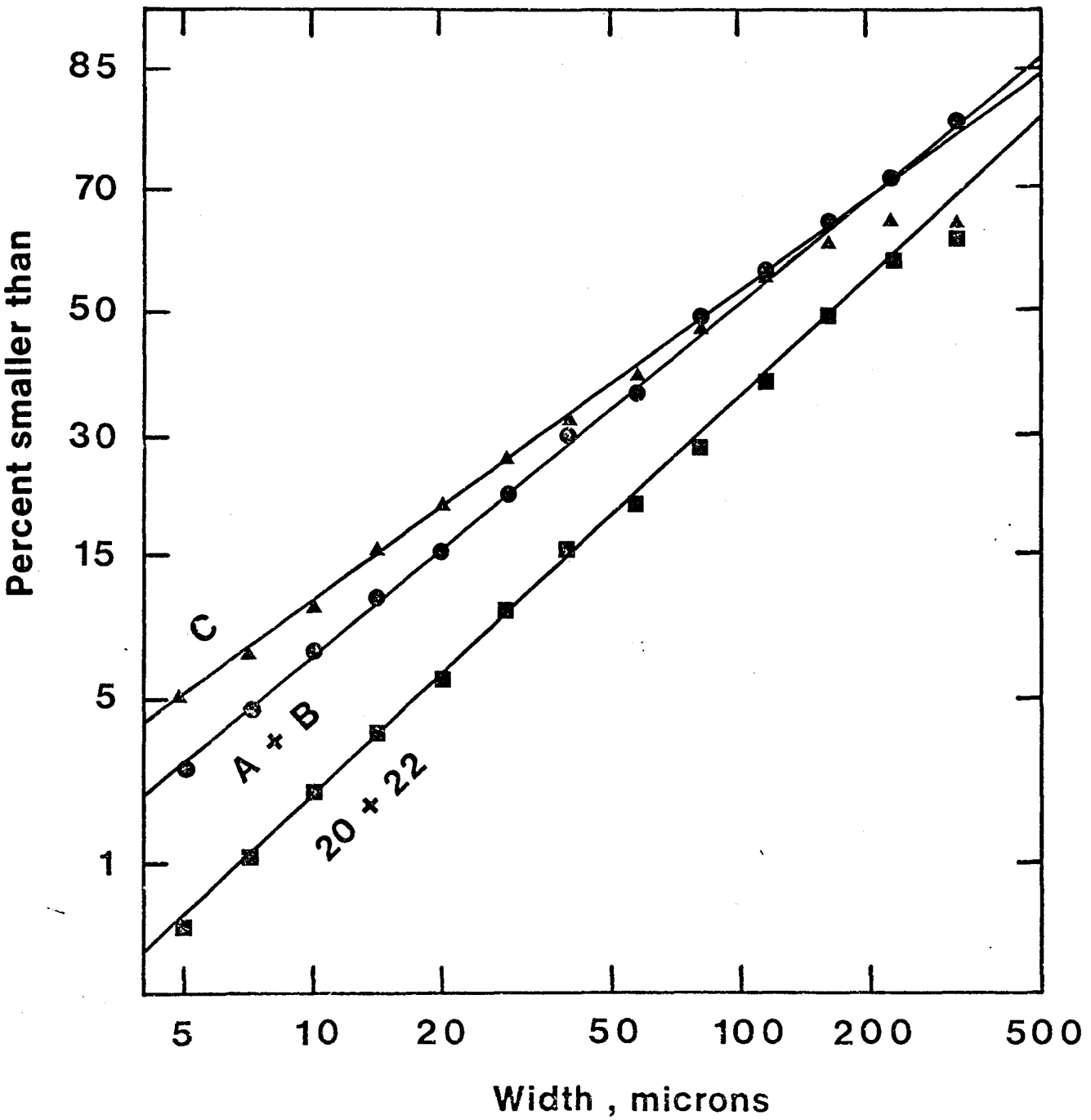

Figure 22. Cumulative particle size distribution, by weight, for laboratory samples (20 + 22) and two mine-induced shear zone samples (A + B and C), plotted on log-probability scales.

of the width. The mass distributions were calculated from particle counts for twelve intervals separated by $5 \times 2^{N/2}$ μm, with N = 0,1,2 .....12. Counts at different magnifications were normalised to an areal density (mass per unit area) on the slide. Larger particles very close to the reference line were observed at different magnifications.

The particle-size distributions of comminuted material are generally well described by the log-normal law (e.g. Herdan, 1953, p. 113). Accordingly, log-normal curves were fitted to the observed mass distributions of particles between 5μm and 320μm in width using a least-squares procedure. Particles consisting of more than one grain from the host rock were not considered; this excluded almost all of the particles larger than 320μm. The proportions for all sizes less than 5μm and greater than 320μm were taken from the log-normal curves determined from the data between 5μm and 320μm and varied by less than 25% when different weights are attached to the data in the least-squares determination. The inferred particle size distribution for samples 20 and 22 combined is shown in Figure 22 as 20 + 22. The axes in Figure 22 are log-probability and a straight line describes a log-normal distribution.

The surface area per unit mass determined from particle-size distributions is given by $S = (K/\rho)\ m_i/x_i$, where m_i is the proportion, by mass, of particles of size x_i, K is a geometric shape factor, taken as 11 from Herdan (1953, p. 50) and $\rho = 2{,}7\ gm/cm^3$, the density of quartz.

The summation is taken over the twelve size intervals measured, as well as for all sizes smaller than 5μm. Particles with sizes greater than 320μm contribute little to the total free-surface area.

Table 7 presents some experimentally determined parameters for the three laboratory samples. Driving stresses, $\bar{\tau}$, were calculated using equation (3) where the area of failure was calculated for an angle, θ, of 30° between the axis of the sample and the shear zone, and the shear displacement was calculated from the residual axial strain. By eliminating the maximum principal stress, σ_1, from $\tau = \frac{1}{2}(\sigma_1 - \sigma r) \sin 2\theta$ and $\bar{\sigma}n = \sigma_1 \sin^2\theta + \sigma_r \cos^2\theta$ the average stress normal to the shear plane was calculated from $\bar{\sigma}n = \sigma_r + \tau \tan \theta$

The crushing energy associated with surface areas determined from particle size distributions of gouge from E.R.P.M. quartzite, formed under a normal stress of about 700 bars, was 2,7 x 10^5 ergs/cm^2 for sample 20 and 4,5 x 10^5 ergs/cm^2 for sample 22, with an average value of 3,6 x 10^5 ergs/cm^2. Sample 21, for which W was uncertain due to poorly determined stress-strain conditions, gave a value of approximately 5 x 10^5 ergs/cm^2.

DRIVING STRESS INFERRED FROM SEISMICITY

McGarr (1976) and McGarr and Wiebols (1977) found that the total seismicity in three separate regions of E.R.P.M. was related to the volume of stope closure, ΔV_c, (convergence) due to mining by

$$\Sigma M_o = \mu \Delta V_c \qquad (5)$$

TABLE 7: FAILURE AND GOUGE PARAMETERS OF TWO SAMPLES OF ERPM QUARTZITE TESTED IN TRIAXIAL COMPRESSION

Sample	σ_r (bars)	σ_1 max (Kbars)	W (10^8 ergs)	$\bar{\tau}$ (bars)	$\bar{\sigma}_n$ (bars)	M (gm)	S (cm^2/gm)	G (10^5 ergs/cm^2)
20	138	3,40	7,3	800	600	3,50	780	2,7
21	276	4,32	5,4	1550	1170	1,81	600	5,0
22	276	4,24	11,0	930	810	3,04	800	4,5
20 + 22	-	-	18,3	-	-	6,54	790	3,6

where ΣM_o is the sum of all the seismic moments of seismic events which occurred during the time for ΔV_c of convergence and μ is the modulus of rigidity.

Combining (5) with the definition of seismic moment, $M_o = \mu AD$,

$$\Sigma AD = \Delta V_c \qquad (6)$$

The gravitational energy, W_G, released by convergence, is related to the ambient vertical stress, σ_1, by

$$W_G = \sigma_1 \Delta V_c \qquad (7)$$

from Cook et al, (1966, equation 3 - 43).

Equation (3) can be generalised as

$$\Sigma W = \bar{\tau} \Sigma AD \qquad (8)$$

where $\bar{\tau}$ is the mean driving stress acting during shear displacement on the fault planes of the entire suite of events associated with the convergence of ΔV_c. W is the resulting work done by the shear stress driving the faulting.

From equations (6) and (8)

$$\Sigma W = \bar{\tau} \Delta V_c \qquad (9)$$

ΣW and W_G are equivalent to W and $V\int \sigma_1 d\epsilon_1$ in equation (2). About 30% of the work done by $V\int \sigma_1 d\epsilon_1$ on the laboratory samples used for this study went into work done against the confining stress; therefore $W \approx 0,7 \int \sigma_1 \; d\epsilon_1$. The role of horizontal stresses in the strain energy balance at E.R.P.M. is unknown. However, seismic events at E.R.P.M. have fault mechanisms consistent with normal faulting (e.g. Spottiswoode et al, 1971) and a certain amount of work has to be done against the horizontal stresses. Assuming $W = 0,7\ W_g$ and using equations (7) and (9),

$$\bar{\tau} = 0,7\ \sigma_1 \qquad (10)$$

The mean driving stress is therefore equal to about 70% of the weight of the overburden, $\sigma_1 = \rho gh$, where $\rho = 2,7$ gm/cm^3 and $g = 980$ cm/sec^2. For the burst zone studied here, the depth below surface, H is 2,1 Km. The mean driving stress from this analysis is therefore 390 bars. For H = 3,3 Km, a more typical depth of mining in E.R.P.M. at present (1979), $\bar{\tau}$ = 610 bars.

Ortlepp (1978) correlated shear zone A with a seismic event with a magnitude of 2,1 which occurred on 23 September, 1970. McGarr et al (1979a) used this magnitude and underground observations to determine a mean shear stress drop, $\Delta\tau$, of about 700 bars. McGarr et al (1979b) applied a simplified elastic analysis using the mining geometry near zone A during September 1970 and estimated a maximum shear stress of about 900 bars acting in the region of shear zone A. The shear stress acting on a plane oriented at 30° to the maximum principal stress, a more common failure orientation, was therefore about 780 bars. The average driving stress acting on shear zone A was therefore about $\bar{\tau} = \tau_1 - \Delta\tau/2$ = 430 bars. This is in very good agreement with the value of 390 bars determined above, considering the uncertainties involved. A value of 410 bars will be used for the driving stress acting during the formation of zone A.

The stress normal to zone A before its formation was between 1 and 2 kbar, from the calculations of McGarr et al (1979b). The normal stress should remain constant during the shear stress drop.

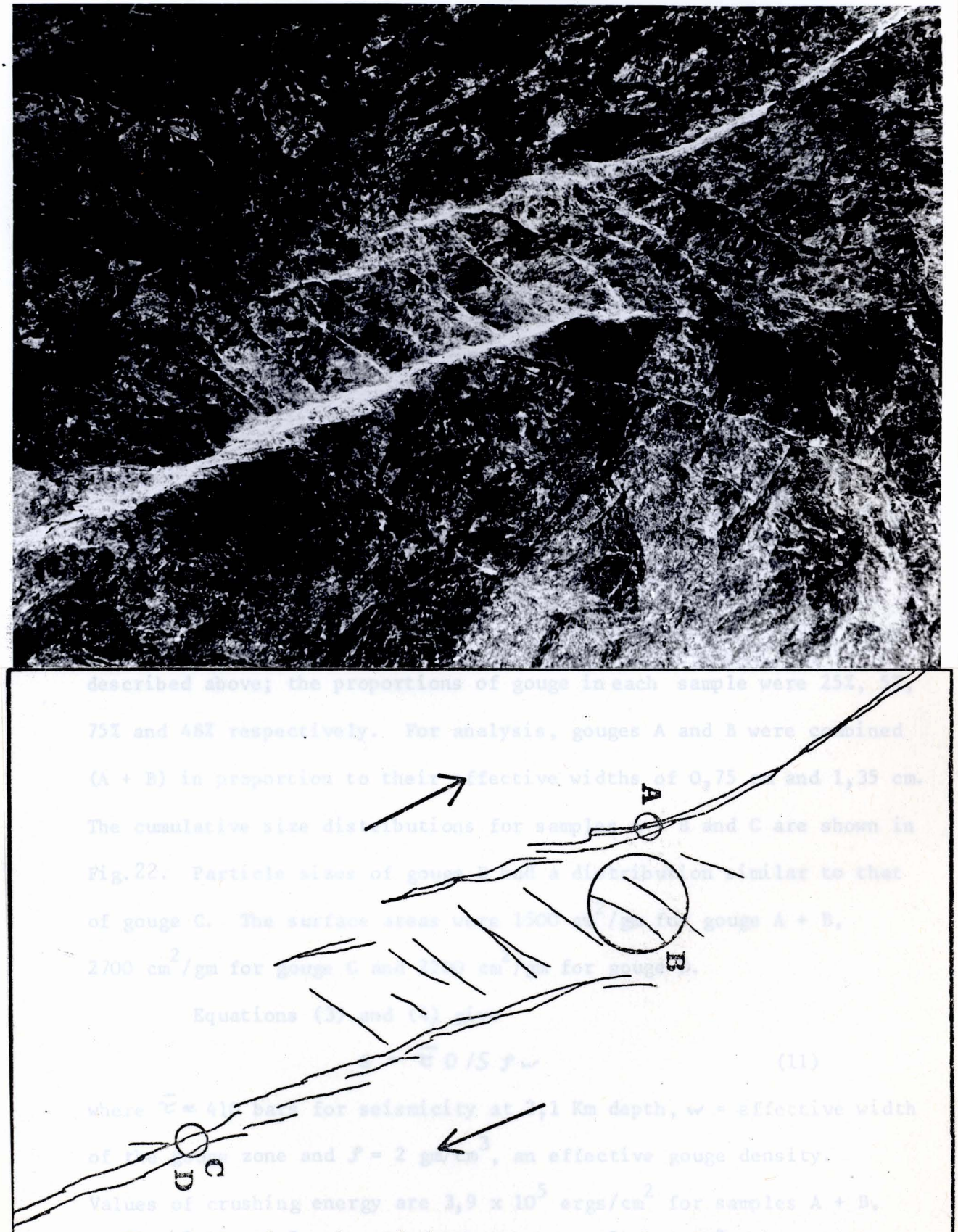

Figure 23. A portion of the burst zone sampled for this study. Regions A, B, C, and D in sketch are similar to regions sampled. Arrows indicate direction of movement.

(photograph courtesy of W.D. Ortlepp)

CRUSHING ENERGY FROM FAULT GOUGE.

Four samples (samples A, B, C and D) were taken from burst zone A, from regions similar to regions A, B , C and D in Figure 23. The samples represented separate regions of the fault zone where it was not widely dispersed. Sample C was taken from an intensely comminuted zone 1 cm wide across which shear displacement of about 5 cm occurred. Sample A and B came from a more diffuse section of the shear zone where it was about 30 cm wide. Throughout most of this width the rock was fragmented. Comminution was more marked in a zone 3 cm wide on one side of the shear zone and sample A was taken from there, while sample B represented the other 27 cm. The total displacement across sites A and B is about 6 cm.

Samples A, B, C and D were sieved and the particle-size distributions and free-surface areas were determined using the method described above; the proportions of gouge in each sample were 25%, 5%, 75% and 48% respectively. For analysis, gouges A and B were combined (A + B) in proportion to their effective widths of 0,75 cm and 1,35 cm. The cumulative size distributions for samples A + B and C are shown in Fig. 22. Particle sizes of gouge D had a distribution similar to that of gouge C. The surface areas were 1500 cm^2/gm for gouge A + B, 2700 cm^2/gm for gouge C and 2200 cm^2/gm for gouge D.

Equations (3) and (4) give

$$G = \bar{\tau} D / S \rho w \qquad (11)$$

where $\bar{\tau} \approx 410$ bars for seismicity at 2,1 Km depth, w = effective width of the gouge zone and $\rho = 2\ gm/cm^3$, an effective gouge density. Values of crushing energy are $3,9 \times 10^5$ $ergs/cm^2$ for samples A + B, $5,1 \times 10^5$ $ergs/cm^2$ for sample C and $4,7 \times 10^5$ $ergs/cm^2$ for sample D (Table 8), close to the values determined above for laboratory samples.

TABLE 8 : CRUSHING ENERGY FROM BURST-ZONE GOUGE

Gouge	w cm	D cm	S cm^2/gm	G_5 10^5 $ergs/cm^2$
A + B	2,1	6	1500	3,9
C	,75	5	2700	5,1
D	1,2	6	2200	4,7
			Av.	4,5

SEISMIC EFFICIENCY

The seismic efficiency, $\eta = E_s/E_{TOT}$, the seismic energy divided by the total energy released during a seismic event, can be expressed as

$$\eta = \mu E_s / \bar{\tau} M_o \qquad (12)$$

(e.g. Wyss and Brune, 1968) where $\mu = 4 \times 10^{11}$ dynes/cm^2 is the modulus of rigidity and M_o is the seismic moment of the event. King (1969) assuming a driving stress of 300 bars, calculated a seismic efficiency of the order of 1% for earthquakes of magnitude 3 to 5. McGarr (1976) calculated a seismic efficiency of 0,24% for E.R.P.M. events by dividing the total seismic energy of a series of mine tremors by the total energy released due to the closure of the workings.

Spottiswoode and McGarr (1975) found that

$$\text{Log } M_o = 1{,}2\ M + 17{,}7 \qquad (13)$$

gave a reasonable fit to data from E.R.P.M. seismic events with magnitudes from 0 to 3 and

$$\text{Log } E_s = 1{,}5\ M + 11.8 \qquad (14)$$

which was derived by Gutenberg and Richter (1956) for surface-wave-magnitudes of large shallow earthquakes, provided a good fit to the observed relationship between the seismic energy in ergs, and local magnitude, M_L for magnitudes between 0 and 3. Using equations (12) (13) and (14) and $\bar{\tau} = 610$ bars appropriate for a typical mining depth at present (1979) (equation (10)), seismic efficiency and total energy release can be expressed as

$$\text{Log } \eta = 0{,}3\ M_L - 3{,}1 \qquad (15)$$

and

$$\text{Log } E_{TOT} = 1{,}2\ M_L + 14{,}9 \qquad (16)$$

McGarr (1976) compared the integrated seismicity with the volume of excavation closure for two periods of time in a region of E.R.P.M. In table 9, equation (16) is applied to the magnitude distribution during these two periods, with magnitudes taken in intervals of 0.4 (McGarr, 1976, Tables 2 and 3). McGarr calculated the total energy release during these two periods as $3,48 \times 10^{18}$ ergs and $3,82 \times 10^{18}$ ergs by multiplying the maximum principal stress of rock at the depth of the region considered, 3.3 km, by the volume of convergence caused by this stress for each period. The total energy release calculated from equation (11) for the tremors is $2,54 \times 10^{18}$ ergs amd $2,83 \times 10^{18}$ ergs for the two periods considered, close to McGarr's estimates of the total available energy. Within experimental error, this agrees with McGarr's conclusion that the total seismic moment accounts for most of the volume of stope convergence, and confirms his estimates of seismic efficiency.

TABLE 9 : TOTAL ENERGY RELEASE FOR TWO SUITES OF E.R.P.M. SEISMIC EVENTS (MAGNITUDE DISTRIBUTIONS FROM MCGARR, 1975) USING

$$\text{LOG } E_{TOT} = 1{,}2\ M_L + 14{,}9$$

M_L	E_{TOT} 10^{16} ergs	N	N E_{TOT} 10^{16} ergs	N	N E_{TOT} 10^{16} ergs
2.5	79,4	1	79,4	1	79,4
2.1	26,3	3	78,9	4	105,2
1.7	8,7	8	69,7	5	43,5
1.3	2,9	4	11,5	10	28,8
0.9	0,95	6	5,7	19	18,1
0.5	0,32	15	4,7	15	4,7
0.1	0,10	35	3,7	27	2,8
		E_{TOT} =	254	E_{TOT} =	283

DISCUSSION

The concept of crushing energy applied to fault gouge has not been applied previously for three good reasons. Firstly, there is no theoretical basis for assuming that the crushing energy will remain constant during different conditions, or even throughout the formation of a single shear zone. Secondly, very few determinations of crushing energy have been made and those that have been made have been for the purpose of judging the efficiency of crushing rock in mills. The third and most important reason is that it is generally impossible to reproduce gouge in the laboratory similar to natural fault gouge.

Mining-induced shear zones are very similar to brittle shear zones in laboratory samples (e.g. Gay and Ortlepp, 1979) and are therefore very suitable for testing the possibility that crushing energy can be used to relate field to laboratory stress conditions. Using $G = 3{,}6 \times 10^5 \text{ergs/cm}^2$ from laboratory samples and equation (11) rewritten as $\bar{\tau} = GS\rho\, w/D$, data from Table 8 give values of driving stress ranging from 290 to 380 bars, close to the value of 410 bars determined above.

Despite the obvious contrast in the rate of formation, the laboratory and mining-induced gouge samples used for this study were remarkably similar. Individual particles are indistinguishable under the optical microscope. The intensity of comminution is similar, with particle sizes fitting log-normal distributions (Figure 22). The same features are observed on both types of gouge using a scanning electron microscope (N.C. Gay, personal communication). No evidence of melting has been seen. The small-scale fracture mechanisms were therefore alike in the two cases: individual particles probably broke down into smaller particles at near sonic velocities.

Engelder (1974) studied the generation of fault gouge in sandstones, considering properties such as grain-size distributions, gouge width and the number of subfractures. $\bar{\tau}$ can be determined from a shear fracture subsidiary to the Bonita fault in Mesa Rica sandstone by applying equation (4) to grain-size distributions presented in Figure 4 of Engelder (1974): curves I and IV are grain-size distributions of undeformed sandstone and sandstone from a shear fracture subsidiary to the Bonita fault. Assuming log-normal distributions, the apparent surface areas corresponding to curves I and IV are 600 and 1800 cm^2/gm, respectively, giving a value of S between 1200 and 1800 cm^2/gm, depending on the degree of cementing in the undeformed sandstone. Using G = $3,6 \times 10^5$ $ergs/cm^2$, determined from laboratory samples of quartz gouge in this study, w/D = 0,063 from Figure 5 of Engelder (1974) and ρ = 2,0 gm/cm^3, equation (11) results in a driving stress between 50 and 80 bars. This technique cannot be applied to faults along which repeated movement has occurred because it does not account for recementing of the gouge between successive displacements.

CONCLUSIONS.

Brittle failure of E.R.P.M. quartzite in controlled laboratory conditions and uncontrolled conditions during a mine tremor produce shear zones filled with very similar gouge. In addition, the crushing energy, defined as the work done in producing the shear zone divided by the total surface areas of particles of gouge, was found to be about 4×10^5 ergs/cm^2 in each case. This value is two to three orders of magnitude greater than free surface energy for quartz (Brace and Walsh, 1962).

The seismic efficiency, $\eta = Es/E_{TOT}$, of E.R.P.M. tremors is empirically related to magnitude by $\text{Log}\eta = 0{,}3M - 3{,}1$ and the total energy release(in ergs)during a tremor is given by $\text{Log } E_{TOT} = 1{,}2\ M + 14{,}9$ for $0 < M < 3$ at a depth of about 2.1 Km below surface.

Further research using crushing energy, or some other measure of gouge development, could give valuable insight into the forces at work during earthquakes, or even creep events, on natural fault zones.

APPENDIX A1.

Seidel's method of successive approximations.

Seidel's method of successive approximations can be illustrated in two dimensions as follows : -

Suppose observations are assumed to satisfy an equation of the form

$$f\ (Xi, \alpha, \beta) = 0, \qquad (1)$$

where i = 1, N, Xi is an independent variable (known), and α and β are dependent variables (unknown).

Preliminary approximations are made for α and β ; a and b.

Let $\delta a = \alpha - a$ and $\delta b = \beta - b$.

Equation (1) can now be written as

$$f\ (Xi,\ a + \delta a,\ b + \delta b) = 0 \qquad (2)$$

Performing a Taylor expansion on equation (2) and neglecting squares, products and higher powers of δa and δb,

$$f\ (Xi,\ a,\ b) + \frac{\partial f}{\partial a}\ \delta a + \frac{\partial f}{\partial b}\ \delta b = 0 \qquad (3)$$

where $\frac{\partial f}{\partial a}$ and $\frac{\partial f}{\partial b}$ are the partial derivatives of $f(Xi, \alpha, \beta)$ with respect to α and β evaluated at $\alpha = a$ and $\beta = b$. δa and δb are now selected to minimise the sum of the squares of f :

$$\sum_{i=1}^{N} (f\ (Xi,\ a,\ b) + \frac{\partial f}{\partial a}\ \delta a + \frac{\partial f}{\partial b}\ \delta b)^2 \qquad (4)$$

The normal equations for δa and δb may be written

$$\begin{aligned} &\sum_{i=1}^{N} \frac{\partial f}{\partial a}\ (f\ (Xi,\ a,\ b) + \frac{\partial f}{\partial a}\ \delta a + \frac{\partial f}{\partial b}\ \delta b) = 0 \\ &\sum_{i=1}^{N} \frac{\partial f}{\partial b}\ (f\ (Xi, a,\ b) + \frac{\partial f}{\partial a}\ \delta a + \frac{\partial f}{\partial b}\ \delta b) = 0 \end{aligned} \qquad (5)$$

On solving these equations and adding δa to a and δb to b, the preliminary approximations are improved. The process can be repeated if necessary and usually converges quite rapidly to a solution. In some cases successive movements might be oscillatory.
Oscillations can be overcome by reducing the movements (δa and δb) after several iterations. This method can be extended to any number of independent and dependent variables.

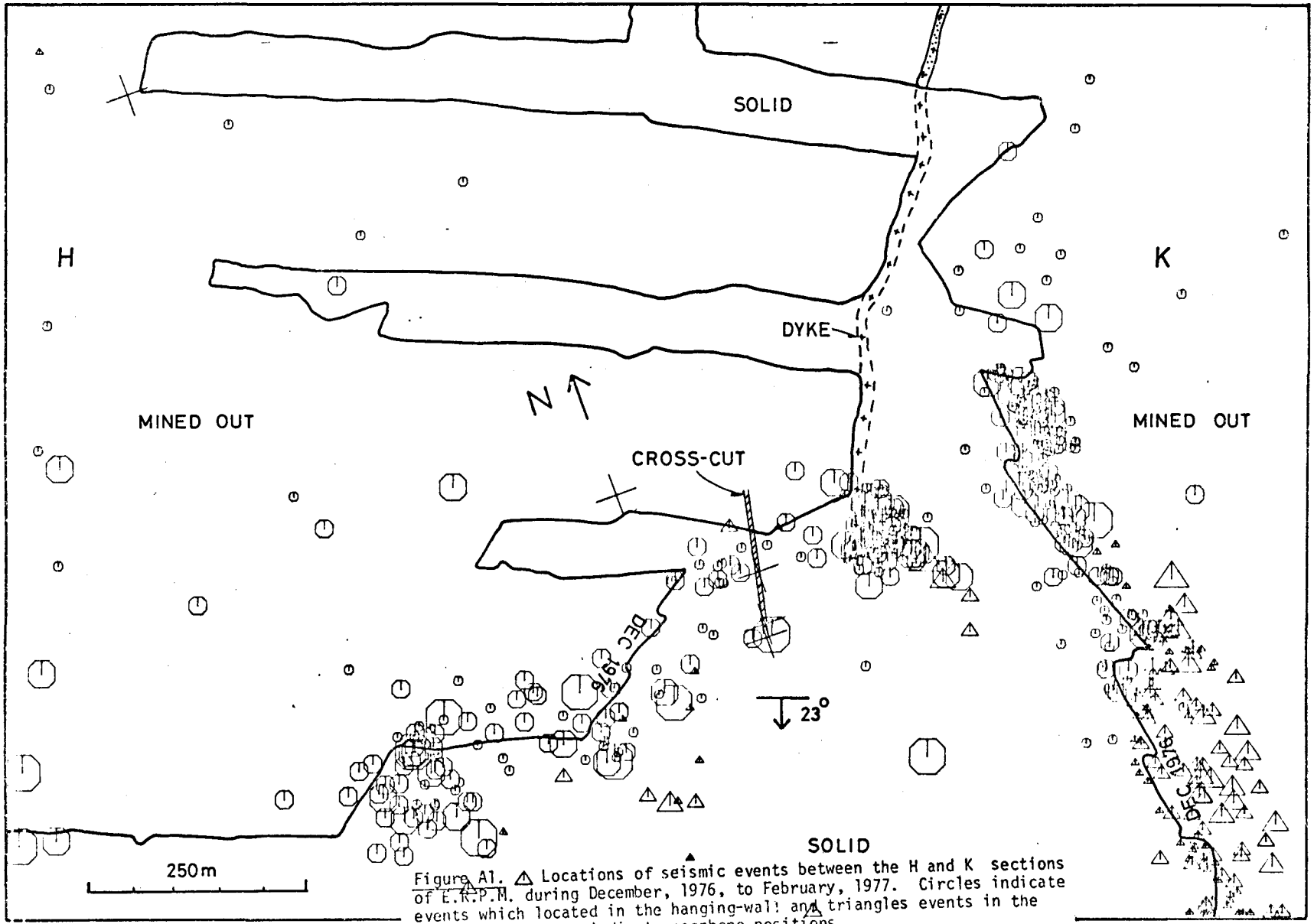

Figure A1. △ Locations of seismic events between the H and K sections of E.R.P.M. during December, 1976, to February, 1977. Circles indicate events which located in the hanging-wall and triangles events in the footwall. Crosses indicate geophone positions.

```
0001            DIMENSION SKU(20),VEL(20),EVENT(3),ARTM(20),DF(4),SS(10),RR(4),
                1         NARR(16),RES(16),DIS(16),XA(10),YA(10),ZA(10),STN(2)
                C****     THIS PROGRAM WAS DEVELOPED BY S. M. SPITTLESWOODE
                C      DURING 1977 FOR LOCATING E.R.P.M. SEISMIC EVENTS.
                C         SEIDEL'S METHOD OF SUCCESSIVE APPROXIMATIONS
                C         IS USED TO IMPROVE AN INITIAL GUESS LOCATION.
0002            REAL RDIR(6)/.228,-.271,.176,-.168,.420,1.0/
0003            LOGICAL LEAP,LDONE
0004            DIST(X,Y,Z) = SQRT(X*X+Y*Y+Z*Z)
0005            WRITE(6,201)
0006      201   FORMAT('1    X',7X,'Y',7X,'Z    HEAD SKEW',4X,'P',6X,'S',7X,
                1       'GEOPHONE')
0007            DO 87 I=1,10
0008            READ(5,10)(XA(I),YA(I),ZA(I),SKU(I),SKU(I+10),
                1          VEL(I),VEL(I+10),STN)
0009      10    FORMAT(7F5.0,5X,5A4)
                C****     10 GEOPHONES ARE USED FOR LOCATIONS, LABELLED 1 TO 10.
                C         (XA(I),YA(I),ZA(I),I=1,10) ARE X, Y & Z COORDINATES IN METERS.
                C         MINE COORDINATES ARE USED : X+ : WEST,
                C                                     Y+ : NORTH,
                C                                     Z+ : DOWN.
                C         SKU(I),I=1,10 : HEAD SKEW CORRECTIONS APPLIED TO P ARRIVALS.
                C         SKU(I),I=11,20 : HEAD SKEW CORRECTIONS APPLIED TO S ARRIVALS.
                C         IN GENERAL SKU(I+10) = SKU(I).
                C         STATION RESIDUALS CAN BE INCORPORATED BY CHANGING
                C         P AND/OR S HEAD SKEW CORRECTIONS.
                C         VEL(I),I=1,10 : P VELOCITIES TO EACH GEOPHONE.
                C         VEL(I),I=11,20 : S VELOCITIES  TO EACH GEOPHONE.
0010      87    WRITE(6,22)(XA(I),YA(I),ZA(I),SKU(I),SKU(I+10),
                1          VEL(I),VEL(I+10),STN)
0011      22    FORMAT(3F8.0,2F5.0,2F7.2,5X,5A4)
0012            NLINE = 14
0013      70    READ(5,13,END=99,ERR=99)EVENT,SCAL,ARTM,NPOOR1,NPOOR2
0014      13    FORMAT(3A4,F4.1,20F3.1,2I2)
                C****     EVENT : EVENT TITLE ; USUALLY DATE & TIME.
                C         SCAL : PAPER SPEED OF HARD-COPY RECORD IN MM/(FIELD) SECOND.
                C         ARTM(I),I=1,10 : 10 P ARRIVALS IN MM
                C         ARTM(I),I=11,20 : 10 S ARRIVALS IN MM.
                C         (P AND S ARRIVALS ARE READ IN IN THE SAME ORDER AS
                C         USED FOR GEOPHONE COORDINATES, VELOCITIES & HEAD SKEWS).
                C****     NPOOR1 & NPOOR2 : GEOPHONE NUMBER (NPOOR = NPOOR+10 FOR S)
                C         OF UNCERTAIN ARRIVALS.
                C      NPOOR2 = 0 IF ONLY ONE ARRIVAL IS CONSIDERED UNCERTAIN.
                C      NPOOR1 = 0 IF ALL ARRIVALS HAVE BEEN READ WITH CONFIDENCE.
0015            NLINE = NLINE+12
0016            IF(NPOOR1.GT.0)NLINE = NLINE+8
0017            IF(NPOOR2.GT.0)NLINE = NLINE+8
                C
                C
                C
                C
                C
                C
```

```
      IF(NLINE.GT.115)NLINE=0
      IF(NLINE.EQ.0)WRITE(6,660)
660   FORMAT('1')
66    IF(NLINE.NE.0)WRITE(6,661)
661   FORMAT(///)
C****    NLINE IS USED TO SKIP TO  A NEW PAGE OF OUTPUT
C        NEAR THE END OF EVERY SECOND PAGE.
      WRITE(6,20)EVENT
20    FORMAT(2X,3A4,/,'  ************')
      IF(SCAL.LE.0.)GO TO 70
      IF(NPOOR1.GT.20)NPOOR1 = 0
      IF(NPOOR2.GT.20)NPOOR2 = 0
      NNEW = 0
      TM = 10000.
C****    ARRIVAL TIMES ARE CONVERTED FROM MM TO MILLISECONDS.
C        HEAD SKEW CORRECTIONS ARE ADDED.
C        EARLIEST ARRIVAL IS IDENTIFIED.
      DO 1 I=1,20
      IF(ARTM(I).EQ.0.)GO TO 1
      ARTM(I) = 1000.*ARTM(I)/SCAL+SKU(I)
      IF(ARTM(I).GE.TM)GO TO 1
      TM = ARTM(I)
      M = I
1     CONTINUE
73    MM = M-10*((M-1)/10)
C****    THE FIRST (GUESS) LOCATION IS CHOSEN CLOSE TO THE GEOPHONE
C        AT WHICH FIRST ARRIVAL IS READ.
      EVX = XA(MM)-400.
      EVY = YA(MM)
      EVZ = ZA(MM)
      EVT = TM-60.
C****    THE ORIGIN TIME OF THE EVENT IS DETERMINED FROM EACH GEOPHONE
C        FOR WHICH BOTH P & S ARRIVALS WERE READ.
      DO 2 I=1,10
      IF(ARTM(I+10).LE.0. .OR. ARTM(I).LE.0.)GO TO 2
      VR = VEL(I+10)/VEL(I)
      T0 = (ARTM(I) - ARTM(I+10)*VR)/(1.-VR)
      EVT = T0
      WRITE(6,221)I,T0,ARTM(I),ARTM(I+10)
221   FORMAT(I5,' , T0 =',F5.0,2F8.0)
      NLINE = NLINE+1
      IF(T0.GT.TM)WRITE(6,222)M
222   FORMAT('+',35X,'THIS IS AFTER ARRIVAL',I3)
2     CONTINUE
      LDONE = .FALSE.
72    IT = 0
      LFAR = M.EQ.9
C
C
C
C
C
C
```

```
                C****     THE ITERATIVE PROCEDURE USED FOR IMPROVING
                C         THE GUESS COORDINATES STARTS HERE.
                C         FOR MOST EVENTS FEWER THAN 6 ITERATIONS ARE REQUIRED
                C         FOR SATISFACTORY CONVERGENCE.
                C         CONVERGENCE IS CONSIDERED TO BE SATISFACTORY IF THE MOVEMENT
                C         BETWEEN SUCCESSIVE ITERATIONS IS LESS THAN 1 METER.
0056            71      IT = IT+1                                                       0340
                C****     ALL THE TERMS OF THE MATRICES SS & RR
                C       (USED FOR IMPROVING THE LOCATION) ARE SET TO ZERO.
0057                    DO 161 J=1,14                                                   0350
0058            161     SS(J) = 0.                                                      0360
0059                    N = 0                                                           0370
0060                    NN = 0                                                          0380
                C****     N ARRIVALS WERE READ.
                C         NN ARRIVALS ARE USED TO LOCATE THE EVENT DURING EACH PASS.
                C         (N-3 <= NN <= N)
0061                    ERROR = 0.                                                      0390
0062                    WMAX = 0.                                                       0400
0063                    DO 164 I=1,20                                                   0410
0064                    IF(ARTM(I).EQ.0.)GO TO 164                                      0420
0065                    IF(N.EQ.15)GO TO 164                                            0421
                C****     NO MORE THAN 15 ARRIVALS ARE USED.
0066                    N = N+1                                                         0430
0067                    II = I-10*((I-1)/10)                                            0440
0068                    X = EVX-XA(II)                                                  0450
0069                    Y = EVY-YA(II)                                                  0460
0070                    Z = EVZ-ZA(II)                                                  0470
0071                    D = DIST(X,Y,Z)                                                 0480
0072                    IF(IT.GE.3 .AND. I.EQ.M .AND. D.GT.1200.)LEAR = .TRUE.          0481
0073                    VV = VEL(I)
                C****     P VELOCITIES ARE FIXED AT 6.1 KM/SEC.
                C       & S VELOCITIES ARE FIXED AT 3.8 KM/SEC FOR DISTANT EVENTS.
0074                    IF(LEAR)VV = 6.1 - 2.3*(I/11)                                   0491
                C****     W : DISTANCE RESIDUAL = (THEORETICAL - OBSERVED) DISTANCE
                C         FROM EVENT TO GEOPHONE , METERS.
0075                    W = D+(EVT-ABS(ARTM(I)))*VV                                     0492
0076                    NARR(N) = ISIGN(I,IFIX(ARTM(I)))                                0500
0077                    RES(N) = W/VV                                                   0510
0078                    IF(I.EQ.NPOOR1)RES1 = W                                         0511
0079                    IF(I.EQ.NPOOR2)RES2 = W                                         0512
0080                    DIS(N) = D                                                      0520
0081                    IF(ARTM(I).LT.0.)GO TO 164                                      0530
                C****     NEGATIVE ARRIVAL TIMES ARE NOT USED FOR LOCATIONS.
0082                    NN = NN+1                                                       0540
                C****     ARRIVALS FROM CLOSE GEOPHONES ARE GIVEN A GREATER EMPHASIS
                C         THAN ARRIVALS FROM MORE DISTANT GEOPHONES.
                C         THE WEIGHTING FACTOR USED HERE (WT) IS CHOSEN
                C         TO BE CONSISTENT WITH ERRORS IN VELOCITIES
                C
                C
                C
                C
```

```
C          TO EACH GEOPHONE AND ERRORS IN PICKING ARRIVALS.
0083            WT = 10000./(600.+D)                                    0541
0084            WW = ABS(W)*WT                                          0550
C****           THE LEAST CONSISTENT ARRIVAL IS IDENTIFIED.
0085            IF(WMAX.GT.WW)GO TO 170                                 0551
0086            IMAX = I                                                0560
0087            WMAX = WW                                               0570
0088       170  ERROR = ERROR+W*W                                       0580
C****           DF(I),I=1,3 ARE THE DIRECTIONAL COSINES
C          FROM EACH (IMPROVED) LOCATION TO EACH GEOPHONE.
0089            DF(1) = X/D                                             0590
0090            DF(2) = Y/D                                             0600
0091            DF(3) = Z/D                                             0610
0092            DF(4) = VV                                              0620
C****           RR(I),I=1,4 & SS(I),I=1,10 ARE COEFFICIENTS OF THE MATRICES
C          USED TO CALCULATE THE CORRECTION FACTOR USED TO IMPROVE THE LOCATION
0093            JK = 0                                                  0630
0094            DO 165 J=1,4                                            0640
0095            RR(J) = RR(J)+DF(J)*W*WT                                0650
0096            DO 165 K=1,J                                            0660
0097            JK = JK+1                                               0670
0098       165  SS(JK) = SS(JK)+DF(J)*DF(K)*WT                         0680
0099       164  CONTINUE                                                0690
0100            IF(NN.GT.5)GO TO 166                                    0691
C****           EVENTS WITH ONLY 3, 4 OR 5 READ ARRIVALS ARE LOOSELY CONSTRAINED
C          TO 100 M. ABOVE (HERCULES) REEF.
0101            W = EVZ - 4554. - .168*EVX + .420*EVY                   0692
0102            RR(1) = RR(1) -.168*W                                   0693
0103            RR(2) = RR(2) + .420*W                                  0694
0104            RR(3) = RR(3) + W                                       0695
0105            DO 167 JK = 1,5                                         0696
0106       167  SS(JK) = SS(JK) + ROIR(JK)                             0697
0107            NN = NN+1                                               0698
0108            N = N+1                                                 0699
0109            NARR(N) = 999                                           0700
0110            RES(N) = W                                              0708
0111            DIS(N) = W                                              0709
0112            IF(NN.LT.4)GO TO 72                                     0700
C****           LEQT1P IS A SUBROUTINE IN THE INTERNATIONAL MATHEMATICAL
C          AND STATISTICAL LIBRARY (IMSL).
C          LEQT1P SOLVES THE EQUATION A*X = B.
C          WHERE A IS AN N BY N MATRIX STORED IN SYMMETRICAL STORAGE MODE.
C          AND B IS AN M BY N MATRIX.
C          FOR THIS PROGRAM N = 4 AND M = 1.
0113       166  CALL LEQT1P(SS,1,4,RR,4,IGDT,D1,D2,IER)                0710
C****           THE AMOUNT OF MOVEMENT DURING EACH SUCCESSIVE ITERATION
C          IS RESTRICTED BY "FIX". THIS GUARDS AGAINST OSCILLATORY BEHAVIOUR
C          SOMETIMES FOUND USING SEIDELS METHOD.
C
C
C
C
```

```
      FIX = 1.2-FLOAT(IT)/20.
      EVX = EVX-RR(1)*FIX
      EVY = EVY-RR(2)*FIX
      EVZ = EVZ-RR(3)*FIX
      EVT = EVT-RR(4)*FIX
      ERROR = SQRT(ERROR/(NN-3.999))
      D = DIST(RR(1),RR(2),RR(3))
C****    EVENT IS CONSIDERED TO DIVERGE IF ITERATION MOVEMENT > 5 KM.
      IF(D.GT.5000.)GO TO 999
C****    EVENT IS CONSIDERED TO CONVERGE IF ITERATION MOVEMENT < 1 M.
      IF(D.GT.1.0 .AND. IT.LE.15)GO TO 71
      IF(LEAR)WRITE(6,220)
220   FORMAT(' VELOCITIES OF 6.1 & 3.8 KM/SEC USED')
C****    EVX, EVY & EVZ ARE THE MINE COORDINATES OF THE EVENT LOCATION.
C        EVT IS THE ORIGIN TIME RELATIVE TO THE COMMON REFERENCE TIME.
C        ON THE HARD-COPY RECORD IN MILLISECONDS.
C        ERROR = SQRT((SUM OF SQUARES OF DISTANCE RESIDUALS IN METERS)
C        /(NUMBER OF ARRIVALS USED FOR LOCATION - 4))
      WRITE(6,21)EVX,EVY,EVZ,EVT,ERROR
21    FORMAT('0X =',F7.0,', Y =',F7.0,', Z =',F6.0,', T =',F5.0,
     1       ', ERROR =',F5.0)
      IF(IT.GT.6)WRITE(6,25)IT
25    FORMAT('+',60X,'OVER',I3,' ITERATIONS')
C****    NARR(N) : GEOPHONE NUMBER OF NTH ARRIVAL
C        (N = 11 TO 20 FOR S ARRIVALS)
C        IF NARR < 0 ,ARRIVAL IS NOT USED FOR THIS LOCATION.
C        NARR = 999 : EVENT IS LOOSELY CONSTRAINED TO 100M ABOVE
C                     (HERCULES) REEF.
      WRITE(6,26)NN,(NARR(I),I=1,N)
26    FORMAT(/,I3,' ARRIVALS ',16I7)
C****    RES : (THEORETICAL - OBSERVED) ARRIVAL TIME , MSEC.
      WRITE(6,27)(RES(I),I=1,N)
27    FORMAT(' RESIDUALS     ',16F7.0)
C****    DIS(I) = (HYPOCENTRAL) DISTANCE BETWEEN GEOPHONE I
C        AND EVENT LOCATION.
      WRITE(6,28)(DIS(I),I=1,N)
28    FORMAT(' DISTANCE      ',16F7.0)
      IF(NPOOR1.EQ.0)GO TO 171
C****    UNCERTAIN ARRIVAL TIMES ARE MADE NEGATIVE AND THE LOCATION
C        IS REPEATED WITHOUT THEM.
C        IF TWO ARRIVALS ARE UNCERTAIN I.E. NPOOR2 NOT EQUAL TO ZERO.
C        LOCATION IS REPEATED FIRST WITHOUT THE UNCERTAIN ARRIVAL
C        WHICH HAS THE LARGER TIME RESIDUAL.
      IF((NPOOR2.EQ.0).OR.(ABS(RES1).GT.ABS(RES2)))GO TO 129
      ARTM(NPOOR2) = -ARTM(NPOOR2)
      WRITE(6,29)NPOOR2
29    FORMAT('0RELOCATE WITHOUT DOUBTFUL ARRIVAL',I3)
C
C
C
C
```

```
                NPOOR2 = 0
                GO TO 72
      129       ARTM(NPOOR1) = -ARTM(NPOOR1)
                WRITE(6,29)NPOOR1
                NPOOR1 = NPOOR2
                NPOOR2 = 0
                GO TO 72
      171       CONTINUE
                IF(NNEW.NE.0)GO TO 173
      C****        DOUBTFUL OR BADLY INCONSISTENT ARRIVALS ARE TESTED TO SEE
      C              IF THEY COULD HAVE BEEN PICKED AS THE INCORRECT PHASE.
      C              IF SO, THE LOCATION IS REPEATED WITH THE "CORRECTED" DATA.
                DO 172 I=1,N
                NOLD = -NARR(I)
                IF(NOLD.LE.0)GO TO 172
                II = ISIGN(1,21-2*NOLD)
                IF(ABS(II*DIS(I)/RES(I)+10.5).GT.2.0)GO TO 172
                NNEW = NOLD+10*II
                ARTM(NNEW) = -ARTM(NOLD)
                ARTM(NOLD) = 0.
                WRITE(6,272)NOLD,NNEW
      272       FORMAT('0TRY ARRIVAL',I3,' AS ARRIVAL',I3)
                GO TO 72
      172       CONTINUE
      173       CONTINUE
                IF((XMAX.LT.300.) .OR. LDONE .OR. (NN.LE.6))GO TO 72
      C****        IF ANY ARRIVAL IS INCONSISTENT BY MORE THAN ABOUT 50 M
      C              (AT 1 KM.) COMPARED TO THE EXPECTED LOCATION,
      C              A FURTHER LOCATION IS DONE WITHOUT IT.
                LDONE = .TRUE.
                WRITE(6,23)IMAX
      23        FORMAT('0****',I3,' ???? ****')
                ARTM(IMAX) = -ARTM(IMAX)
                NLINE = NLINE+3
                GO TO 72
      999       WRITE(6,24)IT
      24        FORMAT('+',40X,'DIVERGES AFTER',I3,' ITERATIONS')
                WRITE(6,21)EVX,EVY,EVZ,EVT,ERROR
                WRITE(6,26)NN,(NARR(I),I=1,N)
                IF(NPOOR1.EQ.0)GO TO 72
      C****        DIVERGENT LOCATIONS ARE REPEATED WITHOUT UNCERTAIN ARRIVALS.
                ARTM(NPOOR1) = -ARTM(NPOOR1)
                WRITE(6,29)NPOOR1
                NPOOR1 = NPOOR2
                NPOOR2 = 0
                GO TO 73
      99        STOP
                END
```

APPENDIX A3 PRE Long-Period response.

System parameters generally used to describe the response of a seismograph system consisting of a seismometer driving a galvanometer are maximum gain, Ts, hs , Tg and hg, where Ts and hs are the free period and damping coefficient of the seismometer and Tg and hg are the free period and damping of the galvanometer These parameters can be determined for WWSSN stations from the daily calibration caused by a step in acceleration achieved by passing a constant current through a calibration coil adjacent to the seismometer coil. The response to an impulse in displacement is required when synthetic seismograms are generated and can be determined in theory by differentiating the calibration pulse three times with respect to time. This procedure is not feasible as it would exaggerate microseismic and higher-frequency noise enormously.

System parameters were determined from calibration pulses using Seidel's method (Appendix A2, Jarosch and Curtis, 1973). In addition, the time at which the calibration pulse started was also considered as a variable and was calculated simultaneously (Mitronovas, 1976). Calibration pulse records were digitised by hand for 64 samples at two second intervals after the D.C. level was carefully chosen. Corrections were made for the ramp effect of the recording drum. The noise level at PRE is quite high and some problems were experienced with this noise.

Groups of three calibration pulses were considered together and the five system parameters and three starting times were determined simultaneously. The system response constants are shown in Table A1 for the three components and the impulse response of the three long-period components at PRE is shown in Figure A1.

TABLE A1 PRE L - P RESPONSE CONSTANTS.

COMPONENT	Max. gain	Ts sec.	Tg sec.	hs	hg
Z	1539	15,6	96,5	0,86	0,93
E - W	1645	11,1	95,2	1,09	0,96
N - S	1633	14,5	98,8	0,81	1, 05

KEY:

Ts : Free period of seismometer.

Tg : Free period of galvanometer.

hs : Damping coefficient of seismometer.

hg : Damping coefficient of galvanometer.

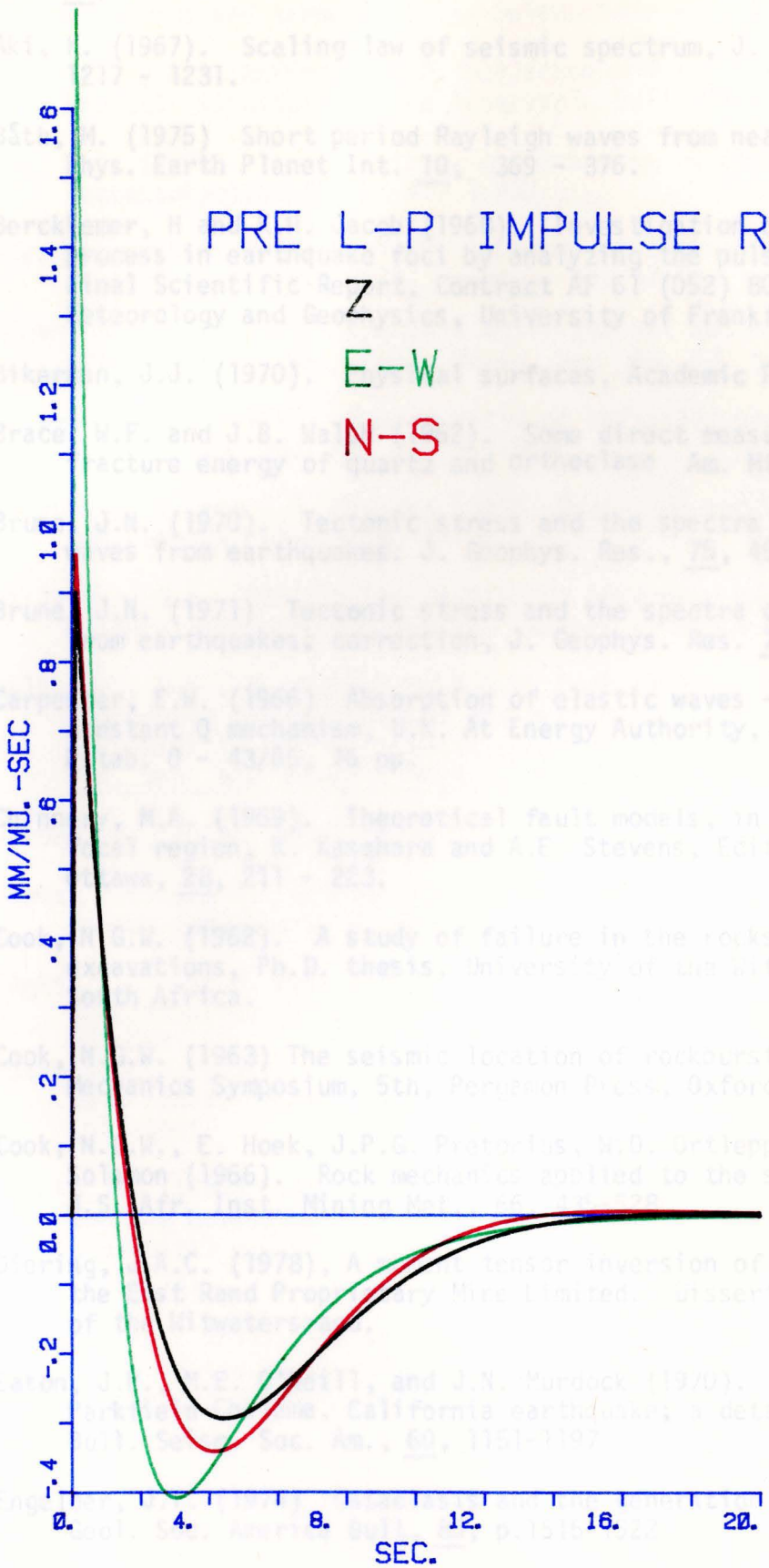
PRE L-P IMPULSE RESPONSE
Z
E-W
N-S
MM/MU.-SEC
1.6
1.4
1.2
1.0
.8
.6
.4
.2
0.0
-.2
-.4
0.
4.
8.
12.
16.
20.
SEC.

Figure A2.

REFERENCES

Aki, K. (1966) Generation and propagation of G waves from the earthquake of 16th June, 1964, Bull. Earthquake Res. Inst., Tokyo Univ., 44, 73-88.

Aki, K. (1967). Scaling law of seismic spectrum, J. Geophys Res. 72, 1217 - 1231.

Båth, M. (1975) Short period Rayleigh waves from near-surface events, Phys. Earth Planet Int. 10, 369 - 376.

Berckhemer, H and K.H. Jacob (1968). Investigation of the dynamical process in earthquake foci by analyzing the pulse shape of body waves. Final Scientific Report, Contract AF 61 (052) 801, Institute of Meteorology and Geophysics, University of Frankfurt, Germany 85.

Bikerman, J.J. (1970). Physical surfaces, Academic Press, London, pp. 214.

Brace, W.F. and J.B. Walsh (1962). Some direct measurements of the fracture energy of quartz and orthoclase Am. Miner, 47, p.1111-1122

Brune, J.N. (1970). Tectonic stress and the spectra of seismic shear waves from earthquakes. J. Geophys. Res., 75, 4997 - 5009

Brune, J.N. (1971) Tectonic stress and the spectra of seismic shear waves from earthquakes; correction, J. Geophys. Res. 76, 5002

Carpenter, E.W. (1966) Absorption of elastic waves - An operator for a constant Q mechanism, U.K. At Energy Authority, At. Weapons Res. Estab. O - 43/66, 16 pp.

Chinnery, M.A. (1969). Theoretical fault models, in A Symposium on the focal region, K. Kasahara and A.E. Stevens, Editors, Publ. Dom. Obs. Ottawa, 28, 211 - 223.

Cook, N.G.W. (1962). A study of failure in the rocks surrounding underground excavations, Ph.D. thesis, University of the Witwatersrand, Johannesburg, South Africa.

Cook, N.G.W. (1963) The seismic location of rockbursts, in Proc. Rock Mechanics Symposium, 5th, Pergamon Press, Oxford, p 493-561

Cook, N.G.W., E. Hoek, J.P.G. Pretorius, W.D. Ortlepp, and M.D.G. Solamon (1966). Rock mechanics applied to the study of rockbursts. J.S. Afr. Inst. Mining Met., 66, 435-528

Diering, J.A.C. (1978), A moment tensor inversion of two rockbursts at the East Rand Proprietary Mine Limited. Dissertation, University of the Witwatersrand.

Eaton, J.P., M.E. O'Neill, and J.N. Murdock (1970). Aftershocks of the 1966 Parkfield-Cholame, California earthquake; a detailed study, Bull. Seism. Soc. Am., 60, 1151-1197

Engelder, J.T. (1974) Cataclasis and the generation of fault gouge, Geol. Soc. America Bull., 85, p.1515-1522

Gane, P.G., A.L. Hales and H.A. Oliver (1946). A seismic investigation of the Witwatersrand earth tremors, Bull. Seism. Soc. Am., 36, 49-80.

Gane, P.G., P. Seligman and J.H. Stephen (1952). Focal depth of Witwatersrand tremors, Bull. Seism. Soc. Am., 42, p.239-250

Gane, P.G., A.R. Atkins, J.P.F. Sellschop and P. Seligman (1956). Crustal structure in the Transvaal, Bull. Seism. Soc. Am.,46, 293-316.

Gay, N.C. (1975), In situ stress measurements in Southern Africa, Tectonophysics, 29, p. 447 1 459.

Gay, N. and W.D. Ortlepp, 1979. Anatomy of a mining-induced fault zone, Geol. Soc. America Bull., part 1, 90, 47-58.

Green, R.W.E. (1973), A portable multi-channel seismic recorder and a data processing system. Bull. Seism. Soc. Am.,63, 423-432

Gutenberg, B. (1944). Energy ratio of reflected and refracted seismic waves, Bull. Seism. Soc. Am. 34, 85-102.

Gutenberg, B. and C.F. Richter (1956) Magnitude and energy of earthquakes, Ann. Geofis. (Rome), 9, 1-15.

Hallbauer, D.K. (1967). The continuous recording of seismic events at Western Deep Levels, Limited, Chamber of Mines Project 109/64.

Hallbauer, D.K., H. Wagner and N.G.W. Cook (1973). Some observations concerning the microscopic and mechanical behaviour of quartzite specimens in stiff, triaxial compression tests. Int. J. Rock Mech. Min. Sci. and Geomech. Abstr., 10, 717-726

Herdan, G. (1953) Small particle statistics, Elsevier, Amsterdam, p. 50 and 11

Hanks, T.C. and W. Thatcher (1972). A graphical representation of seismic source parameters, J. Geophys. Res. 77, 4393-4405.

Hanks, T.C. and M. Wyss (1972). The use of body-wave spectra in the determination of seismic source parameters. Bull. Seism. Soc. Am. 62, 561-589

Haskell, N.A. (1964). Total energy and energy spectral density of elastic wave radiation from propagating faults, Bull. Seism. Soc. Am. 54, 1811-1841

Heunis, R. (1976). Improvements in the design of seismic location systems and the development of a seismic method for the delineation of geological dykes in mines (in Afrikaans). MSc. Thesis, University of Pretoria.

Hodgson, K. (1967). The behaviour of the failed zone ahead of a face, as indicated by continuous seismic and convergence measurements, Chamber of Mines Research Report No. 31/67.

McGarr, A. and R.W.E. Green (1972). A comparison of the focal mechanism and aftershock distribution of the Ceres, South Africa earthquake of September 29, 1969, Bull. Seismol. Soc. Am, 62, 869-871

McGarr, A (1974). Earthquake prediction: Absence of a precursive change in seismic velocities before a tremor of magnitude $3\frac{3}{4}$, Science, 185, p. 1047-1049.

McGarr, A. and Green, R.W.E. (1975) Measurement of tilt in a deep-level gold mine and it's relationship to mining and seismicity. Geophys. J.R. Astr. Soc., 43, p. 327-345

McGarr, A., Spottiswoode, S.M. and Gay, N.C. (1975). Relationship of mine tremors to induced stresses and to rock properties in the focal region. Bull. Seismol. Soc. Amer., 65, p.981-993.

McGarr, A. (1976). Seismic moments and volume changes, J. Geophys. Res. 81, p. 1487-1494.

McGarr, A. and Wiebols, G.A. (1977), Influence of mine geometry and closure volume on seismicity in a deep-level mine. Int. J. Rock Mech. Min. Sci. and Geomech. Abstr., 14, p.139-145.

McGarr, A, I.S. Sacks, A. Linde, S.M. Spottiswoode and R.W.E. Green, 1978, Coseismic strain steps recorded by Sacks-Everton volumetric strainmeters in a deep mine, South Africa, Abstract, EOS, 59, 1209.

McGarr, A., S.M. Spottiswoode, N.C. Gay and W.D. Ortlepp (1979a) Observations relevant to seismic driving stress, stress drop, and efficiency. J. Geophys.Res., 84, 2251-2261.

McGarr, A., D. Pollard, N.C. Gay and W.D. Ortlepp (1979b) Observations and analyses of some consistent structures in two exhumed mine-induced shear zones, Open-File Report 79-1239, Proc. of Conference VIII. Analysis of actual fault zones in Bedrock, U.S. Geological Survey, Menlo Park, California.

McNally, K.C. and T.V. McEvilly (1977). Velocity contrast across the San Andreas fault in Central California: Small-scale variations from P-wave nodal plane distortion, Bull. Seism. Soc. Am., 67, 1565-1576.

Mitronovas, W. (1976). Accuracy in phase determination of L.P. electromagnetic seismographs based on transient calibration pulse. Bull. Seism. Soc. Am., 66, 97-104.

Molnar, P., B. Tucker, and J.N. Brune (1973). Corner frequencies of P and S waves and models of earthquake source. Bull. Seism. Soc. Am. 63, 2091-2104.

Ortlepp, W.D. (1978). The mechanism of a rockburst, Proc. 19th. U.S. Rock Mech. Symp., Stateline, Nevada, 476-483, 1978.

Perret, W.R. (1972). Seismic source energies of underground nuclear explosions, Bull. Seism Soc. Am., 62, 763-774.

Hojem, J.P.M., Cook, N.G.W. and C. Heins (1975). A stiff, two mega-Newton testing machine for measuring the work-softening behaviour of brittle materials. S. Afr. Mech. Engr. 25, p. 250-270.

Iida, K. (1965). Earthquake magnitude, earthquake fault, and source dimension, J. Earth Sci. Nagoya Univ. 13, 115-132.

Jaeger, J.C. and N.G.W. Cook (1969) Fundamentals of Rock Mechanics, Methuen, London.

Jarosch, H. and A.R. Curtis (1973). A note on the calibration of the electro-magnetic seismograph, Bull. Seismol. Soc. Am. 63, 1145-1155

Johnson, L.R. (1974). Greens function for Lambs' problem, Geophys. J. 37,99-131

Johnson, L.R. and T.V. McEvilly (1974), Near-field observations and source parameters of central California earthquakes. Bull. Seismol. Soc. Am. 64, 1855-1886.

Joughin, N.C. (1966). The measurement and analysis of earth motion resulting from underground rock failure, Ph.D. Thesis, University of the Witwatersrand, South Africa.

Kennellopoulis, A. and Ball, A. (1975). The fracture and thermal weakening of quartzite in relation to comminution. J.S. Afr. Inst. Min. Metall., 76, p.45-52.

King, C.Y. (1969). Seismic efficiency. J. Geophys. Res., 74, p.1702.

Keilis- Borok, V.I. (1960), Investigation of the mechanism of earthquakes, Sov. Res. Geophys.(English Transl.) 4, 29.

Knopoff, L. and F. Gilbert (1960) First motions from seismic sources. Bull. Seism. Loc. Am., 50, 117.

Knopoff, L. and M.J. Randall (1972). The compensated linear-vector dipole. A possible mechanism for deep earthquakes. J. Geophys. Res. 75, 4957-4963.

Langston, C.A. (1976). A body-wave inversion of the Koyna India earthquake of December 10, 1967, and some implications for body-wave focal mechanisms. J. Geophys. Res., 81, 2517-2529.

Liebermann, R.C. and P.W. Pomeroy (1970). Source dimensions of small earthquakes as determined from the size of the aftershock zone, Bull. Seism. Soc. Am. 60, 879-890

Logie, H.J. (1951). The velocity of seismic waves on the Witwatersrand. Bull. Seismol. Soc. Am., 41, 109-121.

McGarr, A. (1971a). Violent deformation of rock near deep level, tabular excavations - seismic events. Bull. Seism. Soc. Am. 61, p.1453-1466.

McGarr, A. (1971b) Stable deformation of rock near deep-level tabular excavations. J. Geophys. Res. 76, p. 7088-7106.

Prentice, T.K. (1946). Crushing and grinding efficiencies, Trans. Inst. Min. and Met. 55, p.427-461

Press, F. (1967). Dimensions of the source region for small shallow earthquakes. in Proc. VESIAC Conf. Current status and future prognosis for understanding the source mechanisms of shallow seismic events in the 3-5 magnitude range, VESIAC rept. 7785 - X, 155-163

Pretorius, P.G.D. Contribution to 'Rock Mechanics applied to rockbursts' J.S. Afr. Inst. Min. Metal., 66, p.705-713.

Spottiswoode, S.M., A. McGarr and R.W.E. Green (1971). Focal mechanisms of some large mine tremors on the Witwatersrand, Circ. 3/71 Chamber of Mines of South Africa, Johannesburg.

Spottiswoode, S.M. and McGarr (1975), Source parameters or tremors in a deep-level gold mine, Bull. Seismol. Soc. Amer., 65,p.93-112.

Richter, C.F. (1958), Elementary Seismology, W.H. Freeman, San Francisco.

Savage, J.C. and M.D. Wood (1971). The relationship between apparent stress and stress drop, Bull. Seism. Soc. Am. 61, 1381-1388.

Savage, J.C. (1972). Relation of corner frequency to fault dimensions. J. Geophys. Res., 77, 3788-3795.

Smith, R.B., P.L. Winkler, J.G. Anderson and C.H. Scholz (1974). Source mechanisms of micro-earthquakes associated with underground mines in Eastern Utah, Bull. Seism. Am., 64, 1295-1317

Thatcher, W. (1972), Regional variations of seismic source parameter in the Northern Baja California area, J. Geophys. Res., 77, 1549-1565.

Thatcher, W. and T. Hanks (1973), Source parameters of Southern Californian earthquakes. J. Geophys. Res., 78, 8547-8576.

Tocher, D. (1958). Earthquake energy and ground breakage, Bull. Seism. Soc. Am. 48, 147-153.

Trifunac, M.D. (1972a). Stress estimates for the San Fernando, California, earthquake of February 9, 1971; main event and thirteen after-shocks. Bull. Seism. Soc. Am. 62, 721-750.

Trifunac, M.D. (1972b) Tectonic stress and the source mechanism of the Imperial Valley, California, earthquake of 1940. Bull. Seism. Soc. Am. 62, 1283-1302

van der Heever, P.K. (1978) A seismic investigation of mine tremors in the Klerksdorp mining complex, S. Afr. Assoc. Mine Managers, 2/78,20 pp.

van Proctor, R.J. (1978). An investigation of the nature and mechanism of rock fracture around longwall faces in a deep gold mine, Ph.D. Thesis, University of the Witwatersrand, Johannesburg.

Wilson, J.T. and O. Baykal (1948). Crustal structure of the North Atlantic Basin as determined from Rayleigh-wave dispersion, Bull. Seismol. Soc. Am., 38, 41-53.

Wyss, M. and J.N. Brune (1968) Seismic moment, stress, and source dimensions for earthquakes in the California-Nevada region, J. Geophys. Res. 73, 4681-4694.

Wyss, M. and T.C. Hanks (1972). The source parameters of the San Fernando earthquake inferred from teleseismic body waves, Bull. Seism. Soc. Am. 62, 591-602.